https://doi.org/10.15388/vu.thesis.117
https://orcid.org/0000-0002-1292-4783

VILNIUS UNIVERSITY
CENTER FOR PHYSICAL SCIENCES AND TECHNOLOGY

Monika
KIRSNYTĖ

Semiconductor polymeric composites formation by bioinspired *in situ* polymerization process with non-conductive substrates

DOCTORAL DISSERTATION

Natural sciences,
Chemistry (N 003)

VILNIUS 2020

This dissertation was carried out from 2015 to 2019 at the Center for Physical Sciences and Technology.

The research was supported by the Research Council of Lithuania.

Academic supervisor:
Dr. Arūnas Stirkė (Center for Physical Science and Technology, Natural sciences, Chemistry – (N 003)

https://doi.org/10.15388/vu.thesis.117
https://orcid.org/0000-0002-1292-4783

VILNIAUS UNIVERSITETAS
FIZINIŲ IR TECHNOLOGIJOS MOKSLŲ CENTRAS

Monika
KIRSNYTĖ

Puslaidininkinių polimerinių kompozitų sudarymas bio-inspiruotu *in situ* polimerizacijos būdu su nelaidžiais substratais

DAKTARO DISERTACIJA

Gamtos mokslai,
Chemija (N 003)

VILNIUS 2020

Disertacija rengta 2015 – 2019 metais Fizinių ir technologijos mokslų centre.

Mokslinius tyrimus rėmė Lietuvos mokslo taryba.

Mokslinis vadovas:
Dr. Arūnas Stirkė (Fizinių ir technologijos mokslų centras, gamtos mokslai, chemija – (N 003).

TABLE OF CONTENT

LIST OF ABBREVIATIONS

CPs	Conducting polymers
ICP	Intrinsically conductive polymers
Py	Pyrrole
PPy	Polypyrrole
MS	Microfluidic system
PDMS	Polydimethylsiloxane
SRR	Split-ring resonators
PVA	Poly(vinyl alcohol)
PVAc	Poly(vinyl acetate)
PVB	Poly(vinyl butyral)
PSSA	Poly(4-styrene sulfonic acid)
FIB-SEM	Focused ion beam scanning electron microscope
OM	Optical microscope
EMR	Electromagnetic radiation
EMI	Electromagnetic interference
XPS	X-ray photoelectron spectroscopy
DBS	Sodium dodecylbenzene sulfonate
DOSS	Dioctyl sulfosuccinate sodium salt
SDS	Sodium dodecyl sulphate
CAD	Computer-aided design
PET	Polyethylene terephthalate
PA	Polyamide
BPPy	Bacteria synthesized polypyrrole
EPPy	Electrochemically synthesized polypyrrole
MPPy	Microfluidic polypyrrole
EM	Electromagnetic

INTRODUCTION

The concept of conducting polymers (CPs) has emerged in recent decades with Shirakawa and colleagues discovery of synthetic metals[1] and still to this day continues to interest scientific community because of its tremendous potential for a variety of applications[2,3]. Research in this area is continuing to grow with the objective of tuning the intrinsic electrical conductivity properties of various CPs which offer multiple functionalization possibilities in radar absorbent materials[4], smart textiles[5], flexible electronics[6], biosensors[7] or energy harvesting[8] or energy storing materials[4].

A growing interest in conductive polymers for biomedical applications led to a biofriendly polymer synthesis search. An important source for various novel materials synthesis methods can be found in nature. Living microorganisms have the ability to create a variety of sophisticated biostructures.[9] Therefore is a growing study for the development of polymeric microstructural materials using bioinspired polymer synthesis, such as bacteria or other microorganism instigated synthesis, can not only be used for already widely distinguished metal nanoparticle[10,11] formation but also for novel polymer particle fabrication. Therefore, there is a demand to develop more environmentally benign ways to synthesize conductive polymers with more advanced characteristics.

Microfluidic systems are an attractive solution for the miniaturization of biological[12] and chemical polymerization processes and opens up entirely new experimental approaches for novel tunable polymer microstructure formation. Various CP synthesis techniques have been studied, although only a few are adapted and investigated polymeric synthesis in novel microfluidic systems.

A wide variety of CPs have a unique conducting mechanism, electrical properties, reversible doping/dedoping process, controllable chemical and electrochemical properties and easy processability, which have drawn special attention to conductive plastics field. The most important conjugated polymers feature is their electrical conductivity. Which has been explained by the band model theory, and has been successfully applied to tune electrical conductance in inorganic semiconductors and elucidate many of the physical and observed chemical phenomenas[13].

Polypyrrole is one of the most extensively studied conducting polymer mainly because of its intrinsic conjugated state, simple synthesis, good redox properties, biological compatibility and environmental stability when doped. This intrinsic conjugated polymer is already widely used in electronics and especially in the development of chemical biosensors and potentially in the

future can be used in specific electronic devices as a substitute for highly electrically conductive metals[14]. This electrically conductive polymer has also been successfully utilized in the pharmaceutical industry as a transport container for substances in the blood by placing various types of proteins or other types of active drug delivery systems[15].

Also, CP are widely used in textile fabric composite production. Electrically conductive textiles (E-textile) can be described as flexible conductive smart fabrics that feature incorporated electronics or other different interconnections woven into the textile fabric. It is noteworthy to mention that CPs application plays a crucial role in the development of commercially available and affordable various smart textile products, including medical textiles, efficient radar absorbing materials, touch screen displays, flexible fabric keyboards and various sensor[16] applications.

Goal of the thesis

In this work, a novel PPy *in situ* polymerization process was applied to produce an array of conductive polymer composites by measuring their conductance efficiency with contactless microwave method and by using one of the most examined polypyrrole as model-like conductive polymer, therefore we investigate few areas of interest:

- Synthesize biogenic PPy microspheres utilizing biocatalytic polymerization process with *Streptomyces* spp. bacteria.

- To design and compose chemical microsphere by microemulsion polymerization process in microfluidic system (bioinspired polymerization).

- Form and characterize a conductive PPy layer on a non-conductive surface.

- Produce and analyse conductive polymer composites using textile fabric substates.

- Compare and analyse dopant incorporation dependence on composites electrical conductivity and electromagnetic shielding effectiveness.

Key statements for the defence

1. A synthesis of hollow polypyrrole microsphere formation is possible using a biogenic polymerization method, and to reproduce such spherical structures, microfluidic polymerization technology can be used to obtain polymeric polypyrrole microspheres having a sponge-structure.

2. Conductive polypyrrole composite can be formed with a non-conducting, flexible and porous substrate using an adhesive polymeric matrix together with embedded radical polymerization oxidating agent.

3. Microwave-absorbing materials and flexible textile composites produced by the radical *in situ* polymerization in an adhesive polymeric matrix, shielding effectiveness is directly dependant from dopant incorporation into pyrrole monomer aqueous solution.

Author's contribution

This dissertation is an original author's work on CPs synthesis innovation and composite formation processes. The dissertation author has formulated and presented novel scientific ideas, performed most experimental investigations, analysed the obtained data and together with co-authors prepared two publications and wrote a patent (section *14.1.*).

PPy polymerization process and microsphere analysis using *Streptomyces* spp. bacteria, was performed in close collaboration with dr. Roxana-Mihaela Apetrei in Bioelectrics laboratory. The author also co-wrote the publications manuscript. Dissertation author, with the help of student Algimantas Janarauskas planned and performed experimental investigations concerning microfluidic systems in Vilnius University Life Science Center, Microfluidics laboratory. Also, author carried out the study of conductive PPy layer/composite characterization on non-conductive substrates in collaboration with student Marijus Jurkūnas, which eventually led to the writing of a patent and therefore, second publication manuscript. The author also, performed experimental investigations with textile composites and their dependence on dopant incorporation by carrying out composite synthesis and

measurement data configuration analysis. Parts of the aforementioned experimental research was performed with the collaboration of student Augustas Šukys.

LITERATURE OVERVIEW

CHAPTER 1. SEMICONDUCTIVE POLYMERS

1.1. From Polymers to Conductive Plastics

Historically polymers have always been acknowledged as good dielectric and insulation materials. One of the base characteristics of polymers is that they are composed of extremely large molecules which are often constituent of long, threadlike chains, sometimes branched, sometimes chemically cross-linked with each other so that they could form a solid network. Polymers molecular mass ranges from 10.000 to more than 1.000.000 g/mol, in contrast to better known compounds of low-molecular substances, which in general are in the order of 100 g/mol (e.g. H_2O 18 g/mol, NaCl 58.4 g/mol, H_2SO_4 98 g/mol)[17].

Some polymers of natural origins are often found in nature. These organic polymers are harvested from natural materials and can be used for technological purposes. Therefore, polymers can be divided into groups 'natural polymers' and 'synthetic polymers'. Aforementioned group is synthesized from low-molecular components, mostly organic monomers.

Over the years, studies of 'synthetic polymer' led to the origins of 'synthetic metals'. The term originated in 1911 from Herbert McCoy work when via electrolysis of $(CH_3)_4N^+$, he synthesized the first organic metal[18]. Not enough credit is shown to his fundamental conclusion that is it possible to create an electrically conductive substance constituent of non-metallic materials. Then Alfred Ubbelohde in 1951 first reported example of organic composite with embedded graphite that exhibited conductivities of 2.5×10^5 S/cm, but did not describe them as 'synthetic metals' till 1969[19,18]. It is also important to note that in 1963 Donald Eric Weiss and his co-workers[15,20,21] made a huge contribution by describing iodine oxidation of polypyrrole which later will be called polymer p-doping phenomena. Significant electron spin resonance studies then confirmed of a strong charge-transfer complex between the polymer and iodine molecules[21].

Taking into account all previous studies in 1979 the collaboration of MacDiarmid, Shirakawa and Heeger[22] led to the discovery of intrinsically conductive polymers (ICP) that changed our view to of 'synthetic metals'. While conductive polymers were described constituted of non-conductive polymer matrix and metal particles. More precisely polyacetylene doping[1], changed our view to these intrinsically conductive polymers. The importance

of this discovery lies in possibility of substituting metallic conductors for more unique polymeric compounds designed for specific applications.

This body of work alongside other researchers paved the way to the understanding of today's electrically conductive plastic materials otherwise known as conductive polymers.

1.2. Definition of Conducting Polymers

Conductive polymers are exclusive class of variable poly-heterocyclic organic polymers combining both good stability and high electrical conductance properties[3]. This class of polymers consists of over 25 conductive polymer derivatives[23,24]. Most generally researched CP includes polyacetylene (PA) polypyrrole (PPy), polythiophene (PTh), polyfuran (PF), polyphenylene (PP), polyaniline (PANI), poly(p-phenylenevinylene) (PPV), poly(3,4-ethylene dioxythiophene) (PEDOT).

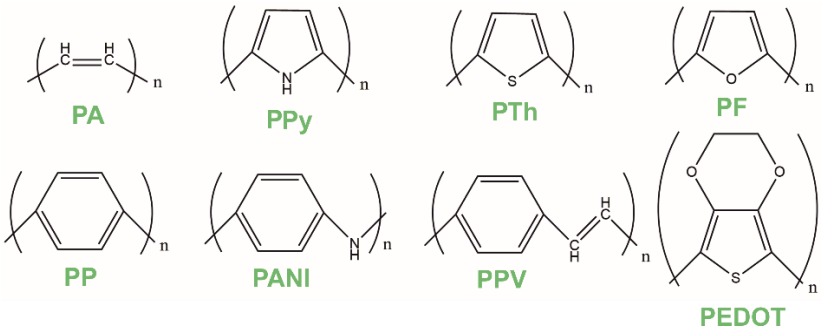

Fig. 1. Chemical structures of the most common conductive polymers.

Over the years CP has attracted much attention for their inherent characteristics, combining unusual material properties like flexibility of plastics and electrical conductivity of metals. CP is a type of material made from metal powders mixed within a non-conductive polymer matrix. The discovery of intrinsically conductive polymers let to a possibility of substituting metallic conductors with cheaper, lighter and more economically efficient products. This unique accomplishment motivated researchers to investigate more conductive material possibilities.

Semi-conductive polymers or otherwise synthetic metals can be described as intrinsically conductive materials constituted of 'metal-like' chemical structure which enable them to transfer electrons through delocalized orbitals. Semiconductor polymers are organic conjugated polymers designed to mimic

electrical conductivity. Organic polymers can be insulators or electrically conductive substances. Therefore, it is noteworthy to underline the importance of doping process. The concept of conjugated polymer doping is generally a tunable and reversible increase in their conductivity levels. Insulators or semiconductors insufficient conductivity range is converted into conductive regime.

1.3. The Phenomena of Conductive Polymers

Conductive polymers electrical conductivity phenomena is considered to be a novel field of research regarding its tremendous potential for a variety of applications. Conducting polymers not only can exhibit near-metal electrical conductivity but also so extraordinary properties such as magnetic, wetting optical, mechanical and microwave absorbing properties[25].

Nowadays we recognise the definition of conductive polymer (CP) as a type of conjugated organic plastics that exhibit metallic conductivity when chemically doped. Either their oxidized (*p*-doped) or reduced (*n*-doped)[26,27]. It is noteworthy to mention the early investigations of polyacetylene that eventually led to the discovery of chemical doping[28]. Metallic conductivity can be usually explained by simple band theory, however to explain this conductivity phenomena we have to implicate the use of solitons, polarons and bipolarons.

Doping techniques can be classified into 3: redox doping, doping involving no dopant and non-redox doping[1]. Most widely used technique is redox doping. Dopants also can be classified as strong reductors or oxidising agents. The origin of these dopants is of great importance: whether it's neutral molecules, compounds, ionic dopants (from inorganic salts), organic dopants or polymeric dopants.

This class of CP and their derivatives undergoing redox doping can be *p* and/or *n*-doped. *P*-doping occurs when CP π backbone undergoes partial oxidation treatment, whereas less frequent *n*-doping occurs when conjugated polymers π system undergoes partial reduction. Both *p* and *n*-doped methods can be utilized by chemical or electrochemical polymerization processes. Also, counter dopant anions (counter-anions) act as conjugated polymer charge stabilizers, creating such highly conductive polymer charge carrying forms. In general doping leads to formation of conjugational defects as solitons, polarons and bipolarons[29]. These electron rearrangements result in effective charge carrier systems or otherwise polarons. The presence of localized structural defects in polymer backbone chain is directly associated

with the existence of polarons (radical cations) and bipolarons (dications diradicals)[30,31]. For example, in Fig. 2 under alkaline conditions polypyrrole backbone chains exited state can be rearranged to form polarons, on the other hand by electron delocalization it results in bipolarons. In general low doping levels give rise to polarons, whereas higher doping levels produce bipolarons[32]. Therefore, polypyrrole chain in Fig. 2 B includes reduced and oxidized units in its molecular structure.

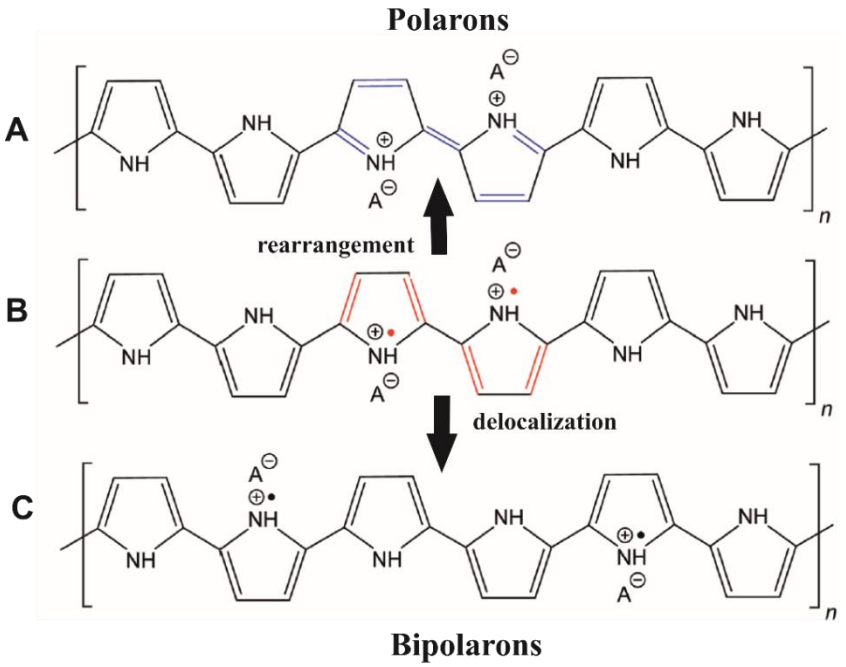

Fig. 2. The rearrangement and delocalization of electrons in exited polypyrrole backbone state with effect of counter-anion B can generate accordingly: A – polarons, C – bipolarons. A^- corresponds as a counter ion.

1.4. Polypyrrole as a Conductive Polymer

Over the years, PPy stands out to be the most extensively studied conducting polymer mainly because of its intrinsic conjugated state, simple synthesis, good redox properties, biological compatibility and environmental stability when doped. As a result of its good intrinsic conductive properties, PPy has proven to be very useful materials for several applications such as antistatic coatings[33], biosensors[34], photovoltaics[35], solar energy harvesting,

fuel cells[36], actuators[37], batteries, tissue engineering[38], drug delivery systems[31] and energy storage materials.

Polypyrrole was first synthesized in 1915 in the name of 'nerro di pirrolo' or 'pyrrole black' by an Italian Chemist Angelo Angeli. His work on pyrrole and indole chemistry led him to find that PPy could be obtained using a variety of different oxidizing agents[24]. Although another Italian chemist produced PPy in 1921[39], he considered it to be an intermediate form of graphite. However precious work did not go to waste then in 1963 based by Ciuta's research, Donald Weiss and his colleges produced an organic polymer PPy and were the first to measure it's conductivity[40,41,14]. Pyrrole was oxidized with iodine vapour[42,43] under base conditions and resulted in PPy with 0.005-0.09 Ω^{-1} cm^{-1} electrical conductivity. Since then various improvements were made for polypyrrole synthesis and more derivatives were produced.

Pyrrole monomer is a heterocyclic organic compound which after getting into contact with a strong oxidant polymerizes into polypyrrole. PPy is described as a very dark blue, almost black colour polymer of organic origin, π-conjugated chain and intrinsic electrical conductivity properties therefore is considered as a semiconductor polymer. There are three most commonly used methods to prepare polypyrrole synthesis, they are: chemical pyrrole oxidation process using a strong oxidant such as anhydrous iron (III) chloride, electrochemical monomer oxidation in an electrolyte solution or enzymatic polymerization process.

Although pyrrole polymerization process is fairly simple, unfortunately the achieved PPy polymer particles is known to be highly brittle, mechanically rigid[44,45], and insoluble after synthesis[46]. Consequently, an area of research emerged to develop a simple, more economically efficient intrinsically conductive polymer layer or composites for numerous technological applications[47,36,37,48,4].

1.5. Polypyrrole Polymerization Mechanism

Most common methods for pyrrole monomer synthesis are electrochemical and chemical oxidations. The chemical oxidation is an easy method that involves the oxidation of pyrrole in aqueous medium, commonly using ferric chloride or ammonium persulfate as oxidizing agent, resulting in an electrically conductive emeraldine or black powder. On the other hand, monomer electrochemical oxidation[7] is carried out without adding any chemical oxidizers, but it is limited to a PPy layer deposition on a non-

electrically conducting substrate. Other methods, such as vapour-phase[49] induced polymerization process, produced PPy without using a solvent. Nevertheless, the synthesized polymer contained a significant amount of oxidation by-products.

However, despite the amount of work already done in polypyrrole polymerization, there has not been a conclusive attention given to the mechanism of PPy synthesis (Fig. 3).

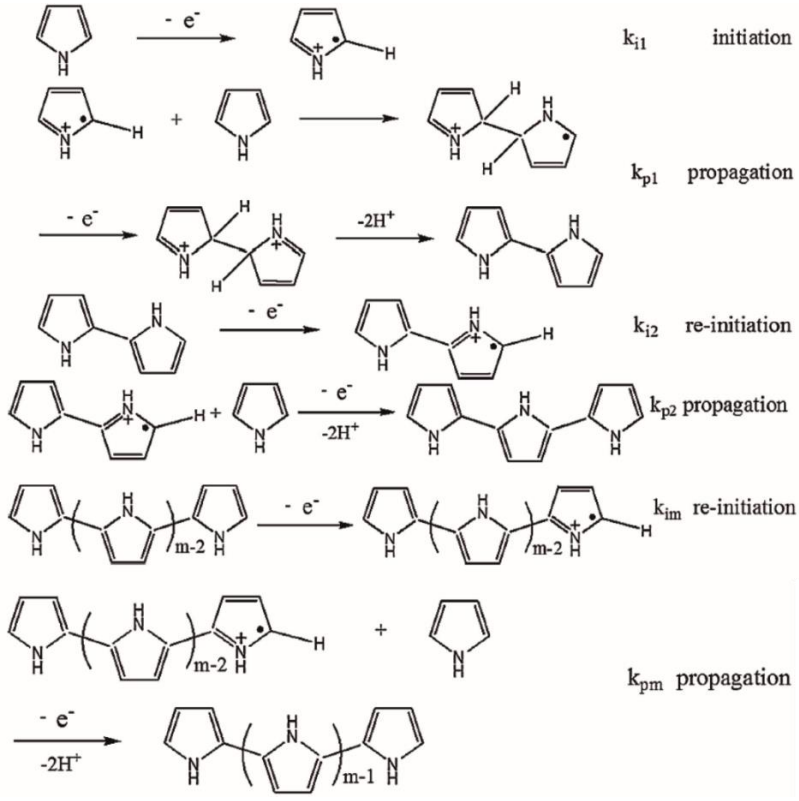

Fig. 3. Oxidative pyrrole polymer polymerization process. Monomer propagation scheme.[50]

Conducting polymers usually have an amorphous structure, in some cases with ordered domains. The charge-transporting mechanism in conducting polymers differs from that in the crystalline CP where their existing conduction bands, valence bands and the charge carriers can move freely in the energy bands. In CP the charge carriers are located in the local doping energy levels (limited length of conjugated polymer chain) or in a very narrow

doping energy band in the case of ordered domains. The charge carriers can move easily on the conjugated polymer main chain, but the charges have to hop for the transportation between the conjugated polymer chains. The activation energy for the hopping of the charge carriers is much higher than that of the charge transportation within the conjugated polymer main chains. Obviously, the charge transportation in conducting polymers is limited by the hopping between the conjugated polymer chains. Therefore, the conductivity of conducting polymers shows characteristics of hopping transportation[51].

1.6. Conductive Polymer Synthesis

A wide variety of conductive polymer films[52,2,53], composites or particles has been prepared from heterocyclic organic molecules. There is no singular method for synthesizing this class of conductive polymers. Conventionally most of conductive polymers may be synthesised using standard polymerization methods: chemical or electrochemical oxidation polymerization or by chemical catalytic synthesis[54,55,56,7].

Conductive polymers can be synthesised by either one of the following techniques[29], followed by coupling of the charged monomers to produce the polymer chains, which is the simplest system.:

1. Radical Chemical polymerisation
2. Electrochemical polymerisation
3. Photochemical polymerisation
4. Metathesis polymerisation
5. Emulsion polymerisation
6. Inclusion polymerisation
7. Solid-state polymerisation
8. Plasma polymerisation
9. Pyrolysis
10. Soluble precursor polymer preparation
11. *In situ* polymerization
12. Chemical vapour deposition polymerization[57,58].

In order to further understand conductive polymer synthesis, it is noteworthy to compare two of the main methods for CP synthesis (e.g. radical chemical polymerization and electrochemical polymerization processes).

Simply put during CP synthesis the monomer solution is mixed with an oxidizing agent of inorganic nature e.g. iron (III) chloride, ammonium persulfate, hydrogen peroxide, copper (II) perchloride etc. Subsequently

oxidative coupling is followed by the oxidation of monomers to a cation radical and their coupling to form dications and the repetition of this process creates a CP chain which leads to powder or a thick film formation. Radical chemical polymerization process is considered to be the most useful technique allowing to produce all classes of conjugated polymers in bulk, since it is fabricated without any additional equipment (e.g. electrodes)[59,60]. Therefore, chemical polymerization process is a method of choice for economically viable commercial applications[20]. However, the conductivity of the polymers synthesized using the chemical technique has always been lower than their electrochemically synthesized materials[3].

Electrochemical polymerization occurs by applying an electrical current through electrodes placed into a solution containing monomer, solvent and the doping agent[61,62]. The electrical current causes the monomer to oxidize and deposit on the positively charged working electrode while forming an insoluble polymer chains[58]. Conditions are recommended to obtain thin films is potentiostatic, while galvanostatic conditions are recommended to obtain thicker films[29].

Composite formation helps to compensate the disadvantages of pure conductive polymer materials by combining the best qualities of both materials. For example PPy is brittle after synthesis[44]. In order to achieve flexibility, PPy composite has been formed with polyester[63] and polyethylene terephthalate fabrics[64] by using vapour phase deposition polymerization process, enabling to be further applied *in vitro* biocompatibility studies.

Moreover, CP particles can be fabricated with the help of templates during the polymerization process. Therefore, two main approaches for the controlled synthesis of CP particles and CP based hybrid nanocomposites[65] as well as heterostructures, which are the template-based synthesis[66] and the template-free synthesis[67,68], are presented in numerous studies. Thus, aqueous solutions containing pyrrole and calix-6-arenehexasulfonic acid were found to undergo polymerization in the absence of either a chemical oxidant or electrochemical oxidation resulting in unstable colloidal suspension consisting of spherical polypyrrole particles[69].

There is growing interest to an enzymatic polymerization method that is more efficient and environmentally-safe. Since usual chemical polymerization techniques for the production of PPy were based on application of strong oxidants and mostly were performed in strongly acidic media, therefore the biomedical application of CP has been problematic, due to traces of toxic materials present in the formed polymer, which become entrapped during the course of polymerization[70].

CHAPTER 2. BIO-INSPIRED MICROSTRUCTURES

2.1. Enzyme Instigated CP Polymerization Processes

Nature is our prominent example for various novel methods of materials synthesis, wherein microorganisms create a variety of sophisticated biostructures. Recently a considerable amount of research has been focused on the development of polymeric microstructural materials using common resources that are abundant in nature[9].

Enzymatic polymerization is an *in vitro* chemical polymer synthesis (in test tubes) using an isolated enzyme as catalyst via non-biosynthetic (non-metabolic) pathways[71,72]. Enzymatic polymerization of aromatic compounds (e.g. CP and their derivatives) provides an alternative method of a "green process" for the formation of soluble and processable conducting polymers. Water-based systems at ambient temperatures and pressure for microorganism-assisted biogenic (enzymatic) polymerization process is safe and economically viable prospect for novel material synthesis approach. Although development in bio-inspired CP polymerization of nano-, micro-particles and polymers on a commercial scale are still in their beginning stage, but are attracting attention of many material scientists throughout the world.

Bacterial, fungi[9] or other microorganism-assisted synthesis can be used for polymer, metal nanoparticle[10,11] or other diverse material[73] synthesis. Therefore, there is a demand to develop more environmentally benign ways for the synthesis of more advanced conductive polymers.

Two of the most popular CP are polyaniline and polypyrrole. Normally, polymerization reaction requires quite harsh conditions with extreme pH levels, high temperature, strong oxidants, and highly toxic solvents. Therefore, conductive polymer fabrication using enzymatic polymerization method has been investigated as a way to address biocompatibility and environmental issues associated with common CP production methods[74].

As early as 1990 Aizawa performed enzymatic polymerization of aniline by using another enzyme, bilirubin oxidase, that resulted 1,4- and 1,2-substitution structures[75]. Both aforementioned structures appeared to partially differ from those of chemically or electrochemically prepared polyaniline derivatives. Another enzymatically synthesized polyaniline is considered Water-soluble conducting PANI was formed by horseradish peroxidase catalysed polymerization of aniline using hydrogen peroxide (H_2O_2) oxidant

and sulfonated polystyrene, which acted as polyanionic template[76]. This entails a particularly attractive, completely benign, one-pot synthesis where the desired final product requires little or no further purification process.

Ideal conditions for PPy synthesis would be at neutral pH and in aqueous environment[77]. In order to fulfil these conditions huge interest is growing on synthesizing more environmentally friendly polymers. Studies have shown that environmentally friendly chemical oxidant H_2O_2 is also able to polymerize pyrrole[65]. However, the disadvantages lie in large production of side products caused by very fast polymerization process. Other reported polymerization methods for PPy have included using catalytic amounts of ferric chloride hexahydrate ($FeCl_3$*$6H_2O$)[78], iron porphyrin enzyme mimics[79], glucose oxidase, and laccase[80] and already mentioned enzymes horseradish peroxidase[81].

In order to develop a 'green' CP synthesis there is a need of utilization of new environmentally friendly polymerization initiators for example such as *Streptomyces* spp. bacteria. It is Gram positive bacteria involved in the formation and/or degradation of complex biopolymers like lignin, melanin and humid substances. *Streptomyces* spp.[82] was deeply studied because of their capacity to produce antibiotics and enzymes of industrial importance, such as glucose isomerase, protease, amylase, xylanase, laccase and tyrosinase, which are synthesized intracellular and then transported into the growth medium[83]. In this way it is possible to synthesize polymers using synthetic routes that can be carried out in mild environments and even around living cells.

2.2. Microfluidic Systems

Microfluidic systems are miniaturized liquid handling devices. MS has the potential to influence elaborated scientific research from chemical synthesis[84], biological, chemical[85] and cell analysis[86,87] to optics[88] and information technology. Microfluidic systems have endless advantages over methods that require large solution volumes to perform complex experiments. Because of their small-scale sample reagent volume requirements, ease of automation, low-cost, shorter reaction times, disposability and the possibility of parallel operation with other microfluidic devices have a possibility to become a valuable tool for various 'lab on a chip' applications. By understanding and controlling this microscale phenomenon, microfluidics can be used to perform techniques and experiments not possible on the macroscale variations, allowing new functionality and experimental models to emerge[89,90].

The basic principle of droplet microfluidic systems is simple[91,92,93]: highly monodisperse aqueous droplets flow in an inert carrier oil in MS microchannels on a chip where each droplet functions as an independent microreactor. In order to perform a high-quality experimental investigation in a microfluidic system, a device compatibility is required – when all pumps, microscope and the slow imaging chamber are calibrated in conjunction.

Aforementioned MS chips require an ongoing droplet observation under microscope and maintaining precise control over long-term flow rates, which requires connecting macroscale plumbing to the chip[94] (e.g. syringe pumps or air pressure controllers). Ultimately, this increases the complexity of systems, and presents a big hurdle to the widespread use of microfluidic chips.

One of the most important variables for a well operating MS is choosing appropriate materials and conditions for the reaction process. Conditions can be easily varied to change the yield or quality of the obtained materials. The system itself is well suited to work in a microscale size environment and can be composed of various flexible and soft polymers[95]: some of polyurethane, polycarbonate, polymethyl methacrylate, polystyrene, polyethylene terephthalate glycol, polyvinyl chloride, polydimethylsiloxane[96] or polyethylene[95].

2.3. PPy Polymerization in Microfluidic System

An entirely new experimental approach for the miniaturization of biological and chemical proceses increasingly emergeged by the utilization of microfluidic systems. Although many different properties and synthesis studies of polypyrrole formation has been performed using different techniques[97,98,99], few is known about the intrinsic properties, methodology, advantages or disadvantages of polypyrrole synthesis in novel microfluidic systems.

Microemulsion polymerization in microfluidic system[100] has many advantages. Firstly, experimental investigations require significantly smaller system size – large-volume experiments are usually performed in volumes of a few or several millilitres, while in the MS system volumes can range from 50 to 500 μl of materials per experiment. Also, superb level of spatiotemporal control is possible by facilitating highly parallelized assays with drastically increased throughput and reduced cost. The design flexibility, reduced energy consumption, increased reaction rate and detailed monitoring of individual

process stages are the most important advantages of polymerization process in microfluidic device. However, MS devices also have some drawbacks: high hardware cost, low final product volume and production efficiency. Thus, there is a lack of information concerning polymeric derivatives synthesis in 'lab on a chip' microfluidic devices.

2.4. Microfluidic Device Formation

Microstructures were traditionally patterned into glass or silicon, making use of such as photolithography and etching techniques. However, this approach requires highly specialized equipment, is rather expensive, and does not allow rapid prototype manufacturing.

In 1996 the emergence of soft lithography is considered to be a real breakthrough for MS device fabrication, which enabled rapid and cheap replica moulding[101]. Instead of patterning microchannels directly into potentially opaque (such as silicon) and expensive materials from which only one device could be produced, therefore a master mould is used for the fabrication of numerous microfluidic devices made from transparent and cheap elastomers such as polydimethylsiloxane[94] (PDMS).

MS systems can be manufactured in three stages of soft lithography, rapid imaging and replication casting. First is soft lithography stage which is commonly used methodology in the fabrication of MS systems. It is a process in which using elastomeric seals, templates and appropriate 'photo masks' are required. Soft lithography stage is a particularly useful non-photolithographic technique for extracting a particular template of the MS system. In the soft lithography stage, the desired structure is repeated on a soft elastomer (most commonly used PDMS). No special conditions are required for this step – it can be performed under standard laboratory conditions for structures ranging in size from 20 to 100 μm[102,103]. It also allows you to use the following quick imaging technique. The first step that begins to create a wanted structural design is a specific computer-aided design (CAD) program. Next, a template of the created design is printed on the transparent film. The film needs to obtain the reverse template of the MS system by photolithography. Everything is irradiated with UV rays leading to uninsulated space polymerization. After dissolving the unpolymerized photoresist, the main template of the MS system remains, which will be further used as a multiple template to produce the same MS system from the PDMS polymer. If a multi-level MS system is to be extracted, the previous process can be repeated several times[103]. The whole

MS manufacturing process is shown in Fig. 4.[12]. The last stage of MS system production is fixing the PDMS plate on the glass and punching holes to connect the duct system. Fixation occurs initially by-passing air plasma through the bottom of the PDMS structure (which will be reinforced with glass). This process helps to form Si-O-Si bonds that are strong and unbroken without breaking the polymer itself. The MS system produced in this way is less expensive and requires significantly less time, design, production and testing of new configurations than other production techniques[104]. It is precisely because the cost of this system is relatively lower than that of other methods that more MS systems can be produced, which allows more experiments to be performed, resulting in greater reproducibility and accuracy of the results.

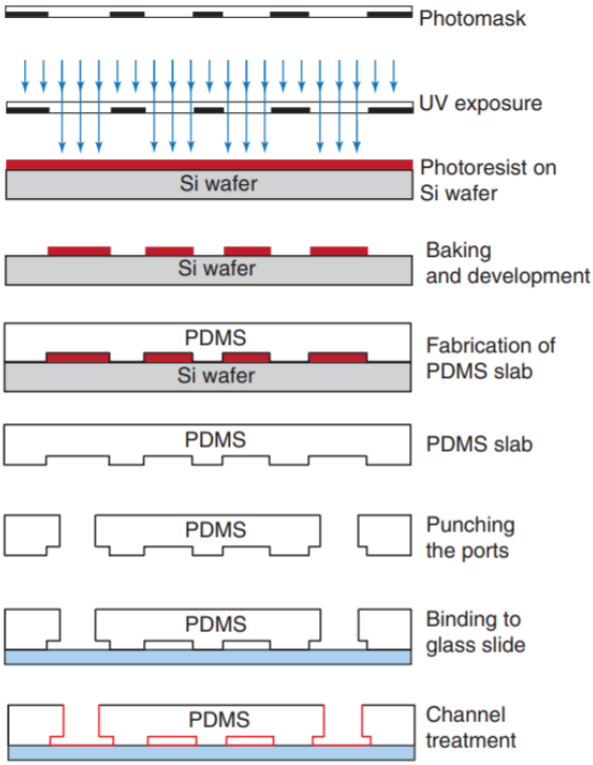

Fig. 4. Schematic microfluidic device fabrication with soft lithography[12].

Microfluidic device formation process precisely includes: mask design using computer-aided design (CAD) software, mask printing, fabrication of the master, polymerization of the PDMS using the master as a mold, bonding

of the PDMS slabs to a glass substrate and surface treatment of the microfluidic channels[12].

Microchannels diameter of such a system is from 10 to 100 μm. The microchannels network must be hydrophobic[105] in order to ensure reliable and monodisperse droplet production and prevent reaction mixture possibility of degrading the overall microfluidic system or PDMS template. To achieve this, the system can be constructed of a hydrophobic polymer that or commercial water repellent Aquapel[106] is used to ensure reliable and monodisperse droplet production[12]. Aquapel is injected into the MS system with a syringe, held for a few seconds and removed with compressed gas. During this process, the MS system is coated with a hydrophobic aquapel layer and becomes inert to aqueous solutions[107].

2.5. Droplet Based Microfluidics

One of the central aims of droplet-based microfluidics is to develop methods for reliable manipulation of droplets to produce special materials for fabrication and development of biological arrays[108], polymeric particles, nanoparticles, inorganic or microgel particles.

A combination of biochemistry, soft matter physics, and microsystems engineering is a rapidly growing interdisciplinary field of research for droplet-based microfluidics utilization. Its applications range from synthesis of advanced materials or fast analytical systems to biological assays for living cells and even protein crystallization. For example, droplet-based microfluidics has been used for sample preparation for targeted DNA sequencing[109]. One of the central aims of droplet-based microfluidics is to develop methods for reliable manipulation of droplets to produce special materials for fabrication and development of biological arrays[108], polymeric particles, nanoparticles, inorganic or microgel particles.

Combination of biochemistry, soft matter physics, and microsystems engineering is a rapidly growing interdisciplinary fields of research for droplet-based microfluidics utilization. Its applications range from synthesis of advanced materials or fast analytical systems, to biological assays for living cells and even protein crystallization. For example, droplet-based microfluidics has been used for sample preparation for targeted DNA sequencing[109]. Reliable droplet manipulations such as individual droplets ability to coalescence, a precise control of droplet volumes, thus the mixing of their contents, and sorting in combination with fast analysis tools allow us

to have and perform chemical reactions inside the droplets under precise conditions[12,110].

Microfluidic 'lab on a chip' devices can produce monodisperse droplets by applying several geometric techniques: 'T-junction', 'co-flow' (flow focusing), and 'step emulsification' in their geometries for the sake of droplet homogeneity, simplicity of device fabrication, and controllable operational parameters[111].

Two of the most important conditions determining droplet size and distribution are carrier phases and various surfactants. Typically, surfactants are added to the continuous phase provides an energy barrier to stabilize the dispersion in a metastable state[112,113]. Surfactants facilitate the formation of new interfaces and to stabilizes the formed emulsion droplets from coalescence by adsorbing at the liquid/liquid interface[113-114].

Standard surfactants such as polysorbate-type non-ionic surfactants (e.g. Span 80 or Tween 20) are also often used with organic carrier phases for example hexadecane and mineral oil. The latter solution combination is used to form aqueous droplets. However, coming into contact with various continuous organic phases PDMS microchannels has a tendency to swell and change their geometry over time[110]. Therefore, one of two possibilities can be adjusted: carrier phase must be changed or surface modification must be applied as discussed in previous section *2.4.*

CHAPTER 3. SEMI-CONDUCTOR POLYMERIC LAYER IN NON-CONDUCTIVE SUBSTRATE

3.1. CP *in situ* Polymerization in Matrix, Conductive Layer Formation

There have been many attempts to improve the chemical and physical properties of CP layers, while ensuring that its electrically conductive properties are maintained. Usually, conducting material layers are obtained by electrochemical or chemical oxidative polymerization of selective exclusive monomers or its respective derivatives. There is a growing interest of the influence of various factors in the preparation of aforementioned CP layers that would allow us to optimize growth conditions where the properties of conductivity, adherence, morphology, and flexibility could all be varied.

Some recent studies have already discussed *in situ* polymerization process by synthesizing series of PANI nanocomposites based on combining nanostructured polyaniline, gold nanoparticles and graphene nanosheets[115]. Ergo varying the

concentration of graphene and chloroauric acid to optimize the formulation of conductive stable films. Also, CP polymerization in polymeric matrix was presented by Percec and his colleagues[116]. A few water-soluble polymers were used as model-like templates for the *in situ* polymerization of pyrrole to determine their effect on the production of nanosized PPy particles. PVA M_w=85,000–124,000 was considered to be best choice in polymeric matrix for PPy nanoparticle formation. Thus, PPy particles size distribution was dependant on water-soluble polymeric matrices molecular weight and concentration. As a matrix base PVA was also used in free-standing Ag-PVA/PS film formation with *in situ* synthesis of highly monodisperse silver nanoparticles[117].

Electrochemical synthesis enables rapid *in situ* deposition of conductive polymers, but the number of bioactive molecules that can be this way doped into the polymeric matrix is limited for thin films[118]. For bioengineering applications, a neural electrode was interfaced with the surrounding brain tissue through the *in situ* polymerization of inherently conductive PEDOT polymer[119]. It is noteworthy to mention biological matrix examples as acellular muscle tissue for chemical *in situ* polymer deposition[120].

The resulting materials display an array of applications in biomedical area with sensors and peripheral nerve repair, as well as in technological applications for EMI shielding, nanoelectronics and batteries where electrical conductivity is critical to material functionalization.

3.2. Polymeric Composites

Polymer composites are useful as they combine properties of flexible polymers with rigid inorganic materials. One component in composites can strengthen other component providing new useful and novel properties for commercial applications.

For example, graphene/polypyrrole composites have been successfully synthesized where polypyrrole was uniformly surrounded by graphene sheets and thus increasing conductivity six times to 6.85 S/cm compared to bare polypyrrole[121]. Polymer composites are convenient to produce flexible and stiff layers which facilitate the manufacture and shaping of the polymer products. Other PPy-polymer composites can be obtained by *in situ* polymerization of pyrrole in the polymer mixture. For example, dodecylbenzene sulfuric acid/poly(4-stirensulfon acid)/PPy composite was produced by spin coating the mixture of components[122]. It is possible to load PPy, for example, on textile fibers by *in situ* polymerization[123] or into polypropylene by polymerization of pyrrole in the presence of sodium bis(2-

ethylhexyl) sulfosuccinate, which minimized the polypropylene–polypyrrole interfacial tension[124]. Polypyrrole/poly(vinyl alcohol-co-ethylene) (PPy/PVA-co-PE) nanofiber composites on polyethylene terephthalate (PET) substrates demonstrated low resistivity (less than 1 Ω·cm)[125]. In another study conductive polymer pyrrole acts as polymeric host matrix as appose to most cases then represents a filler or a conductive layer. Thus, aqueous ferrofluid has been successfully incorporated in a polypyrrole matrix by *in situ* chemical oxidative polymerization process[126]. Aforementioned polypyrrole composite containing Fe_3O_4 nanoparticles demonstrated electrical conductivity in the order of 10^{-2} S/cm. L. Jiang et al.[127] prepared a methanol sensor using PVA-PPy composite and pure PPy and observed that the composite sensor exhibits longer response and recovery time and higher sensitivity. PVA-PPy sensor was prepared by vapour polymerization on the spin coated PVA-$FeCl_3$ (PVA: $FeCl_3$ ratio of 1:3) steaming pyrrole and water vapours. Another paper introduced PVAc-PPy layer which were synthesized immersing PVAc layer impregnated with $FeCl_3$ in aqueous pyrrole solution[128]. Authors explained the mechanism of PPy formation and penetration into a polymer matrix during the polymerization of pyrrole which has impact on modification to polymer surface by creating microchannels thus increasing active surface area for enhanced microwave absorption.

All in all, polymeric composite formation is an area of research that is still under development. Therefore, a large amount of research has been dedicated to in depth analysis and fabrication of conductive composite materials with flexible and economically viable applications for wearable electronics.

CHAPTER 4. FUNCTIONAL TEXTILES FOR WEARABLE ELECTRONICS

4.1. Conductive Fabrics to Smart Textiles

Functional textiles are textile materials to which a specific function is added by means of material, composition, construction and finishing e.g., applying dopants and other additives. Electrically conductive textiles or also in literature called electronic textiles (e-textiles) are fabrics that enable digital components such as a battery, light or including small computers and other electronic components to be embedded in them[129]. Conductive textiles include conductive fibres, yarns and fabrics, which are then incorporated in smart textile production. Conductive textile materials, strictly speaking are not

intelligent. Therefore, they are not able to react to environmental change, but they make many smart textile applications possible, especially those that monitor body functions[130]. Whereas, smart textiles are defined as fabrics that possess the ability to sense external conditions or stimuli thus to respond and adapt fabrics behaviour by increasing their research in health, sport, automotive and aerospace field areas[16,131,5]. It is noteworthy to mention that such e-textiles have to meet special requirements concerning wearability[132].

Textile fabrics are mostly porous, flexible materials made by weaving or fiber pressing, which gives them intrinsic characteristics such as flexibility, stretchability, and lightweight. Therefore, there has been a growing interest in textile-based conductive materials preparation, with attributed utilization in electronic textiles and wearable electronics[133,5].

Conductive polymers have a crucial role in the development of commercially available smart textile products such as medical textiles, protective clothing, touch screen displays, flexible fabric keyboards, and sensors for various scientific areas[16]. Also, Ferrero[134] discussed the influence of various dopants on weight increase and surface resistivity of PPy-coated synthetic fabrics. These fabrics supported the argument that when composite comprises of conductive polymer and dopant one can observe not only an increase in fabric weight but also in surface resistivity.

Nowadays, the convergence of conductive textiles and electronics can result in the development of smart textiles by modifying non-flexible and rigid commercial electronic products. Regarding smart textiles exclusive electronic behaviour they can be utilised in a variety of application and can be divided into three groups[16] according to complexity: 1) passive smart textiles: sensor based textiles for environmental sensing; 2) active smart textiles: reactive sensing to stimuli from the environment (modified with function actuator and a sensor); 3) very smart textiles: has the ability to sense, react and adjust their behaviour to the given environmental change.

Some other functional application can offer energy generation[135] for micro powered electronics, energy storage, radio frequency functionality (e.g. RFID antennas) or health monitoring sensor technology[136]. Also, electric power generation can be achieved through piezoelectric[135] fabrics that harvest energy from motion.

4.2. CP Fabrication for Electrically Conductive Textiles

Metals, conductive polymers as well as conducting materials are already being used in many textile applications, like antistatic materials,

electromagnetic interference shielding, heating or transport of electrical signals, sensors and etc. Over the years, metals have attracted increasing interest as conductive fillers in formation of conductive textile coatings and printings, for implementing electronic conductivity to novel textile fabric formation, in particular, for wearable textile applications[132,16]. Nevertheless, considering the adhesion between metal and the textile fibers as well as corrosion resistance aforementioned textile fabrics can lead to multiple conductivity problems (e.g., drop in conductivity levels). Therefore, more research is dedicated to modify electrically conductive textiles, including conductive fibres production, conductive fibers insertion during/after fabric manufacturing and coating textile techniques.

Dependent upon the nature of the conducting component, electrically conductive polymer fibers are mainly divided into two classes[137]: intrinsically conductive polymer fibers and extrinsically conductive polymers fibers. Intrinsically CP fibers can be manufactured from metal, carbon or intrinsically CP components. Further, only organic conjugated polymers fabrication into conductive fiber or yarns will be discussed as a consequence of excellent CP electrical and optical properties previously found only in inorganic systems[138]. Therefore, various approaches were developed due to intrinsically CP high conductivity, good environmental stability and non-toxicity properties for the production of electrically conductive smart textiles.

Intrinsically CP fibers/yarns are fabrication is demonstrated by few techniques: melt spinning, electrospinning or wet spinning. PANI multifilaments prepared by the wet spinning process revealed 145-1440 S/cm conductivity[139] whilst comparing to one-step wet-spinning process of poly(3,4-ethylenedioxythiophene): poly(styrenesulfonate) (PEDOT: PSS) fibers conductivity[140] exhibited 223 S/cm. Moreover, Jalili et al. experiment with polyethylene glycol resulted in fibres with enhanced electrical conductivity from 9 to 264 S/cm. Non-conjugated polymers with double bonds in the backbone were also found to be conductive when doped. Hence, same overall fabrication approach is used to produce low-cost thermoplastic trans-1,4-polyisoprene doped with iodine exhibited electrical resistivity as low as 10^{-2} Ωm with 0.01 mm thickness[141].

Extrinsically conductive polymers fibers/yarns made by the combination between conductive fillers (e.g. metallic powder, metallic nanowires, conductive nanoparticles and ICP) and non-conductive materials (e.g., polypropylene, polystyrene or polyethylene). Aforementioned fibers production involves wet spinning, melt spinning[142] or coating processes. The

wet spinning process guarantees fibres/yarns with improved electrical and mechanical properties over those produced by the melt spinning[142].

Additionally, studies on fiber flexibility with conductive polyblend of polypropylene/polyamide-6 complex filaments was performed by melt spinning process and then modified by polyaniline. The ternary blend of PP/PA6/PANI complex revealed a matrix/core-shell droplet which dispersed phase morphology exhibited a smoother surface and more even formation for production of conductive fibers or yarns.

Despite of previously discussed intrinsically and extrinsically CP fibers/yarns fabrication methods most commonly electrically conductive textiles fabrication relay on various coating techniques. For a thin film production electrodeposition, electroless (chemical or autocatalytic) plating, thin films sputtering, vapor deposition[16], printing, spraying and knife-over-roll coating can be applied. Whilst for a thicker film coating can be applied manually or by masking techniques, dip-coating, soft lithography or embossing[143]. The influence of ICP coating on the mechanical properties of the yarns is dependent on the ICP and yarn type, concentration of ICP and oxidative agent, coating uniformity and thickness.

Conductive polymers can also be incorporated into E-glass fiber fabrics[144] also multifunctional polymer foams[145] (e.g. polyimide, polyurethane and silicone). These foams can later be applied for use in EMI suppression against high intensity radar absorption, antistatic surface formation[144].

All in all, CP smart textile fabrics development has a crucial role in many commercial areas. These fabrics can be used for EMI shielding e.g. to shield the household appliances, cellular phones, buildings, various electronic gadgets, as well as applications in medical textiles, protective clothing, touch screen displays, flexible fabric keyboards, and sensors for various areas.

4.3. CP in Thermoelectric Materials

Nowadays, most common energy generation comes from fossil fuels[25]. However, there is a lot of development in eco-friendly renewable technologies harvesting energy from natural sources by incorporating sun, wind, waves and etc. Nevertheless, energy harvest from latter natural resources comes with many disadvantages such as time, cost and capacity to efficiently harvest energy from these natural energy sources[146]. Thermoelectric materials are attracting a great deal of attention due to their probability to utilize them for developing environmentally friendly and renewable energy sources to replace

fossil fuels. Consequently, the study of thermoelectric materials e.g., thermoelectric textiles or devices has attracted the scientific community.

Thermoelectric (TE) materials are enabled to convert thermal energy into more useful electrical energy via Seebeck effect[147],[148]. Therefore, by reusing waste heat and thermal energy, TE devices are able to generate electrical power. The combination of polymer elastic and thermoelectric properties seems to be unique for conducting polymers and likely difficult to achieve with inorganic thermoelectric[149] materials. The key point of enhancing TE material performance is independent regulation of their electrical conductivity, Seebeck coefficient, and thermal conductivity[146].

Conducting polymers (CPs) have an intrinsic low thermal conductivity, but they are electrically conducting. They should thus have potentially promising thermoelectric properties. In order to generate electrical power, a thermoelectric material should have the following three properties: a) it should transport the current efficiently, i.e., possess a high electrical conductivity; b) a significant thermo-induced voltage should be produced, i.e., have a high Seebeck coefficient c) low thermal conductivity should be endured, to ensure that a large temperature difference is maintained[150].

CPs display high TE properties close to inorganic materials and are considered to be the next generation TE materials for wearable devices[151]. Thus, CP suitability arises from their intrinsic low thermal conductivity estimated 1–3 orders of magnitude lower than inorganic materials[152], also mechanical and economic advantages including their lightweight, high flexibility and durability, good film formation, low cost-effectiveness and stable performance at near room temperature[153,146].

First strategies of designing thermoelectric materials with high Z factor started with electrically conductive materials of high Seebeck coefficient, in which defects or vacancies were created to lower their thermal conductivity, as in alloys or doped semiconductors, with semiconductors generally displaying higher values of Seebeck coefficient than metals due to the respective band structures[154].

In the past few decades, a large number of CPs have been explored for potential TE materials[155], such as polyacetylene (PA)[156], polyaniline (PANI)[157], polypyrrole (PPy)[158,159], poly(3,4-ethylenedioxythiophene) (PEDOT)[160],[161] and other CPs. The improvement in power factor (S2) of CPs has been considered to be a vital method to improve their TE conversion efficiency, because these CPs have inherent low thermal conductivity near room temperature. Their electrical conductivity can be significantly increased several orders of magnitude for increasing carriers after doping, although

intrinsic CPs exhibit low electrical conductivity, which is ascribed to the fact that the polarons in CPs are generated during the oxidation and reduction.[146,155]

In the future, thermoelectric systems could harness waste heat and/or provide efficient electricity through co-generation. All in all, the key advantage of thermoelectric materials is their flexibility and ability to be applied in a small portable waste heat co-generation device.

CHAPTER 5. ELECTROMAGNETIC WAVE ABSORBING MATERIALS

5.1. Problematics of Electromagnetic Radiation

The growth in the application of various electronic devices has resulted in a new form of pollution[162] – electromagnetic radiation causing electromagnetic interference (EMI). Each electronic device generates an electromagnetic field while in operation. Therefore, mutual interference among different electronic devices can disturb their performance. Thus, regarding to widespread use of electronics, wireless systems, computers, navigation, space technology and other purposes has led to an increase in EMI shielding product development.

EMI consists of many unwanted radiated signals, which can cause severe damage not only to communication systems, electronic equipment performance but also can affect human health[163,164,163]. Moreover, the electromagnetic radiation can form electrostatic charges on devices, which in severe conditions can result in an explosion[165]. Therefore, there is a great need for effective EMI shielding materials to prevent those undesirable effects. Electromagnetic wave absorbing materials of metallic origin are considered the best for any shielding purpose, but conductive polymers are better for practical and cost-effective device fabrication.

5.2. Shielding Effectiveness of Conductive Metal Composites

Metals are outstanding electricity conductors and are able to absorb, reflect and transmit electromagnetic waves. Therefore, metals tend to have a very high degree of EMI shielding effectiveness. Depending on various metal/metal powder employment possibilities, metallized shielding products can be divided by their most common production techniques[166,167,168]:

1. Conductive metal coatings (e.g., use of foil tape with a conductive adhesive);

2. Conductive coatings with conductive filler (e.g., conductive paints)

3. Conductive sputtering coating;

4. Conductive vacuum depositions;

5. Conductive electroless plating;

6. Conductive composite formation (e.g. metallization of textile fabrics).

Conductive metal coating of aluminium/copper foil tape (Al/Cu) with conductive adhesive offers an effective EMI shielded cable assembly without soldering the tape to the braid[169]. While technically acceptable thin metal films performs very poorly in low frequency magnetic field and is difficult to use in irregular shapes[168].

Conductive filler paints utilize silicone, acrylic, polyurethane as suitable matrices for metal particle distribution. They can be applied by conventional coatings: spraying, brushing, dipping, and silk screening otherwise screen printing. Studies reveal that all of the abovementioned metallization techniques result in different conductive composites with various application fields. The conductivity of the coating based on different fillers decreases in the following order: silver, copper, nickel, graphite. These metals are some of the most conductive compounds/fillers that are used for conductive layer/composite formation. The experimental results indicate that different coating materials have different SE, with a thicker coating film having a higher SE.

Graphite coating exhibits surface resistivity ranging from a few Ω to several kΩ/□. In the 10 Ω/□ range it still gives about 20 dB of electromagnetic wave SE, which may be enough in many consumer or industrial applications[170]. Baker et al.[171] reported the EMI SE of stainless steel fibers as conductive fillers in a polymer matrix of acetonitrile-butadiene-styrene. Thus, obtained shielding effectiveness in X-band frequency range was ~11 dB.

Although sputtering is done in a vacuum chamber, the process is completely different from vacuum metallizing. The composition of metal with conductive stuttering coating on the substrate is the same, but in a vacuum metallizing process two more processes occur vaporization and condensation leading to condensed layer composition, which differs from the initial alloy composition[172].

A research of copper electroless plated PET substrate reported[173] the role of surfactant concentration, acid etching, activators and so on in the multistep electroless processes for coating with this technique a polyester fabric. Further, woven fabrics made of metal wire yarns were investigated[174] and their

electromagnetic shielding characteristics were measured. And the measurements obtained in the frequency range of 30 MHz-9.93 GHz for the woven fabric samples have exhibited 25-65 dB SE.

However, metal incorporated composites have certain limitations, heavyweight, prone to corrosion, inflexibility and difficulty in tuning their SE, restrict conductive metal-incorporated materials utilization possibilities. For example, carbon/graphite products suffer from brittleness, aluminium based has low impact resistance, and stainless steel has high density. But one of the main disadvantages of metallic electromagnetic shields is their susceptibility to corrosion[175], which leads to composites drop in efficiency. In some cases the use of two different metals for EMI shielding causes galvanic corrosion which leads to nonlinearity and a decrease in SE of the metallic shields[175]. Also metallic and metal coated materials tend to have particularly high electrical conductivity, therefore they cannot be used as electromagnetic wave absorbers since high conductivity makes them shield by surface reflection[168]. Therefore, there is an area for research of metal-free conductive materials.

5.3. Shielding Effectiveness of Intrinsically Conductive Polymers

Since the discovery of the metallic properties of molecularly doped conjugated polymer polyacetylene[1], there has been a rapid expansion in research and application in the field of conductive polymers. Recent advancements in electromagnetic wave absorbing polymers field make them an eligible material for electromagnetic interference shielding applications. Electromagnetic wave reflection, absorption and transmission are three of the main parameters determinant of EMI shielding practical application. Since electromagnetic wave absorption and transmission rather than reflection can be more important for many applications, electrically conducting polymers can be preferred, because they are capable of reflecting and also absorbing the electromagnetic wavefront and therefore, exhibit has significant advantage over the metallic shielding materials[168].

In order to produce EMI shields, various technological approaches have been extensively considered to modify the electrical conductivity of plain plastics. Therefore we can divide CP into 3 areas of study[25]:

1. Conductive coatings on plastics;
2. Conductive filler compounds;
3. Intrinsically conductive polymers.

Conductive coated plastics and conductive filler compounds are mainly conductive plastics with metal insertions in polymer matrix by powder, into

textile with slim wiring, or by the formation of thin metallic layer. Both aforementioned conductive plastic research areas are already discussed in detail in previous section *5.2*. However, intrinsically conductive polymers possibilities have not yet been addressed.

On the basis of being metal-free substances, conjugated polymers are also low-cost, low-weight, high-strength, easily-fabricated intrinsically conductive plastics with good electrical conductivity and electromagnetic wave reflecting and absorbing properties[176]. Hence the numerous technological applications as active electrode materials in energy storage[177], optoelectronic devices[178], display devices[179], and their application as alternative materials for EMI shielding[167],[180],[169].

Among all extensively studied conducting polymers, polyaniline and polypyrrole are mainly used for EMI shielding purposes. One of the examples is PANI preparation by doping with camphor sulfonic acid in an m-cresol solvent, resulted in intrinsic conductivity of metallic PANI of ~ 10^7 S/cm. Kim[181] and colleagues have demonstrated EMI SE values of 94.11%, 82.27%, 53.94%, 38.75%, and 25.83% at frequencies of 750 MHz, 900 MHz, 1.57 GHz, 2.45 GHz, and 3 GHz, respectively, were obtained from an EMI SE test on the testbed. Kathirgamanathan[182] has described that the 3 mm thick, polyaniline coated nickel (spheres) carbon black (3:1), composite in co-poly(ethylene propylene) host matrix which offers SE > 20 dB in the frequency range 10 KHz–100 MHz is suitable for most shielding applications. While in another study, doped acrylonitrile-butadiene-styrene and PANI composite exhibited 60 dB shielding effectiveness, whereas lower loadings of PANI revealed a SE of ~11 dB at 101 GHz frequency. It is also noteworthy to highlight that SE of the specimen increases with the thickness of the sample. For example, 1.26 mm PANI–PU films exhibit the most promising microwave absorption and EMI shielding characteristics corresponding to the specimens thickness[183].

Polypyrrole textiles can have a wide variety of utilization for military purposes, conductive paint industry and radar absorbing material improvement.

5.4. Split-Ring Resonators in Functional Textiles

Nowadays, a lot of new shielding structures, materials and composites are investigated, developed and commercially available. The fabrication of organic electronic devices on flexible substrates has recently attracted much

attention. One promising trend is the application of organic conductors with tunable properties. The structures and composites containing a variety of conductive polymers are convenient in the application as shielding additive material in fabrics making functional textiles for use in electromagnetic radiation shielding[184] or flexible electronics (wearable electronics) e.g., fabricating radio frequency identification (RFID) antennas.

Significant research and development of conductive textiles have stimulated the fabrication of wearable antennas, exploiting new flexible and conformable smart structures[185].

If the purpose is to develop wearable, responsive and autonomous system, portable antenna is an essential attribute. An antenna can be essential in a few ways. Firstly, a portable antenna allows one to transfer information from the sensors located inside the garment to a control unit or secondly to monitor other preferable electronic parameters. To achieve preferably positive results, wearable antennas have to be lightweight, inexpensive, thin, low maintenance, robust and easily integrated in radio frequency circuits. Specific requirements for wearable antennas consists of planar structures, flexible conductive and dielectric materials[186,187].

Also, RFID textile tags can be a particular antenna solution, for example, in Switzerland Tex Trace is fabricating components for industrial in-house production of woven RFID labels[132]. By integrating RFID into a label fabrication process, one could provide an added function from textile fabric to overall product manufacturing, logistics and sales sectors.

CHAPTER 6. EXPERIMENTAL PART

6.1. Materials and Synthesis Methods

6.1.1. Bacterial Growth Conditions and Biogenic Polymerization

Materials: *Streptomyces* spp. strains MIUG 12p and MIUG 4.88 were chosen from the Microbial Cultures Collection of the Bioaliment (MIUG)[188] in Research Center, Faculty of Food Science and Engineering of 'Dunarea de Jos' University of Galati, Romania. Monomer pyrrole and medium composition components agar, K_2HPO_4, potato flakes, $MgSO_4*7H_2O$, KNO_3, NaCl, $FeSO_4*7H_2O$ were purchased from Sigma-Aldrich, Germany.

First, MIUG 12p and MIUG 4.88 bacterial microorganisms have been cultivated from pure cultures in Petri dishes using Gause's synthetic medium No.1 and incubated at 25 °C temperature for 6 days. The composition of solid

growth medium comprised of: 2.5% agar, 2% potato flakes, 0.05% K_2HPO_4, 0.05% $MgSO_4$ *$7H_2O$, 0.1% KNO_3, 0.05% NaCl, 0.001% $FeSO_4$ $7H_2O$ dissolved in 1000 ml distilled water. The liquid medium had the same components except for agar. Sterilization of both mediums was performed in an autoclave at 121 °C for 20 min.

The biosynthesis of the enzymes entails a submerged fermentation system for the selected strains of *Streptomyces* spp., in a liquid composition, providing intense aeration and mixing of the fermentation broth so that the cells have equal access to nutrients and oxygen during the fermentation. The culture suspension of 5 ml with sterile distilled water was transferred aseptically into 250 ml Erlenmeyer flasks containing 100 ml of liquid growth medium. After inoculation, the flasks were placed on the shaker with a controlled speed of 150 rpm for 10 days at 25 °C temperature. The microorganisms have been multiplying and increasing the turbidity of the culture medium in the specified conditions.

Therefore, after 6 inoculation days, Py monomer was added. In order to estimate the optimum pyrrole concentration used for synthesis, seven 250 ml Erlenmeyer flasks with 100 ml bacterium medium were prepared as described above. After 6 days of inoculation different pyrrole concentrations 10, 20, 30, 40, 60, 80 mM were added into 6 flasks and left in the shaker for 4 more days. In the same conditions, one flask without pyrrole was also analysed as a control example. After 10 days it was evident that the bacteria instigated polymerization exhibited small black particles or biogenic polypyrrole microsphere formation (BPPy).

6.1.2. MPPy Microsphere Bioinspired Microemulsion Polymerization

Materials: monomer pyrrole 98 +% Py = 67.1 g/mol was purchased from Alfa Aesar GmbH & Co KG, Germany. Continuous phase fluorinated oil was obtained from 3M™ Novec™ 7500 Engineered Fluid, Belgium, whilst diamine surfactant D2000 from Huntsman's JEFFAMINE D series products, USA. For phase separation propylene carbonate (PC) (for synthesis) was purchased from Merck, Germany. Polymerization initiator anhydrous iron (III) chloride $FeCl_3$ = 162.2 g/mol > 98.5% was purchased from Carl Roth GmbH + Co.KG, Germany.

Continuous phase solution of fluorinated oil and D2000 surfactant for microemulsion polymerization was bought premade. 0.583 M iron (III) chloride solution and 0.250 M pyrrole mixtures with propylene carbonate were prepared. For $FeCl_3$ preparation, 0.945 g of $FeCl_3$ was dissolved in 7 ml

propylene carbonate and then diluted till 10 ml. 0.250 M pyrrole solution was prepared by mixing 0.173 ml pyrrole with 9.827 g propylene carbonate with vigorous stirring. Freshly prepared solvents were used for syntheses for up to one month. Later solutions were prepared using the same methodology. These solutions were stored in a laboratory fridge at (+2) - (+8) °C at all times and also protected from direct sunlight with a foil wrapping.

Microemulsion polymerization was carried out using a two-phase, droplet-based microfluidics system in a special 'lab on a chip' design. Microfluidic device structure consists of 5 tubular microchannel system with inlet sizes of were 30 μm width and 20 μm high. Microsphere formation was observed with a bright-field inverted microscope (Nikon ECLIPSE Ti series) and "Guppy" camera set. As a separating phase for the iron (III) chloride and pyrrole monomer, a solution of propylene carbonate was used. In order to pump the selected solutions into the microfluidic chip four syringe pumps (Harvard Apparatus, PHD 2000) or equivalent pumps such as those from KD Scientific, Chemyx, Cetoni, New Era were used.

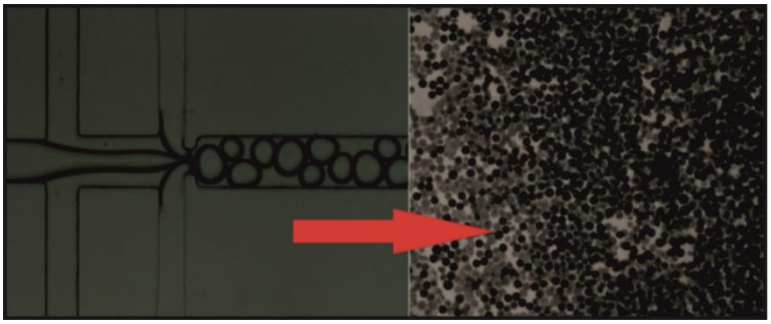

Fig. 5. MPPy microsphere formation using 5 tubular microfluidic system.

In this microfluidic system 2 microchannels were appointed to oil, 2 for pyrrole and PC solution and 1 for oxidant iron (III) chloride solution with PC (Fig. 5). The continuous phase medium chosen for the experiment is fluorinated oil with surfactant. Selected experimental inlet velocities for microfluidic polypyrrole (MPPy) formation were: oil and surfactant D2000 240 μl/h, iron (III) chloride and PC solution 125 μl/h, pyrrole and PC solution 75 μl/h.

6.1.3. Adhesive Matrix Preparation and Conductive Composite Layer Formation

Materials: pyrrole 98 +% and poly (vinyl alcohol) (PVA) 88.000-97.000 g/mol were purchased from Alfa Aesar GmbH & Co KG, Germany. Pyrrole was distilled before use and kept at -18 °C. Anhydrous iron (III) chloride $FeCl_3$ > 98.5% was purchased from Carl Roth GmbH + Co.KG, Germany. Poly (vinyl acetate) average (PVAc) M_w ~500.000 g/mol and poly (vinyl butyral) (PVB) M_w 40.000-70.0000 g/mol were purchased from Merck KGaA, Germany and poly (4-styrene sulfonic acid) (PSSA) 18wt. % aqueous solution, M_w ~75.000 g/mol, was purchased from Sigma-Aldrich Chemie GmbH, Germany. Commercial polyethylene terephthalate (PET) was purchased from 3M Italia S.p.A.

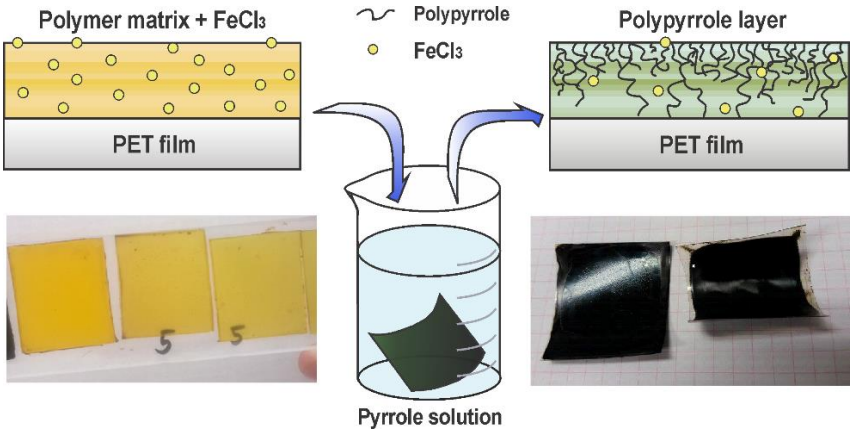

Fig. 6. A schematic image of PPy composite layer formation by *in situ* polymerization in an adhesive polymeric matrix on a PET substrate; before – left and after – right immersion in an aqueous Py monomer solution.

PVA, PVAc, PVB and PSSA were selected for matrix formation as adhesive polymers. 10% PVA 20% $FeCl_3$ adhesive solution was prepared by dissolving 11.4 g PVA in 80 °C aqueous $FeCl_3$ solution (70 g of water contains 22.8 g $FeCl_3$). 17.7% PVAc 19.4% $FeCl_3$ solution was prepared by dissolving 11.4 g PVAc in $FeCl_3$-methanol solution (12.34 ml of methanol contains 3.00 g $FeCl_3$). 20% PVB 10% $FeCl_3$ solution was prepared by dissolving 11.4 g PVB in $FeCl_3$-ethanol solution (17.7 ml of ethanol contains 2.00 g $FeCl_3$ and one drop of HCl). 20% PSSA 40% $FeCl_3$ solution was prepared by rotational evaporating 18% PSSA aqueous solution until 43% PSSA remained. Then 8.25 g of 43% PSSA was added into the $FeCl_3$ aqueous solution (2.15 ml of

water contains 6.94 g $FeCl_3$), thus it produced 20% PSSA 40% $FeCl_3$ solution. The PET substrate base was cut into ~6.3 cm^2 squares. The prepared substrates were cleaned using low pressure plasma treated at 100 power for 3 min in an O_2 environment with a Zepto plasma system (Diener electronic, Plasma – Surface –Technology) device before spin coating. Then 1.5–2 ml of selected adhesive polymer and ferric chloride solution is added on PET substrate and spin coated at 1000 rpm for 1 min. Spin coated polymer matrices were dried in an oven at 70 °C for 30 min.

Pyrrole was purified by distillation under reduced pressure and stored in a refrigerator at 4 °C. PVA-$FeCl_3$, PVAc-$FeCl_3$, PVB-$FeCl_3$ and PSSA-$FeCl_3$ polymeric matrices were spin coated, dried in a laboratory oven and finally immersed in 0.3, 0.5 and 1M aqueous pyrrole solutions. *In situ* radical polymerization in a selected adhesive polymer matrix with entrapped initiator $FeCl_3$, resulted in PPy composite layer formation. The colour of all matrices changed from orange-brown to black, which indicates pyrrole monomer polymerization, thus the presence of polymer PPy within the adhesive polymeric matrix. After the polymerization process, obtained composite layers were washed with distilled water and dried in an oven at 70 °C for 30 min. as shown in Fig. 6.

In order to achieve similar matrix fluidity for all four different matrix compositions, adhesive polymer matrix and radical polymerization initiator $FeCl_3$ quantities slightly vary (Table 1). PVA, PVAc and PVB matrix preparation is similar, despite PSSA where $FeCl_3$ quantity is double compared to other matrices. The difference in density of the aqueous PSSA matrix and 20% $FeCl_3$ solution was visibly noticeable and the formed adhesive composite was brittle and cracked. Since the adhesive PSSA matrix solution was considered too thin, initiator $FeCl_3$ quantity was doubled to achieve the right matrix consistency for spin coating application and prevent a dried matrix layer of cracking. PVA, PVAc, PVB matrices solution quantities were kept more or less in the same ranges, though solvent composition was slightly deviated to improve intrinsic adhesive polymer matrix solubility properties. Spin coating parameters remained the same, although polymer matrix drying parameters and polymerization time alter by taking into account polymeric matrices PVA, PVAc, PVB, PSSA viscosity differences (Table 1).

Table 1. Adhesive polymeric matrix preparation and Py radical polymerization process properties on PET substrate.

Adhesive polymer	Matrix composition			Spin coating parameters, rpm	Drying parameters	Polymerization length, s	Appearance
	Quantity of polymer, %	Quantity of $FeCl_3$, %	Solvent and its quantity, %				
PVA	10	20	H_2O, 70	1 min., ~1000	85 °C, 60 min.	30	Reflective, Flexible, Tend to bend
PVAc	18	19	MetOH, 63		85 °C, 6 min.	60	Matte, Flexible, Flat
PVB	20	10	EtOH, 70 + HCl		50 °C, 15 min.	120	Matte, Flexible, Flat
PSSA	20	40	H_2O, 40		40 °C, 60 min.	10	Reflective Fragile, Loose

6.1.4. PPy Conductive Textile Composite Formation on Various Fabric Substrates

Materials: Wool (88% wool, 12% polyamide) with weight 400 g/m^2 purchased from Velito Presto, Lithuania. Cotton, article: tela voile (100% cotton) with weight 45(+-5%) g/m^2 was purchased from Adalberto Estampados, Portugal. Both 100 % linen purchased from company the 'Linas' and polyester from the textile company 'Audėjas' in Lithuania. Pyrrole monomer, $FeCl_3$ and PVA purchased as mentioned in section *6.1.3. Adhesive Matrix Preparation and Conductive Layer Formation.*

PPy conductive textile composite synthesis technology is very similar to PPy conductive layer formation on a non-conductive surface. *In situ* polymerization process was achieved by submerging or spray coating Py

monomer aqueous solution onto a textile fabric substrate. Four different textile substrates were chosen: linen, wool, cotton and polyester. Specimens were coated with 10% PVA and 20% $FeCl_3$ adhesive mixture (section *6.1.3.*) using flatbed screen printing with a particular squared pattern (9 mm x 9 mm, line width 1 mm) and by fully coating the surface. All coated fabrics were dried at condensation temperature 100 °C for 5 min then submerged in 1M Py aqueous solution or spay coated and again dried in a laboratory oven at 100 °C for 5 min. PPy *in situ* polymerization technique was performed on sheets of size 30 x 45 cm, but the measurements of the microwave transmission and reflection from the coated fabric samples 20 x 30 cm were used. Adhesive PVA polymeric matrix was used for $FeCl_3$ catalyst overall distribution throughout the textile fabrics to ensure a strong PPy conductive layer bond to the fabric.

6.1.5. Split-Ring Resonators Formation

Materials: Pyrrole monomer, $FeCl_3$ and PVA purchased, as mentioned in *6.1.3. Adhesive Matrix Preparation and Conductive Layer Formation.* Wool was purchased as mentioned in section *6.1.4.*

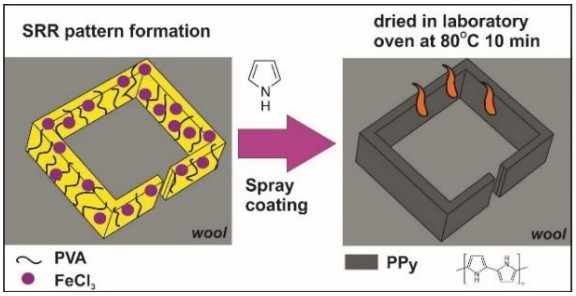

Fig. 7. Split ring resonators formation scheme on wool substrate.

PPy split-ring resonators (SRR) were formed using *in situ* PPy polymerization in polymeric matrix on wool fabric (electrically conductive composite formation). The coating procedure was performed on fabric sheets of size 35 x 25 cm 10% PVA and 20% $FeCl_3$ (section *6.1.3.*) mixture using screen printing with a particular split-ring pattern (17 mm x 17 mm gap 2 mm, width 2 mm) spaced out 8 mm away from each other. SRR pattern was screen printed with several PVA matrix layers. An adhesive polymeric matrix is used for $FeCl_3$ catalyst overall distribution throughout the textile to ensure conductive layers strong bond to the fabric. Coated fabrics were dried at condensation temperature 80 °C for 10 min then spray coated with monomer

Py aqueous solution and again dried in laboratory oven as shown in Fig. 7. Experimental investigations have been performed in far-field area 2-20 GHz frequency range using a semi-anechoic chamber.

6.1.6. Textile Composite Synthesis on Natural Fabric

6.1.6.1. PPy *in situ* Polymerization Process when Dopant is in Monomer Solution on Wool Substrate

Materials: Woven wool fabric 100%, weight 123 g/m^2, warp 31.0 x 2S twisted, weft 31.0 x 1Z single, fabric code: 10078 was obtained from Drobė CO, Lithuania. Anionic surfactants or dopants sodium dodecylbenzene sulfonate (DBS) technical grade and dioctyl sulfosuccinate sodium salt (DOSS) > 97% were purchased from Sigma-Aldrich Chemie GmbH, Germany. Pyrrole monomer, $FeCl_3$, PVA, PSSA and PET purchased as mentioned in *6.1.3. Adhesive Matrix Preparation and Conductive Layer Formation.*

During the production of 20% $FeCl_3$ and 10% PVA (2.33: 1, $FeCl_3$: Py) adhesive matrix, distilled water and oxidant $FeCl_3$ was added to a continuously stirred beaker. Then portions of PVA granules are poured into the solution and heated to 80 °C (section *6.1.3.*). The solution was stirred until became homogeneous. The resulting brown solution (adhesive matrix) is stored in a dark container, protected from moisture and light. PVA adhesive matrix is coated onto the woven wool surface through a specific screen printing template (3 cm x 3 cm square image). Screen printing technique helps for even adhesive matrix distribution throughout the fabric. Woven wool fabrics coated with a (PVA+$FeCl_3$) adhesive matrix are then dried in a laboratory oven at 60 °C temperature for 1h. Since our substrate is a nylon 6,6 fabric, adhesive matrix has a tendency to soak the fabric and mesh with the textiles yarns, which result in PA/PVA composite formation.

Anionic surfactants PSSA[189], SDS[190], DBS[191] and DOSS[192] were chosen and optimal concentrations considered (Table 2), which were selected as a starting point for preparation of an aqueous solution of dopant reagent in 1 M Py solution. Three different molar concentrations were used for each dopant. An aqueous solution of dopant in pyrrole and dopant solution is prepared by mixing already prepared 1M Py solution with the corresponding dopant (PSSA, SDS, DBS, DOSS) concentrations in an appropriate amount of distilled water until the solution is homogeneous.

Pyrrole polymerization process on a woven wool fabric/PVA composite is performed by spray coating 1 M Py monomeric solution with corresponding dopant concentrations on a woven wool textile substrate. The polymerization takes place for ~3 min till PVA adhesive matrix surface turns black. Then PPy composites are washed with a large quantity of distilled water and dried in a laboratory oven at 60 °C temperature for 1h.

6.1.6.2. PPy *in situ* Polymerization Process when Dopant is in Adhesive Polymer Matrix on Wool Substrate

Aforementioned anionic compounds (section *6.1.6.1.*) are also used in PPy *in situ* polymerization process when dopant is embedded into polymer matrix and later penetrated onto a woven wool substrate. The preparation of 20% $FeCl_3$ and 10% PVA adhesive matrix was performed as discussed in section previous section *6.1.6.1.* Latter appropriate amounts of PSSA, SDS, DBS, DOSS dopant is then mixed in an adhesive polymer matrix with various molar concentrations (Table 2) whilst homogenised solution is obtained. The resulting PVA adhesive matrices containing anionic dopants are stored in a dark place protected from moisture. Further, PVA/dopant adhesive solutions are then coated on a woven wool substrate through a screen printing template, dried at 60 °C temperature for 1h. Lastly, PPy *in situ* polymerization process is implemented by spray coating 1 M Py monomer solution onto the dried woven wool fabric/PVA/dopant substrates as described above, resulting in woven wool/PPy composite.

6.1.6.3. PPy/Dopant Composite Sample Preparation for FT-IR analysis

PET substrates were prepared for spin coating. PET substrates with a radius of 1.5 cm. then put into plasma chamber and cleaned with O_2 plasma, to increase the adhesion of the polymeric adhesive matrix and the PET substrate. spin coating technique is used to evenly spread the adhesive matrix on PET substrates by. PET substrates are coated with the desired amount of 10% PVA/20% $FeCl_3$ matrix that has been prepared in section *6.1.6.1.*

PET substrates coated with an adhesive matrix are dried in a laboratory oven at 60 °C temperature. Then Py polymerization process is carried out according to *6.1.6.1* and *6.1.6.2.* methodologies. To investigate chemical and physical characteristics of doped PVA/PPy layers on PET substrate.

Table 2. Spin coating parameters on PET substrates.

Matrix Composition	Dopant concentration, M	A spin coating rate, rpm	A spinning time, s	B spin coating rate, rpm	B spinning time, s
$FeCl_3$ 2.33 M, PVA 10 %	control	1000	10	1300	30
PSSA, $FeCl_3$ 2.33 M, PVA 10 %	0.071			1300	
	0.143				
	0.286			1500	
SDS, $FeCl_3$ 2.33 M, PVA 10 %	0.084			1300	
	0.168				
	0.336			1500	
DBS, $FeCl_3$ 2.33 M, PVA 10 %	0.083			1300	
	0.167				
	0.333			1500	
DOSS, $FeCl_3$ 2.33 M, PVA 10 %	0.094			1300	
	0.188				
	0.375			2000	40

6.1.7. Textile Composite Synthesis on Synthetic Fabric

Materials: Cordura 100% polyamide fabric containing in the warp and weft directions textured 56 tex Nylon 6,6 yarn and 213 g/m^2 surface density was obtained from Invista. In this study employed multiwalled carbon nanotubes (MWCNT) with parameters: NC7000 series (AQ0302) with an average diameter of 9.5 nm and length 1.5 μm; surface area 250−300 m^2 g^{-1}; containing 90% carbon purity, were purchased from Nanocyl S.A., Belgium in the form of water dispersion of 3 wt.% of MWCNT containing anionic surfactant. The MWCNTs were used as received, without any chemical modification. Anionic surfactants SDS., PSSA, DBS, DBS and other materials purchased, as mentioned in section *6.1.6.1. PPy in situ Polymerization Process when Dopant is in Monomer Solution on Wool Substrate.*

Five different anionic dopants were chosen for PPy composite fabrication on synthetic nylon 6,6 fabric: PSSA, SDS, DBS, DOSS and 3% aqueous

solution of MWCNT. Nylon 6,6/PPy/dopant composites were synthesized in variation of dopant incorporation: a) in adhesive PVA and $FeCl_3$ matrix, and b) in aqueous monomer pyrrole solution.

Firstly, for a) synthesis an adhesive PVA and $FeCl_3$ matrix solution was prepared with each dopant accordingly PSSA, SDS, DBS, DOSS and MWCNT. In order to embed dopant into an adhesive polymeric matrix $FeCl_3$ solution must be fabricated. An aqueous 20% oxidant solution was prepared by dissolving $FeCl_3$ in distilled water. Then prepared solution is left to cool till it reaches room temperature. Afterwards each anionic dopant of 0.286 M PSSA, 0.336 M SDS, 0.333 M DBS and 0.375 M DOSS is gradually dissolved in different beaker with 20 ml of $FeCl_3$ solution until it becomes homogeneous. Then 10% PVA homogeneous adhesive solutions were prepared by dissolving PVA granules in aforementioned $FeCl_3$ and aqueous dopant solutions at 80 °C with vigorous stirring for 3-4 hours. PVA adhesive polymeric matrix is used for initiator $FeCl_3$and dopant overall distribution throughout the textile fabric to ensure conductive PPy layer strong physical bond to the fabric. Unlike other dopants, MWCNT was already a 3% water dispersion, so it was chosen to use 5.1 g of 3% MWCNT solution in both a) and b) synthesis, which corresponds to 153 mg carbon nanotubes for each sample. All prepared solutions were cooled till they reached room temperature.

Doped PPy composite formation was achieved by patented *in situ* polymerization process on nylon 6,6 fabrics as a dielectric substrate. Firstly, substrate was activated with oxygen plasma because of nylon 6,6 fabric hydrophobic characteristics. PVA/dopant matrix was transferred onto the textile substrate via a screen printing technique with a particular 20 cm x 30 cm to thoroughly coat the entire active surface.

Coated specimens were dried in a laboratory oven at 100 °C for 5 to 10 minutes, spray coated with 15 ml of 1M Py monomer aqueous solution and after quick polymerization reaction dried again, respectively.

Nylon 6,6 fabric /PPy/dopant composites were also synthesized by synthesis b) when aforementioned dopants are incorporated into Py aqueous monomer solution. As previously discussed in section *6.1.3.* the 10% PVA/ 20% $FeCl_3$ adhesive solution was prepared and transferred onto O_2 plasma activated nylon 6,6 fabric surface with screen printing technique and particular 20 cm x 30 pattern. All nylon 6,6 fabric /PVA composites were dried in a laboratory oven at 100 °C for 5 to 10 min. Py/dopant solutions were prepared with each dopant in 15 ml 1M Py solution accordingly 0.286 M PSSA, 0.336

M SDS, 0.333 M DBS, 0.375 M DOSS with vigorous stirring until the solution becomes homogeneous.

6.2. Materials Characterization

6.2.1. FT-IR Analysis

Fourier transform infrared (FT-IR) spectra were recorded on a PERKIN-ELMER Frontier infrared spectrometer using the UATR (Universal Attenuated Total Reflectance) solid sample analysis supplement. Scanning parameters: spectral range 550-4000 cm^{-1}, 25 scans, 1 cm^{-1} resolution.

6.2.2. XPS Measurements

XPS measurements were carried out to obtain information about the elemental chemical states and surface composition considered samples on the upgraded Vacuum Generator (VG) ESCALAB MKII spectrometer fitted with a XR4 twin anode. All spectra were recorded at a 90° take-off angle a calibrated from the hydrocarbon contamination using the C1s peak at 284.6 eV. The non-monochromatized MgKα X-ray source was operated at hν = 1253.6 eV with 300 W power (20 mA/15 kV). The spectra were acquired with electron analyser pass energy of 20 eV for narrow scans and resolution of 0.05 eV and with pass energy of 1000 eV for survey spectra while chamber pressure was lower than 5×10^{-7} Pa during spectral acquisition. Samples core level peaks were analysed using a nonlinear Shirley-type background. The calculation of the elemental composition was performed on the basis of Scofield's relative sensitivity factors.

6.2.3. FIB-SEM Characterization

Specimens were prepared by depositing a few nanometres of thin chromium film atop. Composites morphology and thickness were examined by dual beam system Focused Ion Beam Scanning Electron Microscope, "Helios NanoLab 650 "with Ga^{+} ion beam gun.

6.2.4. Contactless EMI Measurements in Rectangular Waveguides

Samples microwave properties in the frequency range 8–38 GHz were measured using contactless rectangular waveguide technique. Four analogue waveguide type scalar network analysers, connected to data acquisition system were used:

- P2-54 for X band measurements (8.2 GHz–12.4 GHz);
- P2-67 for Ku band measurements (12 GHz–18 GHz);
- P2-66 for K band measurements (18 GHz–26 GHz);
- P2-65 for Ka band measurements (26 GHz–37 GHz);

With waveguide window size 23×10 mm^2 (WR-90), 16×8 mm^2 (WR-62), 11×5.5 mm^2 (WR-42), and 7.2×3.4 mm^2 (WR-28) respectively. Specimen under test was inserted between two waveguide flanges connected to directional couplers with detectors measuring incident, reflected and transmitted power using scalar network analyser. Four different analysers were used for different cross section waveguides. From the measured signals reflectance R, transmittance T, and absorbance A coefficients were determined and stored in computer. Measurement results were further processed allowing to determine shielding effectiveness (SE) of the investigated composite at a normal incidence of electromagnetic wave and its surface conductivity σ (Fig. 1). The scattering problem of TE_{10} mode electromagnetic wave propagating in the rectangular waveguide divided into two parts by thin conductive layer and covering waveguide window was solved in[193]. Accounting the conductive layer as a boundary condition for the transverse component of the magnetic field experiencing a break proportional to the surface current in the layer, the following expressions for reflection *r* and transmission *t* coefficients were obtained[193]:

$$r = -\frac{\sigma\eta_O}{\sigma\eta_O + 2D} \quad (1)$$

$$t = -\frac{2D}{2D + \sigma\eta_O} \quad (2)$$

Here σ is a surface conductivity of the layer, measured in Siemens per square (S/□) η_0 = 376.73 Ω is the impedance of free space, *D* is a multiplier accounting for the dispersion of electromagnetic wave in a rectangular waveguide (3), f denotes a frequency of microwave, and f_c is a cut-off

frequency of TE_{10} mode in a waveguide. It should be noted that dispersion effect did not always accounted for when determining shielding effectiveness of the samples inserted into the rectangular waveguide[194].

$$D = \sqrt{1 - \left(\frac{f_c}{f}\right)^2} \tag{3}$$

As one can see from (1) and (2), due to wave dispersion the both coefficients become frequency dependent even if the surface conductivity is independent of *f*. The dispersion in the waveguide can be intuitively understood considering a TE-polarized uniform plane wave propagating through the waveguide at an angle and for this reason reflecting back and forth between the narrow walls of it[195]. Therefore, changing the frequency, the incident angle changes resulting in the dependence of r and t on frequency. In the limit $f >> fc$, $D = 1$ and the wave falls perpendicularly to the conductive layer inserted into waveguide. Reflection and transmission coefficients for this case read as:

$$r_0 = -\frac{\sigma\eta_O}{\sigma\eta_O + 2} \tag{4}$$

$$t_0 = \frac{2}{2 + \sigma\eta_O} \tag{5}$$

Eliminating from (1), (4) and (2), (5) $\sigma\eta_0$ one can get relations which bind the reflectance ($R_0 = r_0^2$) and transmittance ($T_0 = t_0^2$) coefficients at a normal fall of wave with corresponding coefficients measured in a waveguide ($R = r^2$, $T = t^2$):

$$R_0 = \frac{RD^2}{\left(1 + \sqrt{R(1-D)}\right)^2} \tag{6}$$

$$T_0 = \frac{T}{\left(D + \sqrt{T(1-D)}\right)^2} \tag{7}$$

We used (6) and (7) to determine R_0 and T_0 from experimentally measured *R* and *T*. If T_0 is known the important layer characteristic – shielding effectiveness – can be determined as an inverse of transmittance in dB scale at a normal incidence of electromagnetic wave:

$$SE\ [dB] = 10 \log \frac{1}{T_0} \tag{8}$$

The surface conductivity σ can be easily calculated from squared expressions (4) and (5) determining the dependence of reflectance and transmittance on layer surface conductivity at a normal incidence of electromagnetic wave on the layer under test:

$$\sigma^{(r)} = \frac{2\sqrt{R_0}}{\eta_0\left(1-\sqrt{R_0}\right)} \tag{9}$$

$$\sigma^{(t)} = \frac{2}{\eta_0}\left(\frac{1}{\sqrt{T_0}} - 1\right) \tag{10}$$

where the superscripts (*t*) and (*r)* represents the surface, conductivity calculated from the measurements of transmittance and reflectance, respectively.

6.2.5. Contactless EM SE Measurements in Anechoic Chamber

Experimental investigations of textile composite samples were performed in an anechoic chamber. Dimensions of the chamber are 8.4 m × 4.6 m × 3.7 m. Electromagnetic signal was generated using PSG Analog Signal Generator (E8257D) 250 kHz-40 GHz. The setup of the measurements is shown schematically in Fig. 8. Experimental data was collected over the frequency range from 2 to 20 GHz. Measurements were performed using a set of A-infoMW 10180-NF model broadband horn antennas.

A tunable microwave generator was used as a microwave source. The transmitted power was measured using averaging power sensors. The power meter was connected to the receiving horn antenna using a waveguide to coaxial adapter. The measured transmitted power P_t with a specimen under test was normalized by the power P_{t0} measured in its absence. Therefore, the SE can be expressed in the following way:

$$\mathrm{SE} = 10\log\left(\frac{P_{t0}}{P_t}\right) \tag{11}$$

In the anechoic chamber a specimen under measurement is surrounded by absorber sheets to prevent the diffracted wave from getting directly to the receiving antenna. Whereas transmitting antenna was placed 300 cm in front of the sample, while the receiving antenna was placed approximately 100 cm behind the sample. To assure that the receiving antenna would be in the absorber shadow region, it was situated closer to the absorber panel.

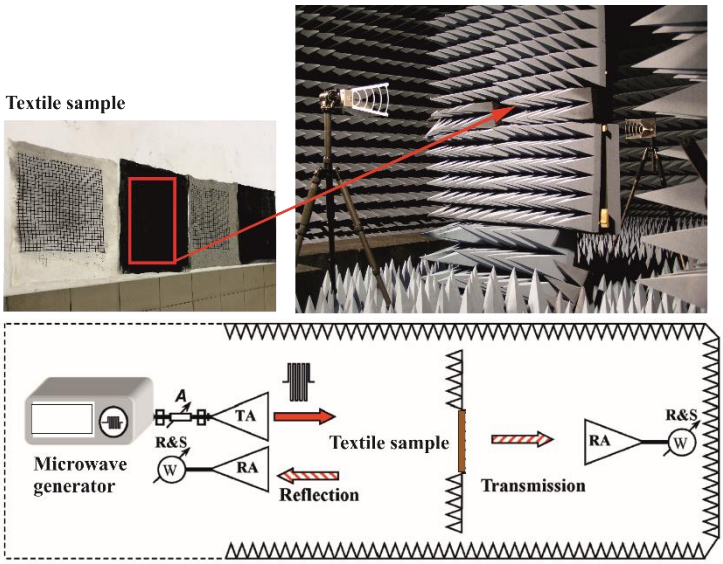

Fig. 8. Measurement setup of the microwave transmission and reflection from the textile sample. TA denotes the transmitting antenna and RA denotes the receiving antennas[196].

6.2.6. Four-Point Probe Resistivity Measurements

The test is performed by the 4-contact method, Aim TTi 1908P 5.5 precision multimeter. For the measurements, the samples are prepared by applying silver paste contacts and drying in an oven at 50 °C.

6.2.7. Surface Resistivity Measurements

Surface resistivity was measured according to standard EN1149-1 (2006), with Terra-Ohm-Meter 6206 (produced by 'Eltex') applying voltage of 10 V (for conductive textiles) and 100 V (for control fabric). Specimens were cut of size between the overall dimensions of the electrodes and of the base plate from the material designed. Specimens were pressed with the load of about 10 N between an assembly of cylindrical and annular electrode arranged concentrically with each other and base plate, on which the specimen was placed in Fig. 10. The diameter of electrode used is 100 mm. The range of measured values is 103–1014 Ω. The conditioning is for 24 h and tests were carried out in dry conditions – air temperature (23± 1) °C, relative humidity (25 ± 5) %, as indicated in the standard used. The assembly of stainless-steel

electrodes, used in measurement of resistances, is presented in Fig. 9. The measuring circuit of electrodes during measurements of resistance is presented in Fig. 10.

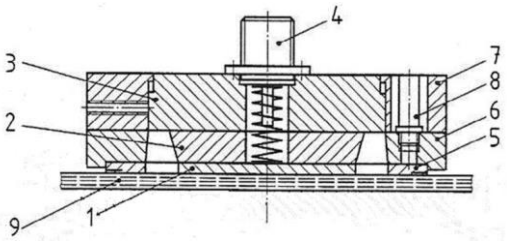

Fig. 9. Assembly of electrodes, where 1 – test electrode, 2 – insulating disc, 3 – guard plate, 4 – coaxial plug-in connection, 5 – annular electrode, 6 – insulating ring, 7 – screening ring, 8 – connector, 9 – sample.

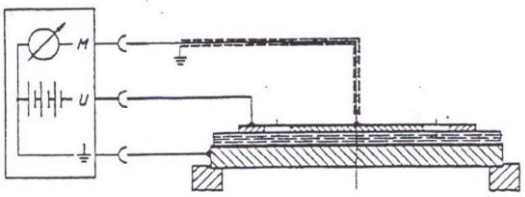

Fig 10. Measuring circuit of surface resistance measurement.

6.2.8. Electrostatic Shielding Factor and Half Decay Time

Electrostatic shielding factor and half decay time were determined according to EN 1149-3, 2nd method (induction charging) in dry conditions – air temperature (23± 1) °C, relative humidity (25 ± 5) %[197]. These parameters were taken with the electric charge metre ICM-1, produced by STFI. Immediately under the test material, which is horizontally arranged, a field-electrode is positioned, without contacting the specimen and a high voltage of (1200 ± 50) V is rapidly (rise time of applied voltage 0.2 V/ms) applied to the field-electrode during the measurement. The instrument is controlled by a microprocessor and makes automatic calculations according to equation (12) and displays the measured data. Arrangement of equipment ICM-1 for induction charging test method is presented in Fig 11.

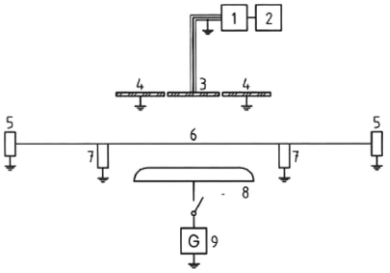

Fig. 11. Arrangement of electric charge metre ICM-1, where 1 – charge amplifier, 2 – recording device, 3 – field measuring device, 4 – guard ring, 5 – specimen clamping ring, 6 – test specimen, 7 – support ring, 8 – field-electrode, 9 – voltage generator.

The value of the shielding factor (*Sf*) is obtained by equation:

$$Sf = 1 - \frac{E_R}{E_{max}} \tag{12}$$

where E_R is the maximum electric field strength indicated on the recording device with the test specimen in the measuring position, and E_{max} is the electric field strength indicated on the recording device with no test specimen present. The half decay time is the time taken for the indicated field strength to decay to $E_{max}/2$.

6.2.9. FLIR Thermoelectric Characterization in Anechoic Chamber

Specimens ability to absorb electromagnetic waves and convert them into thermal energy was measured in an anechoic chamber, in a free space. When collecting data for thermal imaging, Analog signal generator Agilent E8257D was used for generating microwave source signal in the operating field and then was amplified with ETM 2 kW Electromatic incorporated Pulsed SC-Band TWT Amplifier. Aforementioned amplifier was used for reinforcing irradiation intensity to the selected samples with 4.0 GHz strength wave. Transmitting S band antenna was placed 100 cm in front of the sample. Thermal shift in the specimens were recorded with 'InfraCAM, FLIR systems' thermal imager. Electromagnetic irradiation was applied with to the samples

for 60 s and response data is registered every 5 s. After EM irradiation process specimens are left to cool for 100 s and cooling time is registered every 10 s.

RESULTS

CHAPTER 7. BIOGENIC POLYMERIZATION PROCESS FOR BPPY MICROSPHERE FABRICATION

7.1. BPPy Microsphere Optical Microscopy Analysis

Optical microscopy (OM) was the primary analysis tool in the morphological investigations for obtained microsphere samples. Initially, it was used to determine the size, shape and vitality of the bacterial colonies formed in the fermentation medium of *Streptomyces* spp. strains. Subsequently, after the addition of pyrrole monomer, the morphological characteristics of BPPy microspheres were also analysed. Therefore, OM analysis was used in order to provide evidence of polypyrrole microsphere formation in the bacterial medium. The images depicted in Fig. 12 shows the black compact microspheres ranging from 10 to 25 μm in diameter.

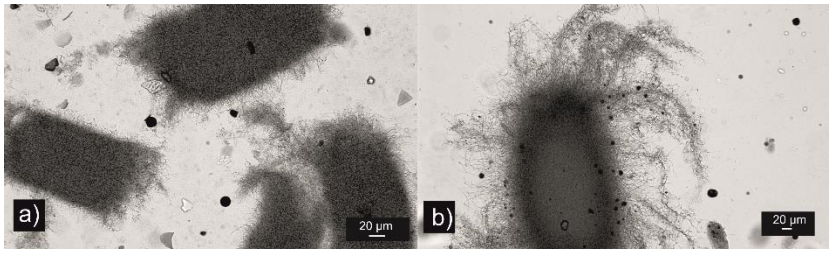

Fig. 12. Optical microscopy images of BPPy microspheres obtained in *Streptomyces* spp. bacterial medium: a) MIUG 12p strain; b) MIUG 4.88 strain.

In order for BPPy microsphere formation, Py monomer was added into the bacterial medium after six days since the initial inoculation process. The optical analysis was performed after two days when polymerization product appears visible in the flask. In each of the samples, optical images revealed black BPPy microspheres. However, while the BPPy microspheres were formed in the MIUG 12p (Fig. 12 a) based medium appeared round in size with 20 μm diameter. On the other hand, BPPy microspheres formed in MIUG 4.88 based medium (Fig. 12 b) were estimated smaller in size. Additionally,

the concentration of BPPy microspheres formed in MIUG 12p medium is 8 times lower with average of 24 microspheres in 1 ml in contrast to the microspheres in the MIUG 4.88 medium with an average of ~188 pcs./µl.

7.2. BPPy Microsphere FIB-SEM Analysis

The FIB-SEM technology was used to increase the accuracy of the analysis because it allows a better resolution and an improved perspective of the cross-section interior of the BPPy microspheres. Scanning electron micrographs of the BPPy samples are depicted in Fig. 13. BPPy microspheres obtained in the fermentation medium of the strain MIUG 12p are about 20 µm in size and prove a dense structure. The concentration of BPPy microspheres obtained in the fermentation medium of strain MIUG 4.88 twice higher but mostly smaller in size what is in agreement with previously presented SEM images. Their structure is not as resistant as one of microspheres formed in MIUG 12p medium, their top bends under the action of vacuum used in the SEM analysis. The inside view though indicates some sort of substance trapped in the middle of the BPPy microspheres.

FIB-SEM microscopy has provided interesting information giving further insight into the morphological and compositional properties of the BPPy microspheres. This microscope has a dual beam that was used to scan the area of interest at low magnification and subsequently zoom in for further analysis on an ultrastructural level, rendering valuable and detailed three-dimensional information of the BPPy microspheres.

Moreover, the ion beam has the ability to cross-section obtained polypyrrole microspheres and therefore revealed that oval shape resistance of the BPPy microspheres is better if they are formed in MIUG 12p than in MIUG 4.88 fermentation medium. MIUG 12p medium microspheres have a more compact and dense morphological structure. The reason for that could be the possibility of more rapid and intense monomer polymerization with MIUG 12p bacteria strain, which gives time for a polymer to grow denser. Also, FIB-SEM analysis of bio-instigated polymerization process resulted in hollow BPPy microsphere formation without any template, unlike generally discussed PPy microsphere formation methods[198].

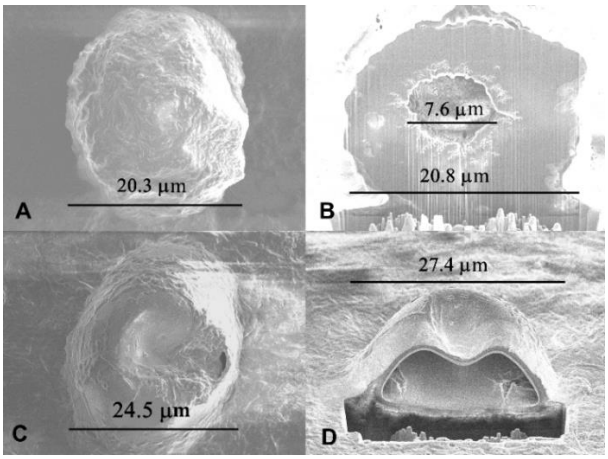

Fig. 13. PPy microspheres FIB-SEM images obtained after Py incubation in *Streptomyces* spp. bacterial medium: A, B – MIUG 12p; C, D – MIUG 4.88 strain. A, C – top view; B, D – cross section, at view angle of 53°.

7.3. BPPy, and EPPy FT-IR Comparison

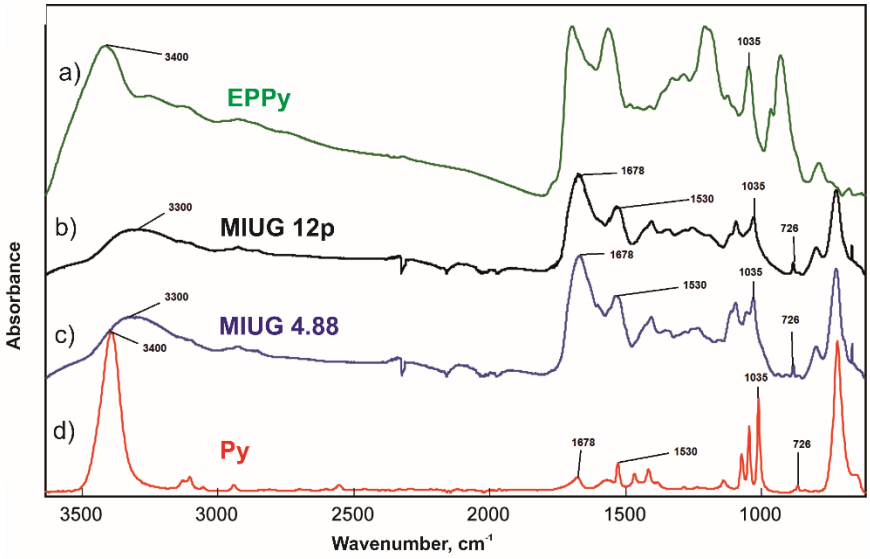

Fig. 14. FT-IR spectrum of polypyrrole synthesized: a) electrochemically; b) MIUG 12p strain; c) MIUG 4.88 strain; d) pyrrole monomer.

FT-IR spectrums of pure pyrrole, bacteria synthesized polypyrrole (BPPy) and electrochemically-synthesized polypyrrole (EPPy) were obtained (section *6.2.1.*). Wet samples for analysis were lyophilized and FT-IR spectrums were

obtained. The FT-IR absorption spectrums of Py, BPPy and EPPy shown in Fig. 14 exhibited characteristic vibration bands at 1530 cm^{-1} for pyrrole ring stretching at C=C band. Wide peaks at 3300 cm^{-1} and 3400 cm^{-1} is attributed to pyrrole ring N-H stretch vibrations. Intense peak at 1678 cm^{-1} is assigned for the stretching vibration of the acetate C=O group which could occur due to enzymes. Peaks between 1450 and 1300 cm^{-1} occurs due to C-C and C-N conjugated stretching. Other peak, which is common for polypyrrole spectrums at 1236 cm^{-1}, is attributed to C-N in plane deformation[199]. Furthermore, peaks at 1035 cm^{-1} and 726 cm^{-1} are due to N-H wagging vibrations. FT-IR was used to identify chemical bonds in microspheres by producing an infrared absorption spectrum[200]. Both spectrums of BPPy that were obtained from biogenic synthesis using *Streptomyces* spp. bacteria strains and spectrum that was obtained from electrochemically synthesized EPPy exhibited characteristic peaks of polypyrrole. The shift of peaks in spectrums from BPPy microspheres that was synthesized using bacteria medium could be because of additional products in the synthesis solution, such as starch, and/or presence of bacterial by-products. This fact is concerning and further use of polymer will demand extra steps of BPPy microspheres purification.

7.4. BPPy and EPPy XPS Comparison

Measured photoelectron survey spectra for all investigated compounds are similar and practically don't differ from the spectra of electrodeposited films of polypyrrole[201]. Major survey spectra peaks of C 1s, O 1s, and N 1s were analysed. For all investigated materials in carbon region, C 1s peak can be deconvoluted into three components with binding energies of ~284.6 eV, ~286 eV, and ~288 eV that corresponds to C-C/C-H, C-OH, and $C-N^{+}$[202] chemical bonds. For example, Fig. 15 a presents more detailed C 1s peak fitting result for bacteria synthesized polypyrrole. Likewise, the deconvolution of O 1s peak for BPPy material is presented in Fig. 15 b. Similar fitting results were obtained for Py and EPPy samples. In all cases O 1s peak consists from three components with binding energies at ~531 eV, ~532 eV, and ~533 eV. The interpretation of given experimental results become complicated because oxygen ions are not involved into the structure of pyrrole. But its derivatives (such as furan, furfural, porphobilinogen, pyrrole-3-carboxylic acid, and so on) comprised of carbonyl, carboxyl groups, and also N-C/N-C-O bindings[203]. Thus, fitting component with binding energy ~531 eV can be attributed to C-

O carbonyl group[204,205]. Then component with binding energy ~532 eV may be accredited as carboxyl groups because the difference between oxygen ions in oxide O^{2-} and hydroxyl OH^- states binding energies is ~1 eV and bindings between oxygen, carbon and nitrogen[206] (carboxyl/N component in Fig. 15 b). The last fitting component with binding energy ~533 eV corresponds to oxygen ions in water molecules[207] (Fig. 15 b). It must be pointed out that a similar approach was applied in Frateur work[208], setting up the chemical bonds of oxygen O 1s peak components.

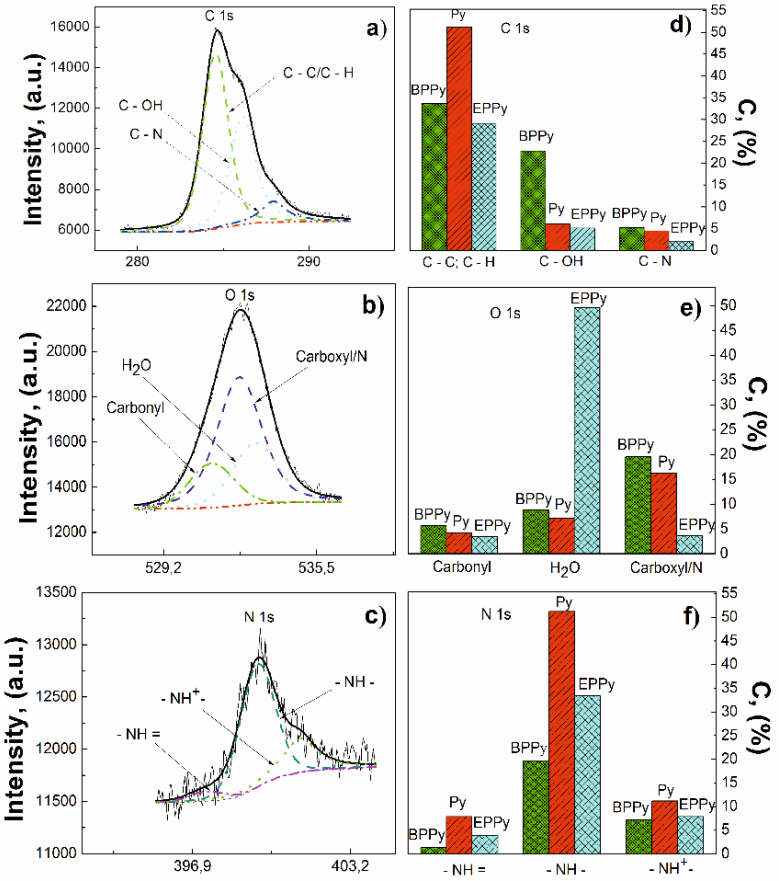

Fig. 15. XPS spectra of bacteria synthesized polypyrrole (BPPy) of: a) C 1s, b) O 1s, c) N 1s histograms of relative concentration of d) carbon e) oxygen and f) nitrogen ions in various chemical bonds of BPPy, Py, EPPy.

For BPPy (Fig. 15 c) as well as for Py and EPPy compounds, N 1s region peak was deconvoluted in three components with binding energies ~398 eV, ~400 eV, and ~401 eV that corresponds to nitrogen in imine state -NH-, amine

nitrogen -NH-[202], and protonated nitrogen -NH^+-[209,210]. The relative concentrations of carbon, nitrogen, and oxygen ions, which are involved in various chemical bonds, are shown in Fig. 15 d, e, and f. The total content of nitrogen in investigated samples is highest for pure pyrrole (Fig. 16, N column) when the distribution of nitrogen ions under their chemical binding is similar for all samples (Fig. 15 f) – the highest concentration of amine group then follows protonated amine and least – for nitrogen ions in imine group. It means that in pure pyrrole (sample Py), the concentration of pyrrole ring is the highest between all used synthesized PPy samples. From results presented in Fig. 15 d follows that the concentration of pyrrole ring in all investigated samples is smaller than the concentration of derivatives of pyrrole, because the concentration of C-N bonds is lower than, the sum of concentrations of C-C/C-H and C-OH bonds. The total carbon concentration (Fig. 16) is fairly large (61.7%, 61.8% and 36.3% for BPPy, Py and EPPy respectively). It may be explained by carbon absorption from environment. The concentrations of carbon, nitrogen, and oxygen ions for all investigated compounds are shown in Fig. 16. The results, which are shown in Fig. 15 a-f and Fig. 16 are calculated from experimentally registered XPS spectra for C 1s, O 1s, and N 1s peaks, and their deconvolution into separate components.

As follows from Fig. 16 results, the chemical formulas of investigated samples may be written as: $C_{0.617}N_{0.043}O_{0.34}$, $C_{0.618}N_{0.107}O_{0.275}$, and $C_{0.363}N_{0.069}O_{0.568}$ for BPPy, Py, and EPPy respectively. The highest concentration of oxygen ions (Fig. 16, O column) is observed for EPPy sample. This fact related with highest concentration of water in EPPy compound (Fig. 16, H_2O column). The appearance of water can be explained in two ways. Firstly, the absorption of water molecules from environment and secondly infiltration of water into the structure of the samples during synthesis process. The amounts of oxygen ions in water molecules in BPPy, Py, and EPPy samples are equal to 8.8%, 7.1%, and 49.7% (Fig. 16, H_2O columns) of total oxygen quantity (total oxygen quantity – 34%, 27.5%, and 56.8% for BPPy, Py, and EPPy samples (Fig. 16). Then the general formulas of BPPy, Py, and EPPy must be written as $C_{0.617}N_{0.043}O_{0.31}$*0.03 H_2O, $C_{0.618}N_{0.107}O_{0.256}$ *0.019 H_2O, and $C_{0.363}N_{0.069}O_{0.286}$*0.282 H_2O, respectively. In this case, the amount of oxygen is approximately equal to 0.3 for all samples. It means that the quantity of pyrrole derivatives is the same for all investigated compounds. In this way, we have to speak about pyrrole as a hydrated compound, which consists of several pyrrole derivatives.

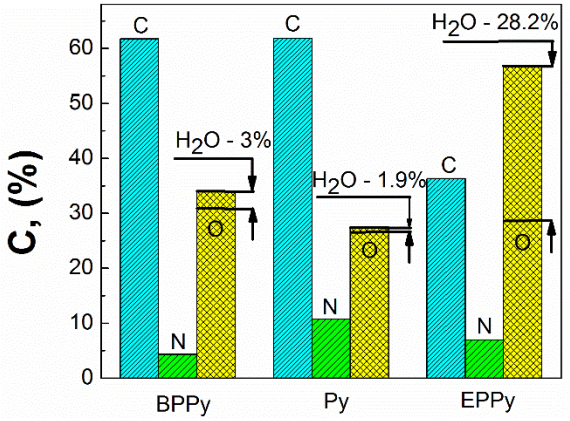

Fig. 16. Histogram of carbon, nitrogen, and oxygen concentrations investigated compounds (BPPy – bacteria synthesized polypyrrole, Py – pure pyrrole, and EPPy – electrochemically synthesized polypyrrole; H_2O – X % – relative concentration of water molecules).

7.5. Discussion of the Main Results

The general aim of this study was to investigate the possibility to polymerize pyrrole monomer using two bacterial strains of *Streptomyces* spp. In this research, the proposed method to polymerize pyrrole is an environmentally friendly route carried out in mild aqueous media and free of oxidation by-products.

Streptomyces spp. bacteria synthesized a novel type of hollow polypyrrole microspheres. Optical microscopy observations revealed that microspheres formed in the bacterial medium was from 10 to 25 μm in diameter. It was found that diameter and interior cross-section of microspheres highly depends from the chosen bacteria strain. Microspheres obtained by strain MIUG 4.88 was smaller in size and not as resistant as the one microspheres formed by MIUG 12p, their top bends under the action of vacuum used in the SEM analysis.

All in all, in this study, we present an innovative biogenic synthesis for hollow BPPy microsphere formation, which could be applied in biotechnology fields: bio-mimetic or EMI shielding materials, drug delivery, molecular electronics, and also in various nanomedicine applications.

CHAPTER 8. BIOINSPIRED POLYMERIZATION PROCESSES FOR POLYPYRROLE MICROSPHERE FABRICATION

8.1. MPPy Microsphere formation in Microfluidic System and Optical Microscope analysis

Polypyrrole microsphere formation was implemented with microemulsion polymerization process using advanced microfluidic system (MS) device. Alternating phase flow speed, substance quantities, arrangement of the microfluidic device or even changing various MS structure designs we can achieve polymeric microsphere formation. Experimental investigations were performed several times to ensure accuracy of the results. After microemulsion polymerization in microfluidic device microspheres were collected from the capillaries to a collection bath and analysed under optical microscope. Overall MPPy microspheres were investigated by OM, SEM, FIB-SEM and FTIR analysis methods.

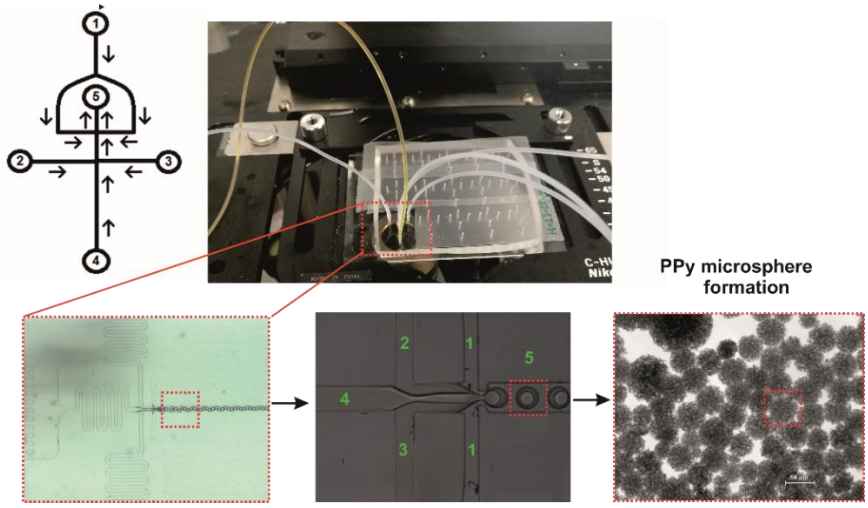

Fig. 17. MPPy microsphere formation scheme in microfluidic system. 1 – fluorinated oil and surfactant D2000 solution, 2 – 3 pyrrole solution with propylene carbonate, 4 – iron (III) chloride in propylene carbonate, 5 – pyrrole microsphere formation microchannel.

PPy microsphere formation in microfluidic system was used as shown in Fig. 17. Microfluidic system was observed by using optical microscope with integrated Guppy F-038B/C camera. 5 microchannels capillary system with filters compile a new design microfluidic system: 1 – fluorinated oil and

surfactant D2000 solution, 2 – 3 pyrrole solution with propylene carbonate, 4 – iron (III) chloride in propylene carbonate, 5 – pyrrole microsphere formation channel. Experiment inlet velocities were chosen in reference to other microemulsion polymerization models[100] were: 1 – 100 μl/h per inlet, 2 – 3 50 μl/h per inlet, 4 – 50 μl/h per inlet (Fig. 17). Microsphere microscopic analysis was performed using optical microscope OLYMPUS BX51 (Japan).

Co-flow drop maker microfluidic device with 4 pumps is used to control the direct solutions flow rate and in which order it is switched, in the microfluidic system. First continuous oil phase and surfactant is released while it fills the microchannels, then pyrrole and propylene carbonate solution and lastly $FeCl_3$ in propylene carbonate solution is released. When all microchannels fill up with solution we observe droplet formation with a high-speed camera and a microscope which are integrated at the end of the microchannel tip. Dripping effect leads to intrinsic Py polymerization in emulsion and MPPy microspheres resulted to be non-isotropic and started agglomerating in the collection bath. Polymerization was too quick, just after 30 s PPy microsphere formation in average size of 45.6 μm, microfluidic system clogs within microchannels where pyrrole solution meets $FeCl_3$ solution and intrinsic polymerization reaction occurs. PPy microsphere various shapes and sizes are represented in Fig 17.

In order to improve the efficiency of MS and also quality and yield of MPPy microspheres, a new type of polymerization scheme has been applied. It was decided to slightly regroup the contact points of the highly reactive solutions in the microfluidic system itself, in order to slow down pyrrole and $FeCl_3$ propylene carbonate solutions polymerization and make them interflow as late as possible into pyrrole monomer droplet in microchannel 5 (Fig. 18 a). A new type of MS solutions inlet rearrangement is shown in Fig. 18 a. The fluorinated oil with D2000 surfactant in this case was transferred to microchannels 2 and 3, whilst Py and propylene carbonate solution was transferred to the site of the previously fluorinated oil (microchannel 1). Oxidative $FeCl_3$ and propylene carbonate solution was left in the same microchannel – 4. As a result, Py and $FeCl_3$ propylene carbonate solutions merged only in the presence of continuous oil phase, and not before, as it was in the case of previous experiment. Such a new mechanism was intended to ensure a prolonged onset and further course of the polymerization reaction, resulting in more uniformly formed MPPy microemulsions as well as MPPy microsphere formation and unclogged microfluidic system. MS phase modification ensured that dispersed phase (Py and $FeCl_3$ in propylene

carbonate) was in the middle of continuous phase droplet (fluorinated oil). In further dissection this rearranged system will be referred as standard reaction.

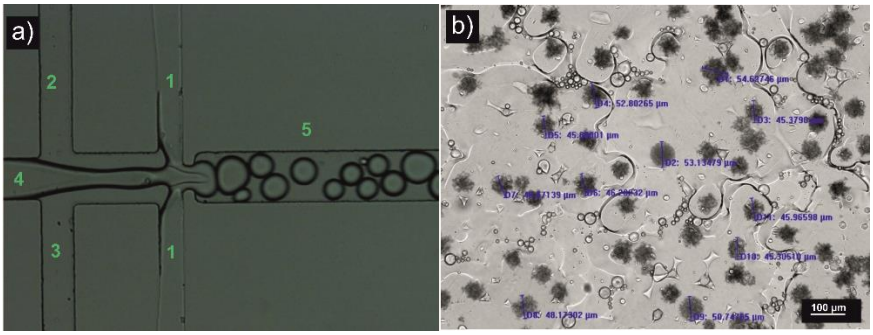

Fig. 18. Microfluidic system standard polymerization scheme. 2, 3 – fluorinated oil and surfactant D2000 solution; 1 – pyrrole solution with propylene carbonate; 4 – iron (III) chloride in propylene carbonate; 5 – polypyrrole microsphere formation microchannel.

During polymerization reaction in microfluidic system, inlet velocities of all liquid media phases were left the same as in previous experiment. After solutions flow rearrangement various shapes and sizes of MPPy microspheres were obtained (Fig. 18 b). MPPy microsphere sizes vary between 45 and 54 µm. Before most of the experiments resulted in microsphere agglomeration and clogged microchannels. Hence the change in phase flow arrangement, almost all PPy microspheres formed singularly and no agglomeration was noticed. However, as can be seen from the examination of optical microscope images (Fig. 18 b), MPPy microspheres were not completely regular in shape. The microspheres had uneven edges and an irregular oval shape. It was decided to try to vary the inlet velocity rates of the reagent solutions to ensure better and more efficient emulsion polymerization process outcome with more orderly and homogeneous microspheres.

In the following experiments, continuous and disperse phase inlet velocities were increased. The arrangement of the liquid media phases was in all cases left the same as in the previous experiment. Three experiments with increased inlet velocities were performed. So due to aforementioned findings inlet velocity rates were increased 1.2 times, the second time – 1.5 times, and the third time – 2 times. Thus, after increasing the rates of the reactive solutions 1.2 times, the inlet velocity rates were: oil – 240 µl/h, Py – 120 µl/h, $FeCl_3$ – 60 µl/h. A comparison images of modified increase in volumetric flow rates for microemulsion polymerization reaction is given in Fig. 19.

After 1.2 times increased emulsion polymerization reaction collected PPy microspheres are shown in Fig. 19 b. The images from the experiment showed that the quality of the polypyrrole microspheres actually improved. More microspheres contained a more regular circular (oval) shape, but some were still either fractured or irregularly polymerized. After microemulsion polymerization PPy microspheres sizes varied between from 26.6 to 50 μm, although on average microspheres formed 33.3 μm size microspheres.

During the next experiment, when inlet velocities were increased even more – up to 1.5 times: oil – 300 μl/h, Py – 150 μl/h, $FeCl_3$ – 75 μl/h. experimental results varying different microspheres sizes reflected in Fig. 19 c. Polypyrrole microspheres appeared to be more constant in uniformity and bigger in size between 46 and 53 μm, but did not obtain smooth sphere surface. Moreover, in time, aforementioned microsphere particles became irregular in shape and appeared more agglomerated than usual. Lastly volumetric flow rates were increased even more – up to 2 times: oil – 400 μl/h, Py – 200 μl/h, $FeCl_3$ – 100 μl/h and resulted microspheres were depicted in Fig.19 d image.

It can be seen from Fig. 19 d image that MPPy microspheres become even more irregular in shape and actually expand. Most of collected microspheres appears to be flat. Microspheres size varies between 34.1 – 63 μm. Furthermore, collected reaction mixture became more agglomerated in the collecting bath within minutes.

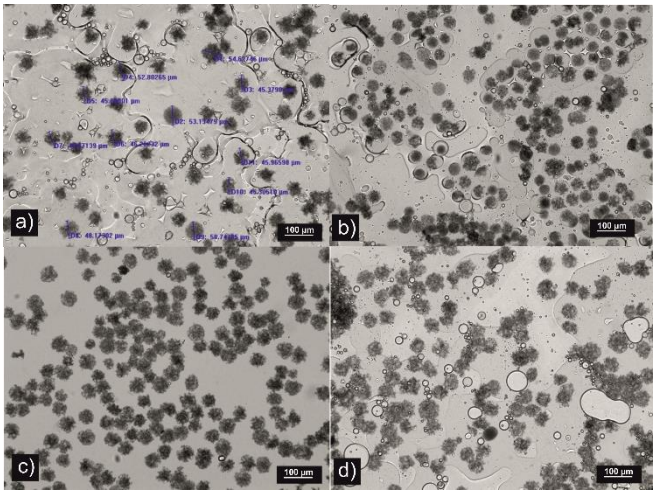

Fig. 19. A comparison of microemulsion reaction mixtures when inlet velocity rates were increased. Liquid phase inlet velocities: a) standard, b) increased 1.2 times, c) increased 1.5 times, d) increased 2 times.

Optical microscopy analysis shows that further increases in inlet velocity rates would only make MPPy microspheres more irregular in shape, flat and over time collected reaction mixture becomes more agglomerated. As inlet velocity flow rates increase microemulsion polymerization tends to be too quick and microspheres do not form anticipated spherical structures, on the contrary forms flat and irregularly spiky MPPy microsphere compositions.

By comparing aforementioned results, it was evident that the most suitable liquid phase inlet velocity rates for the formation of the highest quality MPPy microspheres was achieved by increasing the standard rates by 1.2 times. MPPy microspheres obtained in this experiment were decided to be examined by SEM analysis method which observed collapsed, flat and spiky microspheres Fig. 20 shows the dried microemulsions on a glass substrate when viewed under a scanning electron microscope. After drying MPPy microspheres in 70 °C temperature in a laboratory oven overnight, we observed collapsed, flat and spiky microspheres.

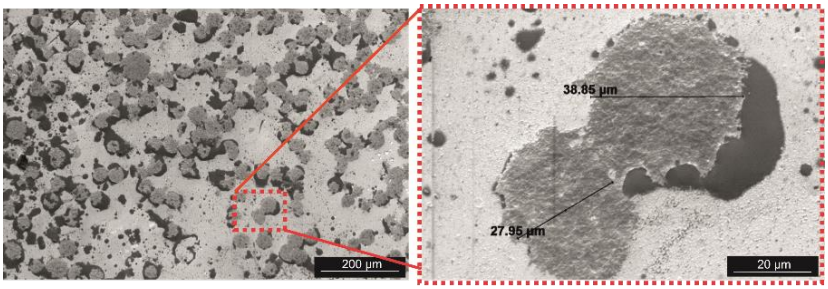

Fig. 20. SEM images of MPPy microspheres after microemulsion polymerization with 1.2 times increased flow rates.

In order to fabricate more homogenous MPPy microspheres the following experiments were performed as flow inlet velocity rates in the MS were reduced. The arrangement of the dispersed and continuous phase positions was left the same in all cases as in the previous experiment. Three experiments with reduced rates of reactive solutions were performed. Firstly, all microfluidic systems inlet velocities were reduced 0.8 times, when – 0.75 times and lastly – 2 times. A complete representation of the inlet velocity rates reduction influence on the PPy microsphere homogeneity, size and overall shape is given in Fig. 21.

After reducing reaction solutions inlet velocity by 0.8 times, the flow rates correspond to: oil – 160 µl/h, Py – 80 µl/h, $FeCl_3$ – 40 µl/h. PPy microspheres obtained from collecting bath reaction mixture is shown in Fig. 21 b. From

experiments with 0.8 times reduced velocity rates reveal that the quality of the MPPy microspheres resulted in almost transparent spheres, meaning slight microsphere deterioration was observed. Generated MPPy microspheres were spiky and in varied in shape and size between 28 and 58.3 μm. It was evident that most of the droplets fractured during polymerization process which resulted in irregular polymerized MPPy microspheres.

In the next experiment, the inlet velocity rates were further reduced 0.75 times: oil – 150 μl/h, Py – 75 μl/h, $FeCl_3$ – 37.5 μl/h. Polypyrrole microemulsion seemed even more irregular Fig. 21 c. MPPy microsphere size was attributed to more or less constant, but almost all of the microemulsions were agglomerated and obtained flat and spiky morphology. During the last experiment the flow of inlet velocity rates were further reduced twice and corresponded to: oil – 100 μl/h, Py – 50 μl/h, $FeCl_3$ – 25 μl/h. The obtained PPy microspheres are completely irregular in shape, has a tendency to collapse and fracture into smaller pieces Fig. 21 d. Over time microemulsion mixture did not agglomerate but also no oval-shaped microspheres were fabricated.

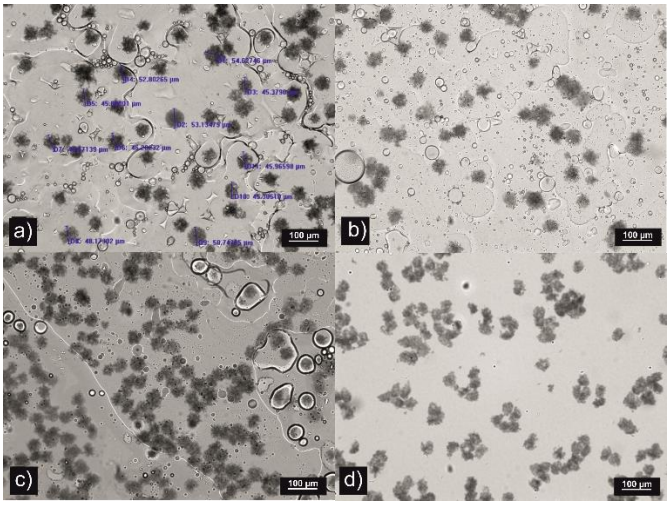

Fig 21. A comparison of microemulsion reaction mixtures when inlet velocity rates were reduced. Images were taken with an optical microscope. Liquid phase inlet velocities: a) standard, b) reduced 0.8 times, c) reduced 0.75 times, d) reduced 0.5 times.

In the following experiments, monomer MPPy, oxidant $FeCl_3$ both in propylene-carbonate and fluorinated oil with 2.5 wt.% D2000 surfactant phase were varied independently of each other. Table 3 shows the sequence of experiments performed in an attempt to find the most appropriate medium

phase inlet velocity ratio for Py polymerization reaction by alternating solutions inlet velocity rates, whilst using rapid and tunable microfluidic mixing system.

In experiment 1.1. the oil phase flow rate was increased without changing velocities of other reactive solutions by 50 μm/h. Obtained microemulsion mixture is shown in Fig. 22 a. MPPy microspheres are more isotropic and maintain a round oval shape with size distribution between 37.5 and 50.5 μm. average MPPy microsphere size is ~41.5 μm. As well as in 1.1 experiment in 1.2 continuous fluorinated oil and surfactant solution was increased to 300 μl/h without dispersed phase alterations. Obtained PPy microsphere quality decreased as a result of accelerated velocity rate. Fig. 22 b image exhibits uneven microsphere distribution where sizes vary from 42.4 to 54.2 μm. Increased fluorinated oil velocity rate most likely prevents efficient droplet formation, therefore MPPy microspheres occur fractured or not fully polymerized. The microemulsions during experiment 1.2 in time were highly agglomerated so it was decided not to further increase the velocity of the oil medium phase. In experiment 1.3, the oil phase velocity rate was reduced to 150 μl/h without changing the rates of other reaction solutions.

Table 3. Experimental solution inlet velocity rates.

Experiment number	**Py solution velocity, μl/h**	**Iron (III) chloride solution velocity, μl/h**	**Fluorinated oil with 2,5 wt.% D2000 surfactant solution velocity, μl/h**
1.1	100	50	250
1.2	100	50	300
1.3	100	50	150
1.4	100	100	250
1.5	50	100	250
1.6	125	75	250
1.7*	125	75	250

*solution inlet velocities stay the same, but MS microchip inlet rearrangement is changed

As a consequence of continuous phase reduction microemulsions were obtained with almost no agglomeration, exhibited oval shape and some of

them were very irregular and spiky Fig. 22 c. MPPy microsphere sizes varied from 36.4 to 54.5 μm. The in experiment 1.4, the inlet velocity rates of $FeCl_3$ and oil were increased to 100 μl/h and 250 μl/h, respectively. The reaction mixture is shown in Fig. 22 d. Generated microemulsions image exhibits agglomerated microspheres which are completely unstable in size and fractured. This was due to the addition of too much oxidant to the reaction mixture which led to an unpredictable and rapid MPPy polymerization process in the droplets. In experiment 1.5, the ratio of pyrrole to $FeCl_3$ solutions was further modified by reducing Py and propylene carbonate inlet velocity rates by 50 μl/h.

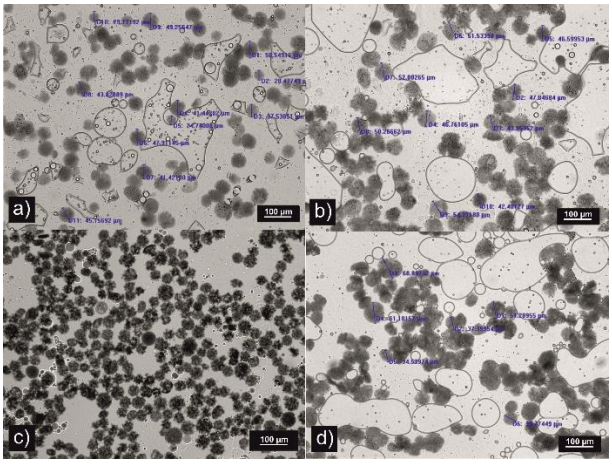

Fig. 22. Polypyrrole microspheres obtained by alternating continuous and dispersed phase inlet velocity rates. Experimental results represent: a) 1.1, b) 1.2, c) 1.3 and d) 1.4 experiment numbers.

The reaction mixture in Fig. 23 a reveal fractured microsphere formation indicating that monomer phase velocity rate was too slow and microemulsions lacked monomer droplet for oval PPy formation. As a consequence, strongly agglomerated microemulsion derivatives of variable size and shape were formed. Some of the produced microspheres were sheer with indistinctive circular shape. The importance of monomer and oxidant velocity ratio is particularly visible from 1.5 experiment since polymerization reaction yield was highly dependent on the appropriate ratio of Py to $FeCl_3$ solutions. Therefore in 1.6 and 1.7 experiments (Fig. 23 b, c) Py monomer and $FeCl_3$ solution velocity rates were enhanced from standard by 25 μl/h each and fluorinated oil continuous phase was left to 250 μl/h. MPPy microspheres

resulted to be more homogenic in shape and their size varied between 25 and 43.5 μm when on average formed about ~33.3 μm circular particles.

In the last 1.7 experiment, it was decided to return to the original scheme when pyrrole solution and fluorinated oil continuous phase where interchanged. Since the optimal volumetric flow rates have already been determined during previous experiments, it was expected that in this case an even better result could be achieved using the original scheme. The original MS scheme used in this experiment is shown in Fig. 17. The reaction mixture is shown in Fig. 23 c. Obtained MPPy microspheres appear to be of a uniform spherical shape and constant size around ~41.5 μm. No agglomeration was observed in the collection bath, although over time MS microchannels eventually became clogged with access MPPy sedimentation.

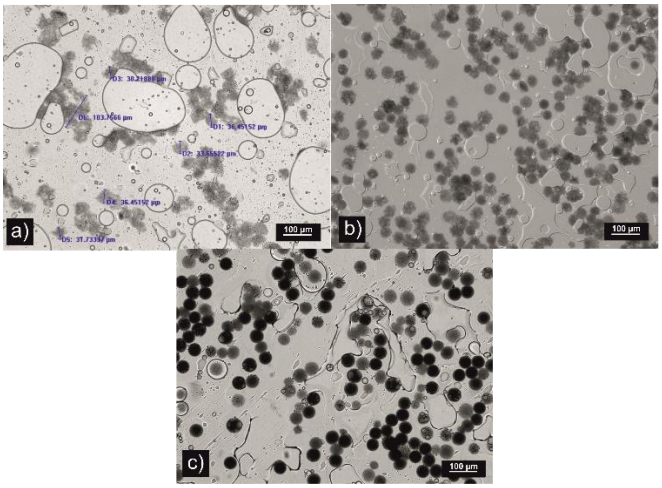

Fig. 23. Polypyrrole microspheres obtained by alternating continuous and dispersed phase inlet velocity rates. Experimental results represent a) 1.5, b) 1.6 and c) 1.7 experiment numbers.

8.2. MPPy Microsphere SEM Analysis

SEM analysis was performed to further investigations of MPPy microsphere surface morphology. As already discussed in previous section *8.1* with 1.2 experiment, more MPPy microsphere examples were analyzed. Firstly, selected emulsions were dried on an optical glass surface and latter sputtered with thin chrome layer. Fig. 24 micrograph shows SEM images of dried three different MPPy microsphere formation results were measured perpendicular to the surface.

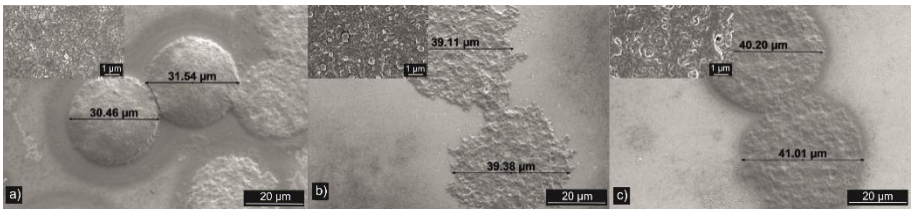

Fig. 24. SEM images of dried a) standard b) 1.4 c) 1.6 MPPy microsphere specimens at 2000 and 25.000 magnifications.

As can be seen from SEM (Fig. 24 a) image standard MPPy microspheres obtained their oval, round shape and were estimated to be around 30.46 – 31.54 µm in diameter. MPPy microspheres contain a circular particle shape even after drying procedure. During drying process, access liquid evaporates from the MPPy microspheres which causes them to fall into a single pile, although still obtaining round particle shape. Also, we can observe that obtained MPPy microsphere surface at higher magnifications is irregular, wavy and reveals a scaly and rough surface morphology without see through any visible pours. However, further FIB-SEM morphological investigations of standard MPPy microemulsions are needed to determine inner particle morphology.

SEM studies were also performed with non-standard polypyrrole microemulsions. SEM micrograph of 1.4 experiment dried microemulsion is shown in Fig. 24 b. Obtained MPPy microsphere do not hold their shape after drying procedure. By comparing 1.4 experiment microspheres Fig. 24 b with two other samples one can observe a collapsed and spiky MPPy surface morphology and obtained microspheres size is around ~39.2 µm in diameter. Also, at higher magnification a porous microsphere surface structure is observed.

Fig. 24 c image depicts particles generated from 1.6 experiment of tuning volumetric flow rates for oval MPPy microsphere formation. Size distribution is constant at 40.5 µm and particle surface contains tight sponge-like structure, whilst compared to the standard MPPy microspheres.

In conclusion an assumption of polypyrrole sponge-like structure formation in microemulsion droplets can be proposed.

8.3. MPPy Microsphere FIB-SEM Analysis

In continuation of MPPy microsphere morphological characterization the next study of polypyrrole microemulsions was performed by FIB-SEM

analysis. This method is very similar to the simple SEM method, although with FIB-SEM to obtain a cross-section view of fixed particle. Only few generated MPPy microspheres were selected for FIB-SEM analysis. Microsphere specimens were prepared in the same way as described in section *8.2.* of SEM study and also adding a narrow and thin layer of platinum.

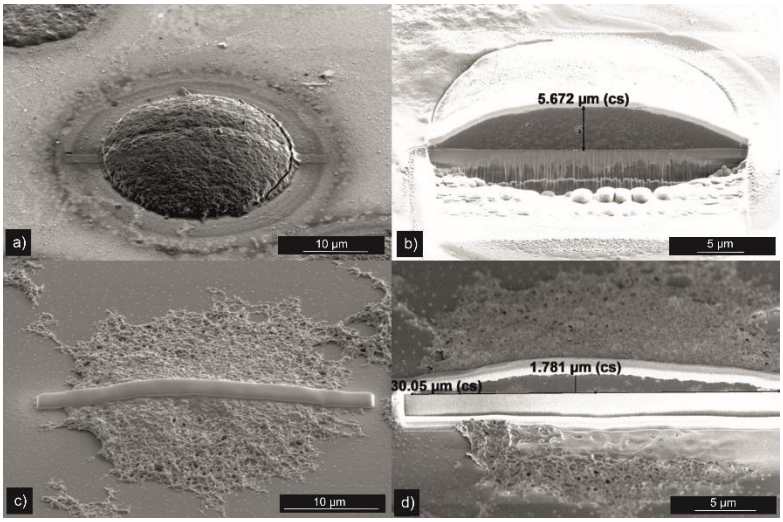

Fig. 25. FIB-SEM images of dried a) b) standard and c) d) 1.4 experiment obtained MPPy microspheres at a) 3500 b) 10.000 c) 5000 d) 13.000 magnifications measured at an angle of 54° from the surface.

While microspheres are dispersed in a liquid medium, they contain their expected smooth spherical shape. In order to obtain detailed description of their inner morphology FIB-SEM analysis is utilised. Results of the FIB-SEM study for standard MPPy microsphere synthesis is shown in Fig. 25 micrograph. After particle drying procedure MPPy microspheres were tent to collapse into lens-shaped structures with 5.67 µm thickness, due to their speculated porosity in inner particle morphology. At high magnification, one can observe open pores of various sizes (Fig. 25 b), comprising a porous inner microsphere morphology. This particle characteristic is of great importance for various applications and has both its positive and negative variables. If the polypyrrole microspheres were solid, their active surface area would only be the surface area of the sphere. Since sponge-like structure is visible throughout the sphere, as a result active surface area increases greatly. Consequently, if MPPy microspheres are dispersed in a solvent, their surface area is much larger compared to conventional solid spherical particles. Overall, the entire

structure of standard MPPy microspheres appears to be uniform from the center of the microsphere to the periphery. Polypyrrole microspheres obtained in experiment 1.4, already established as lower quality (spiky shape) but higher in porosity were also investigated by FIB-SEM method (Fig. 25).

Lens-shaped structure thickness of 1.4 experiment microspheres is much smaller 1.781 μm, compared with standard microemulsion MPPy microsphere thickness, due to their highly porous inner particle morphology. As can be seen from FIB-SEM images at an angle of 54°, in 1.4 experiment produced MPPy microspheres are highly porous and detected pore size distribution is estimated to be from 100 to 700 nm in diameter Fig. 25 d.

These finding apply that at different volumetric flow rates generated microreactor droplets may lead to higher or lower porosity MPPy microsphere formation.

8.4. MPPy Microsphere FT-IR Analysis

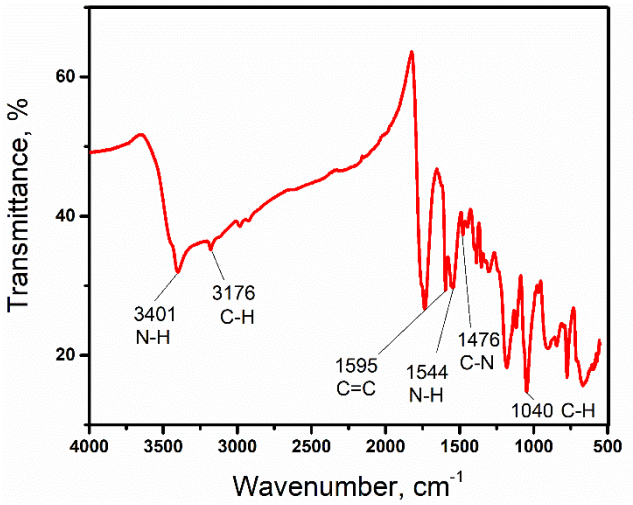

Fig. 26. General FT-IR spectra of MPPy microsphere obtained in microfluidic device.

Individual MPPy microsphere chemical structure was observed with FTIR spectrometer (section *6.2.1.*). Preparing microspheres for analysis they had to be dried on a glass surface at 60 °C in a laboratory oven overnight. Fig. 26 shows a general FT-IR spectrum of MPPy microspheres. The characteristic peaks of 3401 cm^{-1} and 3176 cm^{-1} are attributed to N-H and C-H respectively. The peaks at 2985 cm^{-1} and 2896 cm^{-1} are associated with the asymmetric stretching and symmetric vibration of CH_2[211]. Also microsphere spectra shows

a peak at 1544 cm^{-1} corresponding to the N-H stretching of the monomeric pyrrole unit of the backbone structure[46]. The characteristic peaks at 1595 cm^{-1} and 1476 cm^{-1} correspond to C=C/C-C and C-N respectively, whereas 1040 cm^{-1} is mostly assigned to C-H and N-H deforming vibrations[212] and is described as a complex out-of-plane nature[213].

Although the peaks observed in the present work match well with the ones available in the literature[213] proving the formation of MPPy microspheres the occurrence of a strong peak at 1723 cm^{-1} is offsetting. Though it could correspond to a carbonyl group from oil residue, thus more advanced microsphere purification methods should be applied in the future to ensure pure MPPy microspheres.

8.5. Discussion of the Main Results

The most suitable conditions for the formation of high quality, repetitive structure and size, circular and non-agglomerated MPPy microspheres obtained by using novel MS scheme (Fig. 17). Thus, optimal continuous and dispersed phase inlet velocity rated were determined: fluorinated oil – 250 µl/h, Py– 125 µl/h and $FeCl_3$ – 75 µl/h.

The morphology and structure of MPPy microspheres were analysed by SEM, FIB-SEM, and optical microscopy methods. At optimal reaction inlet velocity rates, the microemulsion solution has resulted in orderly distributed oval and smooth surface spherical moieties, between 30-40 µm in diameter, consisting of sponge-like morphology. The results of optical microscope studies showed that reduction of medium phase inlet velocity rates is not beneficial for MPPy microsphere formation.

Polymerization process was achieved in each singular droplet as an efficient polymerization microreactors. MPPy microspheres analysed under FIB-SEM analysis revealed diverse structures, less efficient solution inlet velocity rates obtained and dried MPPy microspheres collapsed and acquired lens-shape form, although at highly efficient velocity rates microspheres maintained their structure better and revealed a denser inner morphology.

FT-IR studies have confirmed that oval microspheres are composed of pure polypyrrole.

The aforementioned MPPy microsphere future applications could include distinct gel-filtrations systems or composing novel electromagnetic wave absorbing paint or materials.

CHAPTER 9. PPY FORMATION ON A NON-CONDUCTIVE SUBSTRATE

9.1. PPy Composite Layer Morphological SEM Analysis

The morphological characteristics of PPy composite layer after immersion in Py solution visibly changed: Initially, PVA polymeric matrix layers with oxidative initiator obtained orange colour whilst, after radical polymerization they turned black. Monomer colour change during polymerization process in polymeric matrix indicated the success of the process. During scanning electron spectroscopy (SEM) before polymerization all samples, except PVAc-$FeCl_3$, showed $FeCl_3$ crystals on the surface. Further polymerized PVA-PPy composite layers showed dotted surface composition with cracks and small ridges (Fig. 27). PVAc-$FeCl_3$ surface reminded a sponge-like structure that was flat, wavy, with some cracks. PVAc-PPy surface appeared to be porous, with 1-4 μm cavities (Fig. 27). PSSA-$FeCl_3$ surface was porous, uneven and wavy, with few μm pores. PSSA-PPy composite surface was wavy, porous and was easy to crack (Fig. 27). PVB-$FeCl_3$ surface was very flat and even, with 100 nm round cavities. PVB-PPy composite surface appeared to be porous, with small 0.2-1 μm cavities (Fig. 27). From morphological aspect most similarities were observed with PVAc-PPy and PVB-PPy composites because of their unique sponge-like-structure.

Another interesting morphological tendency of PPy composites is that with lower pyrrole concentration, composites appear thinner than those polymerized with higher pyrrole concentrations PSSA-PPy composites remain as an exception with a much thicker composite layer. Taking into consideration unclear PSSA-PPy composite layer thickness matrix swelling[214] effect must be discussed. On the one hand $FeCl_3$ salt is soaked and released while the adhesive polymer matrix is being immersed in water which might be the reason why composite layer thickness is reduced after polymerization which results in conductive composite formation by migrating into adhesive polymeric matrix. But on the other hand, polymer matrix swelling might partake in accelerating Py polymerization process for the same quick $FeCl_3$ release which induces uncontrollable radical polymerization and growing PPy chain passes through the adhesive polymer matrix which results in even thicker conductive PPy composite layer formation.

Probably, higher pyrrole concentration interrupts $FeCl_3$ soaking from the matrix leaving the final layer thicker. In PSSA-PPy case, PPy layer might grow atop of polymer matrix layer. Therefore, Cho et al. reported that PSSA

was found to be a more effective stabilizer for conductive PANI nanoparticles compared with PVA, due to the sulfonic acid group in PSSA[215]. Unlike PVA, PSSA as a polymer with π-π electrons might stack up PPy which has π-π electrons as well.

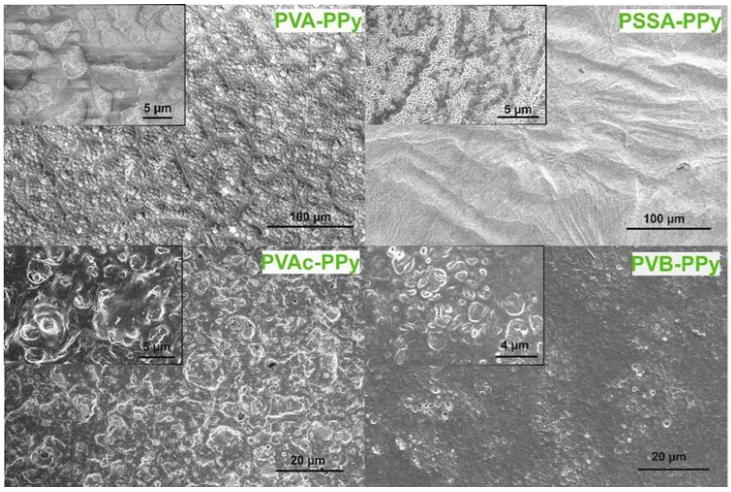

Fig. 27. SEM images of PPy composites surfaces after *in situ* polymerization process.

9.2. PPy Composite Layer FT-IR Spectral Analysis

PPy composite layer spectra were measured according to section *6.2.1.* methodology. The PVA-$FeCl_3$ layer spectra in Fig. 28 before the immersing into pyrrole solution showed significant peaks at 3360, 1640-1610 and 1068 cm^{-1} indicating the presence of O-H and C-O functional groups[128]. The new peaks appeared at 1548 and 1410 cm^{-1} in PVA-PPy spectrum which correspond to the stretching vibrations of C=C and C-N of PPy, respectively[216]. Peak at 3220 cm^{-1} can be attributed to the humidity on PVA-PPy surface.

The PSSA-$FeCl_3$ spectrum in Fig. 28 indicates strong hydrogen bond at 3400 cm^{-1}. C-C aromatic phenyl ring vibration peak was shifted from 1644 cm^{-1} to 1599 cm^{-1} which might be due to π-π electron interaction between phenyl and pyrrole rings. Two new peaks at 1592 cm^{-1} and 1533 cm^{-1} are shown in PSSA-PPy spectrum which could be attributed to the C=C and pyrrole ring skeleton vibrations, respectively. A broad and narrowed band at 3390 cm^{-1} indicates N-H functional group and confirms the presence of PPy

in PSSA matrix O=S=O vibration was shifted from 1190 cm^{-1} to 1226 cm^{-1}. Peaks at 1123 cm^{-1} and 1003 cm^{-1} indicate in-plane skeleton vibration of phenyl ring and in-plane bonding vibration of phenyl ring, respectively[217,218].

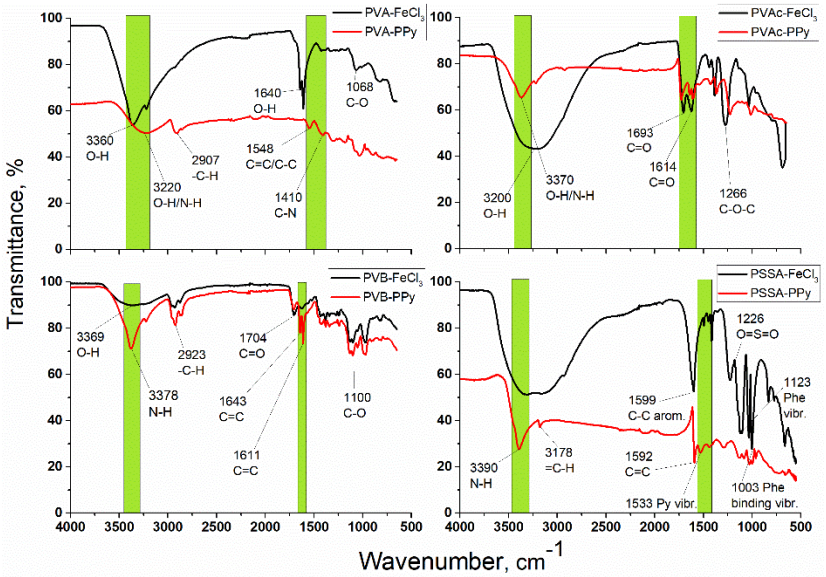

Fig. 28. FT-IR spectra comparison of layers before and after immersing in 1 M pyrrole solution.

9.3. PPy Composite Layer XPS Analysis

XPS measurements were carried out to obtain information about the elemental chemical states and surface composition considered PVA-PPy, PVAc-PPy, PVB-PPy composites polymerized in 1 M pyrrole monomer solution were chosen and their core level peaks of C1s, O1s, Cl2p and N1s were analysed[219,217,220,215] (Fig. 29, 30). PSSA-PPy composite was considered to be unsuitable for XPS analysis because of its cracked composite surface and fast degradation in vacuum chamber.

The N1s core spectra in Fig. 29 (left) has been deconvoluted into three peaks: the neutral pyrrolylium nitrogen N^0 at a binding energy of ~399 eV, the positively charged nitrogen N^+ at ~401 eV and $C=N^+$ at ~402 eV (this peak is absent in PVB-PPy spectra). Basically, peaks at 401 eV and 402 eV are attributed to polaron and bipolaron in PPy backbone and both can be marked as N^+. The N^+/N ratio for PVA-PPy, PVAc-PPy and PVB-PPy is 0.35, 0.43 and 0.38 respectively.

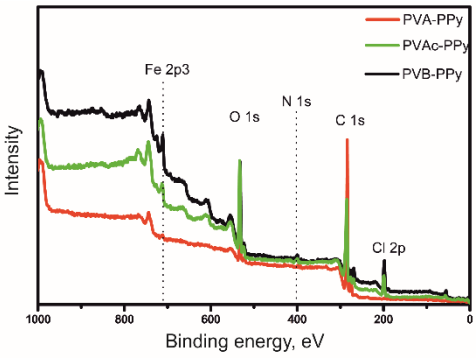

Element	Percentage of element on the surface		
	PVA -PPy	PVAc -PPy	PVB-PPy
Fe2p3	0.57	2.78	4.05
O1s	13.48	23.78	22.28
N1s	1.06	1.79	1.41
C1s	84.17	64.57	60.92
Cl2p	0.71	7.08	11.34

Fig. 29. XPS survey scans of PPy composites on dielectric substrates (left) and XPS composite surface composition (atom %) analysis (right) with polymer matrices (PVA, PVAc, PVB).

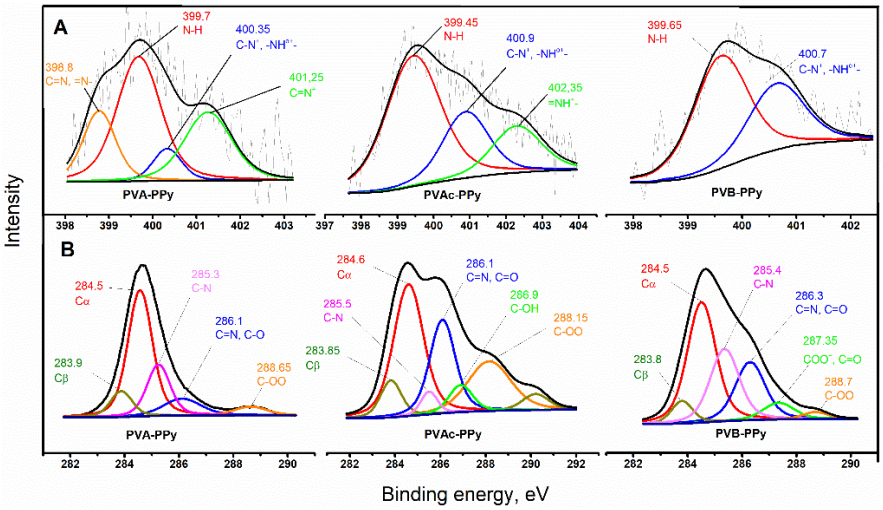

Fig. 30. PVA-PPy, PVAc-PPy and PVB-PPy composites XPS spectra analysis of high-resolution A – N1s, B – C1s regions.

This ratio predicts the percentage of oxidized PPy, a direct characteristic linked to conductivity. According to N^+/N ratio, PVAc-PPy should be the most conductive layer among other two and PVA-PPy should exhibit the poorest conductive properties. Noticeably, bipolaronic structure is absent in PVB-PPy N1s spectra (Fig. 30 A), thus predicts poor surface conductivity as well. Seemingly, unlike other adhesive polymers, PVB adhesive polymer matrix has an impact for PPy conductivity by blocking bipolaronic state. However, XPS elemental analysis uncovered very low percentage of nitrogen atoms on

all surfaces (Fig. 29 right). The survey spectra are hardly noticeable at ~400 eV, making the conductivity prediction unreliable.

The low values of the nitrogen can be linked to the assumed polypyrrole diffusion deep into a polymer matrix during the polymerization, thus little PPy remains atop (Fig. 30).

9.4. Composite Layer SE and Surface Conductivity Measurements

One can note that the aforementioned equations have been derived under the assumption that the conductive composite is infinitely thin, this meaning having no substrate. In fact, all PPy composites were formed on polyethylene terephthalate (PET) substrate, with a thickness of 150 μm and a relative dielectric constant of 3.5. To ensure the validity of simplified theory we compared measurement results of the reflectance performed when samples are irradiated from the conductive composite side and from the substrate side. According to the theory accounting for the finite thickness of the substrate, the measured reflectance values might be different due to influence of the substrate thickness[193]. Experimental investigations have revealed that this difference is less than 7% that is much less than the scattering of measurement results obtained measuring different matrices.

Also, we used exact formulas that account for the thickness of the substrate when determining surface conductivity of the investigated matrices[221]. The difference between values defined using exact and approximate formulas is less than 2%. Based on performed verification, the aforementioned simplified approach has been used when determining T_0 and R_0 as well as of the surface conductivity of investigated composites.

Measurement results of PPy composites with PVA and PVAc adhesive polymer matrices in Fig. 31 A show weak dependence of surface conductivity on frequency. All measured composites with PVA matrix in Fig. 31 A demonstrate almost similar surface conductivity in the range from 12 to 22 S/cm which is practically independent from frequency in the selected 8 to 38 GHz frequency range. Composites formed with 1 M concentration pyrrole solution demonstrate ~15% larger surface conductivity than 0.3 M and 0.5 M formed composites. Measured surface conductivities of 0.3 M and 0.5 M composites are practically equal in all frequency bands (12-22 S/cm) and coincide with surface conductivity of 1 M PPy composites at higher frequencies. We can conclude that pyrrole concentration during the

polymerization has little influence on the measured surface conductivity of PVA-PPy composites.

Measured surface conductivity of 1 M PVAc-PPy composite is roughly 4-6 times lower than the conductivity of the same PVA-PPy composite (Fig. 31 A) and it is independent of frequency. From these results one can conclude that the influence of selected adhesive matrix is much larger on the surface conductivity, than the influence of concentration of pyrrole during *in situ* polymerization process.

PSSA-PPy composites in Fig. 31 B demonstrate more pronounced dependence of surface conductivity on pyrrole concentration during the polymerization reaction. An average surface conductivity of 0.3 M, 0.5 M and 1 M composites is 0.45, 0.8, and 3 S/cm, respectively. It is seen that by changing pyrrole concentration during the polymerization reaction the desirable value of surface conductivity of PSSA-PPy composite can be achieved in the range from 0.4 to 3 S/cm. Some dependence of σ on frequency is also visible. The conductivity has a trend to increase approximately twice, when frequency is growing from 8 to 38 GHz.

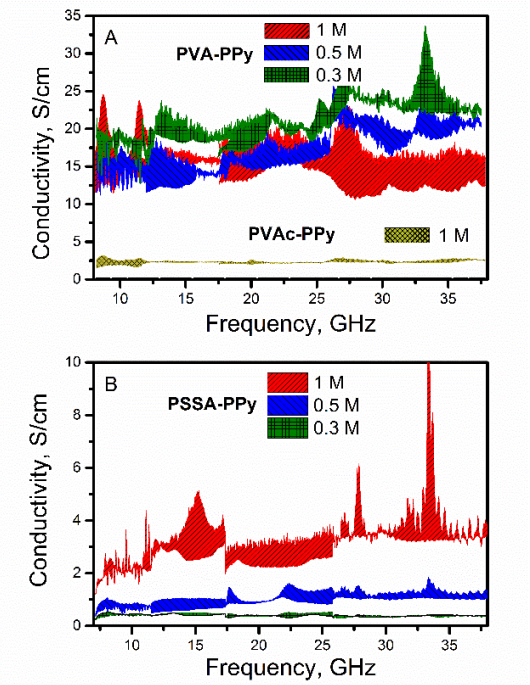

Fig. 31. Surface conductivity of PPy composites for different pyrrole concentrations and polymer matrix: A – PVA and PVAc matrices; B – PSSA matrix.

The DC specific conductivity of mechanically pressed PPy samples measured using 4-probe method was reported 190 S/cm[46] and 90 S/cm[34], [43b, 47]. The highest reliable value of the surface conductivity measured in our experiments using microwave technique is 0.035 S. Taking into account, that the average thickness of the investigated PPy composites in this work was roughly ~15 μm, one can get that the largest conductivity value of the investigated layers was 23 S/cm. It is substantially lower than the results mentioned above. On the other hand, measured surface conductivities of textile coated by polypyrrole were in the range 0.001-0.005 S[34, 43b, 47] that is noticeably lower than the data presented in this study. The discrepancies mentioned above might be attributed by the differences in preparation technology of samples and possible inhomogeneity of our achieved composites.

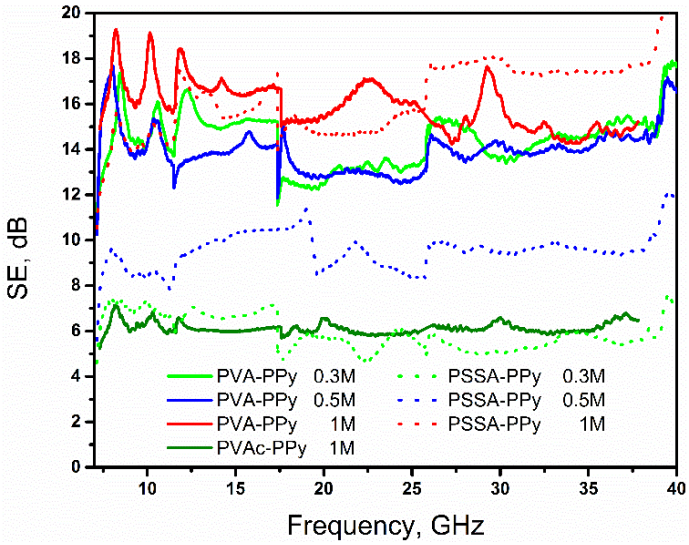

Fig. 32. Shielding effectiveness of PPy composites. Solid lines SE of PVA-PPy and PVAc-PPy composites, dotted lines PSSA-PPy composites.

The peaks on the measured curve as well as some breaks at limiting frequencies of particular waveguide are probably caused by non-uniformity of the composite surface and drawbacks of waveguide holders, where investigated samples are mounted. The latter manifested itself when the cross-section of the waveguide is changed from one frequency band to the other. One can observe that the measurements of layers with lower surface conductivity are less scattered (Fig. 32). At a lower pyrrole concentration

during polymerization the synthesized composites are less conductive but more homogeneous. Dependencies of the shielding effectiveness in Fig. 32 on frequency correlate with data of the surface conductivity, the increase of σ leads to the increase of SE. Depending on the surface conductivity SE ranges from 6 to 18 dB. This value is consistent with the values obtained by Saini and Choudhary[48], where the single layer of textile covered by polypyrrole demonstrates roughly 10 dB attenuation of microwave radiation in the frequency range 8-12 GHz. For PVAc-PPy composite the desirable value of SE in the range 6 to 18 dB can be obtained by changing the pyrrole concentration during *in situ* polymerization reaction. This pronounced feature of the investigated composites might be important for special electromagnetic shielding applications as anti-radar or stealth technology improvement.

9.5. Discussion of the Main Results

In conclusion, polypyrrole was successfully loaded into the adhesive polymer matrix by radical *in situ* polymerization and characterized by FIB-SEM, FT-IR and XPS methods. PVA-PPy, PVAc-PPy, PVB-PPy and PSSA-PPy composites on dielectric PET substrates were successfully synthesized using radical polymerization.

PPy composites surface analysis and morphological SEM characterization has shown sponge-like structure formation throughout adhesive PVAc-PPy and PVB-PPy layers.

PPy composites surface conductivity and shielding effectiveness was measured and calculated using a contactless EMI shielding method with rectangular waveguides in the microwave band from 8 to 38 GHz frequency range, by inserting the samples in rectangular waveguides and measuring transmittance and reflectance. The contactless EM shielding method of surface conductivity measurement used in this thesis can be applied for other conductive films or composites deposited on non-conductive substrates, textile-based materials, etc.

The conductivity of PPy composites with PVA matrix weakly depends on the concentration of pyrrole during the polymerization reaction and typically ranges from 13 to 18 S/cm. The surface conductivity of these composites slightly depends on microwave frequency up to 38 GHz. On the contrary, PPy composites with PVAc demonstrate pronounced dependence of the surface conductivity on frequency. This allows in a rather simple way to synthesize composites with the desirable value of SE in the range 8-18 dB. Conductivity

measurements were taken ignoring PPy and polymer matrix thickness. Although PPy penetration in the polymer matrix during the polymerization is worth further investigation. Neither full or even polypyrrole insertion is not examined and confirmed, nor is PPy density and conductivity at different depth level in the polymer matrix. Additional investigation might give a better understanding about the polymerization mechanism through the polymeric matrix.

Microwave absorption experiment showed that the most promising adhesive polymer matrix for polypyrrole composite formation is PVA, conducting preeminent mechanical and electrical properties that may offer a wide range of applications in military industry, flexible electronic devices, sensors or even smart textiles. PVAc or PVB polymer matrices with PPy produces low conductivity while PSSA-PPy composite might obtain high conductivity but has a tendency to crack as an adhesive layer. Further investigation is required for the PPy dispersion in an adhesive polymer matrix which might explain the uneven surface conductivity and shielding effectiveness.

Future activity in PPy radical *in situ* polymerization process for conductive composite formation can further be applied on other non-conductive surfaces. By choosing PVA matrix as all in all the most promisable polymer for initiator throughout distribution and enhancing conductivity properties with anionic dopants these PPy conductive composites can be used for producing flexible conductive composite wires, smart textiles or with respect to high levels of composites capacitance, energy storing materials.

CHAPTER 10. PPY *IN SITU* POLYMERIZATION ON VARIOUS TEXTILE SUBSTRATES

10.1. PPy Textile Composite Shielding Effectiveness Analysis

PPy textile composites experimental investigations have been performed in far field region at 2-18 frequency range in a semi-anechoic chamber (section *6.2.5.*). Continuous wave signal was passed through specimen and data collected in transmitting antenna. As it is seen in Fig. 8 measured PPy textile fabric composite is surrounded with absorber sheets preventing the diffracted wave to directly get into the receiving antenna. It can be seen that an almost linear dependence between SE and frequency range was obtained with both pattern designs. Collected EMI shielding results depicted in Fig. 33 A, shows

that squared pattern coated design exhibits a much lower SE performance comparing to fully coated surface design.

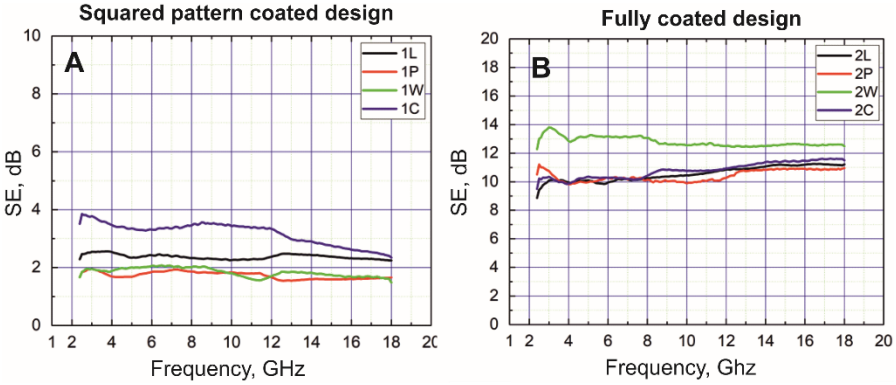

Fig. 33. PPy textile composite shielding effectiveness measurements in different frequency bands S, C, X, Ku in 2-20 GHz frequency range on L – linen, P – polyester, W – wool, C – cotton fabric textile substrates, A – with squared pattern and B – fully coated designs.

Textile/ PPy composites with squared patterned design highlighted two textile materials, cotton and linen woven fabrics with SE of 3.9 and 2.4 dB respectively. Squared patterned polyester and wool/ PPy composite fabrics indicated only 2 dB SE. Highest EMI shielding efficiency levels were demonstrated with fully coated woven wool/ PPy composite fabrics when SE reached 14 dB (Fig. 33 B). On the other hand, woven cotton, polyester and linen/ PPy composite fabrics reached accordingly SE of 10 dB. These findings apply that with different pattern designs produced conductive textile composite can possess varied levels of SE levels. Rybicki[194] noticed an increase in a surface weight of PANI on polyacrylonitrile fabric substrate, which is linearly dependent on the number of PANI layers, leads to an almost proportional increase in SE. Therefore, in our study, wool substrate absorbed more adhesive polymer matrix with $FeCl_3$, which eventually led to a thicker PPy layer on composite formation with higher SE properties. It is noteworthy to point out that wool substrate utilised for conductive composite formation was of unwoven state.

10.2. PPy Textile Composite Surface Resistivity Measurements

Table 4. Surface resistivity of tested samples before and after washing.

Fabric type groups		Surface resistivity ρ, Ω		
		Before washing	**After 1 washing cycle**	**After 5 washing cycles**
Wool	Non treated	2.97×10^{13} 5.15×10^{13}	-	-
	Pattern coated	1.37×10^{5} 5.62×10^{5}	1.12×10^{8}	1.34×10^{9}
	Fully coated	$< 2 \times 10^{3}$	5.5×10^{4}	1.8×10^{5}
Polyester	Non treated	4.95×10^{12} 6.93×10^{12}	-	-
	Pattern coated	$< 2 \times 10^{3}$	5.69×10^{5}	6.99×10^{5}
	Fully coated	$< 2 \times 10^{3}$	3.4×10^{4}	1.91×10^{5}
Linen	Non treated	1.98×10^{13} 2.57×10^{13}	-	-
	Pattern coated	$< 2 \times 10^{3}$	1.83×10^{5}	1.47×10^{6}
	Fully coated	$< 2 \times 10^{3}$	After 1 washing cycle fabric cracked	
Cotton	Pattern coated	$< 2 \times 10^{3}$	1.37×10^{5} 0.82×10^{5}	1.33×10^{5} 0.22×10^{5}

On the basis of knowledge that EMR shielding textile fabrics characteristics exhibit relatively low resistivity levels, surface resistivity (ρ, Ω) was measured according to standard method EN1149-1, with Terra-Ohm-Meter 6206 (produced by "Eltex") applying a voltage of 10 V (for conductive textiles) and 100 V (for control fabric). Specimens were pressed with the load of 10 N between an assembly of cylindrical and annular electrode arranged concentrically with each other and base plate on which the specimen is placed. The conditioning of samples (for 24 h) and tests were carried out in dry conditions – air temperature (23 ± 1) °C, relative humidity (25±5) %. The quality of the coatings was assessed after various washing cycles. The washing procedure was carried out using SCOUROTESTER, FE M–09/A, at 40 °C

temperature, adding to each container steel balls. Duration of one washing cycle – 30 min. A standard detergent with phosphates without optical bleachers was used for washing.

Both pattern and fully coated fabrics samples were washed repetitive five washing cycles, in a solution of ECE standard detergent of concentration – 4g/l. After each washing cycle, the samples were rinsed in cold distilled water ten times, squeezed, and lastly dried at room temperature conditions.

The results of fully coated fabrics after particular washing cycles still indicated textile rigidity. Electrostatic measurement subsequently was evaluated all non-treated, pattern coated and fully coated specimens results presented in Table. 4. Surface resistivity of fully coated wool samples before washing and after one and five washing cycles resulted in a drop in surface resistivity, comparing with untreated fabric, over few orders of magnitude less than the untreated fabrics. For non-treated textile fabrics ρ obtained is 10^{12}-10^{13} Ω orders of magnitude, whilst pattern coated and fully coated fabric samples demonstrate ρ less than $< 2 \times 10^3$ Ω, with the exception of pattern coated wool which resulted in 1.37×10^5-5.62×10^5 Ω resistivity range.

10.3. PPy Textile Composite Half Decay Time and Electrostatic Shielding Factor Analysis

Half decay time (t_{50}) and electrostatic shielding factor (*Sf*) were determined and collected according to the induction charging test method in dry conditions - air temperature (23 ± 1) °C, relative humidity (25±5) %, using electric charge meter ICM-1, manufactured by STFI. The field electrode is positioned under sample without contacting the specimen, a high voltage of 1200 V is rapidly applied to the field electrode. The microprocessor makes automatic calculations.

Sf determines charge migration at the textile surface therefore this parameter shows applied conductive coatings electrostatic properties provided to non-conductive textile fabrics (as substrate). Three woven fabrics consisting of wool, polyester and linen fibers were analysed (cotton specimens did not meet specified size requirements for measurement). Electrostatic shielding factor for wool pattern coated sample after 1 and 5 washing cycles decreased correspondingly only in 0.01. For polyester pattern coated samples it remained constant, but for linen pattern coated sample electrostatic shielding factor decreased by 0.02. Although with pattern coated specimens *Sf* decreased, the achieved results are considered more then, sufficient comparing

with fabric composites with metalized yarns which *Sf* corresponds to 0.89 or 0.78 [184]. Unlike pattern coated samples wool, polyester and cotton fabrics fully coated samples electrostatic shielding factor was obtained (*Sf*=1), which indicates excellent modified textile fabrics electrical properties. However, the determination of *Sf* parameter does not allow to objectively characterize highly conductive fabrics, because *Sf* value 1 is the maximum measurable value.

Table 5. Half decay time (t_{50}) and electrostatic shielding factor (*Sf*).

Fabric type groups		**Before washing**		**After 1 washing cycle**		**After 5 washing cycles**	
		t_{50}, **s**	***Sf***	t_{50}, **s**	***Sf***	t_{50}, **s**	***Sf***
Wool	Non treated	> 30	0	Not washed			
	Pattern coated	<0.01	0.94	<0.01	0.92	<0.01	0.93
	Fully coated	<0.01	1	<0.01	1	<0.01	1
Polyester	Non treated	>30	0	Not washed			
	Pattern coated	<0.01	0.85	<0.01	0.84	<0.01	0.85
	Fully coated	<0.01	1	<0.01	1	<0.01	1
Linen	Non treated	>30	0	Not washed			
	Pattern coated	<0.01	0.98	<0.01	0.97	<0.01	0.95
	Fully coated	<0.01	1	After 1 washing cycle sample was damaged			

Half decay time represents the time required for the charge to reduce to half of its initial value. As seen in Table 5, all of the investigated textile fabrics demonstrate equal half decay time less than <0.01 s in spite of non-treated fabric specimens. That is why this parameter is not going be taken into account for further analysis.

10.4. PPy Textile Composite for Split-Ring Resonators

In this study, split-ring resonators were formed and later analysed in an anechoic chamber (section *6.2.5. Contactless EM SE Measurements in Anechoic Chamber*). The resonant behaviour of the effective SSR-1 and SRR-2 samples is represented in Fig. 34. The nature of the spectrum corresponds to the classical spectrum of ring resonators. Conductive polymeric split-ring resonators were analysed in vertical and horizontal electric field polarization, because of the specific ring structure. SRR transmittance goes to 0 because of resonance peaks, which can be theoretically calculated using eq. (13).

$$f_r = \frac{nc}{2n_{ef}P} \tag{13}$$

when n = 1, 3, 5; and P = 4A

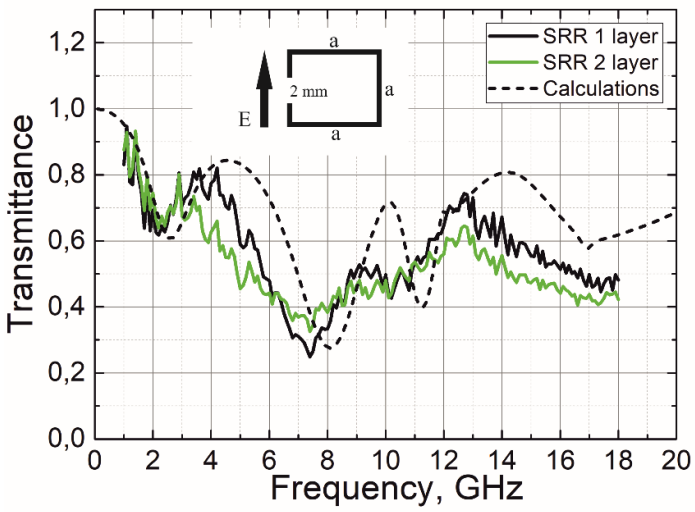

Fig. 34. Dependence of transmittance on frequency in PPy-SRR on wool substrate. Polarization of electric field is depicted in insert.

Therefore, the spectrum shows three decreases in transmittance corresponding to the plasmonic resonances of the split-ring resonators. Theoretically calculated resonance peaks alternate at 2.2, 7.2 and 9.7 GHz frequency ranges. Although experimental results practically correspond to the calculated ones in 2 separate resonance peaks, respectively 2.2 and 7.2 GHz, it was evident that the third peak at 9.7 GHz does not coincide with theoretical resonance calculations. All three experimental resonant peaks are visible in

the experimental transmittance spectra (Fig. 34) however, they are all shifted to the left into a lower frequency range.

Since the conductivity of the resonators is not very high, the minimum wave bandwidth values are not very low. At 2.2 GHz, the first-order plasmon resonance mode is observed, at 7.2 GHz, the third order, and at 9.7, the fifth order. It is known that fifth-order plasmonic resonance is observed only in dense arrays of resonators[15]. At 11.8 GHz, resonant lattice mode is observed, and resonator arrays of this configuration are also characteristic.

In order to get the sharper peaks corresponding to theoretically calculated and the right number of them, one will need to synthesize more conductive PPy composites on textile fabrics. Conductive polymer SRR could then be used in developing new functional textiles with lightweight, cost effective and desired design RFID antennas.

10.5. Discussion of the Main Results

A contactless method of thin film conductivity measurements in a waveguide and in an anechoic chamber was adapted with a fitting of the analytical model.

Best shielding effectiveness on textile was achieved with wool fabric substrate is about 14 dB in 2-20 GHz frequency range. Electrostatic shielding factor after five washing cycles decreased only 0.01 S. Surface resistivity was much higher after five washing cycles, compared to cotton or polyester specimens.

Conductive polymer PPy-SRR composite resonant behaviour is a material parameter and an intrinsic property of a metamaterial. RFID (antennas) tags can be based on a split ring resonator.

CHAPTER 11. PPY COMPOSITE FORMATION WHEN DOPANT IS IN POLYMER MATRIX AND IN MONOMER SOLUTION WITH NATURAL TEXTILE FABRIC

A woven wool textile of natural origin was chosen for this work as it provided promisable EMI shielding properties exhibited in section *10.1. Shielding Effectiveness Analysis*. Although woven wool displays better breathability and characteristics than non-woven, yet the modified textile fabric surface is uneven due to the weave and fibrous nature of the yarns.

Therefore, a flexible polymer interface layer is used to present a more homogeneous surface for the subsequent screen printing.

11.1. Wool/PPy/Dopant Composite FT-IR Analysis

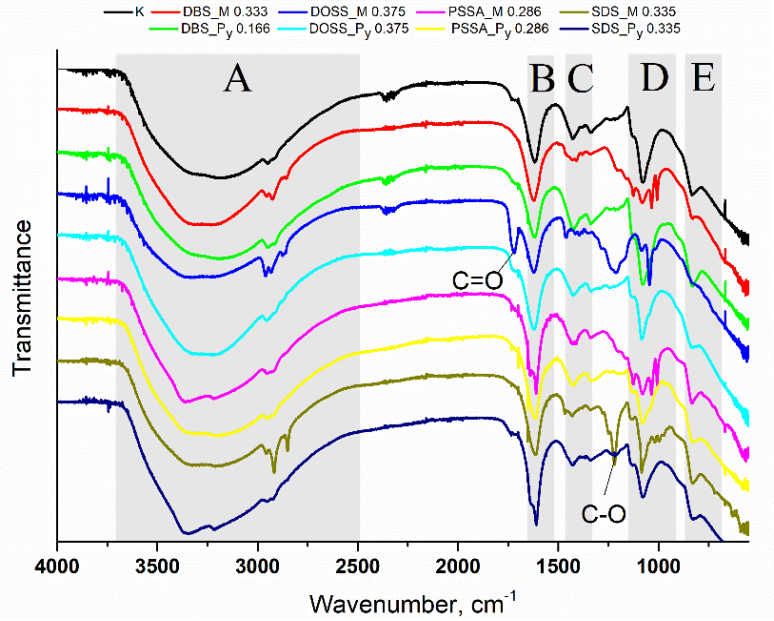

Fig. 35. PPy/dopant composite FT-IR transmittance spectra. Characteristic intervals are labelled in the spectra by characters.

FT-IR spectroscopy was utilised to examine and compare PPy/dopant composites when the dopant is integrated into a polymer matrix and Py aqueous monomer solution by identifying specific chemical bonds on the obtained surface (section *6.2.1.*). Fig. 35 shows the FTIR summary spectra of PPy composites with various ratios of dopant components and, for comparison, the spectra of K – PPy without any dopant.

PPy/dopant composites in A section assigns to the hydrated O-H bonds and is present in all PPy/dopant composites at ~3400–3300 cm^{-1}, proving that the resulting compositions contain PVA polymer[222]. Section B denotes the peaks of the ~1625–1615 cm^{-1} band that indicate aromatic C=C bonds[223,224]. Section C shows ~1430–1425 cm^{-1} band peaks that indicate elastic, deformable C-C, C-N bonds[224,225,226]. Section D, at ~1084–1078 cm^{-1} peaks, which denotes to S=O bonds existing in DBS, PSSA, DOSS, SDS dopants[217], whereas in the control sample, this peak indicates deformation of C-H bonds[224]. Section E

reveals the peaks at ~832–828 cm^{-1} band, indicating that vibrating, planar C-H bonds exist in all specimens[190]. Also, a characteristic peak at ~1723 cm^{-1} corresponds to the C=O carbonyl bond, which proves DOSS[227] incorporation into the composite as well as peaks at ~1221 cm^{-1}, which are attributed to elastic C-O bonds[228].

11.2. Wool/PPy/Dopant Composite SEM Characterization

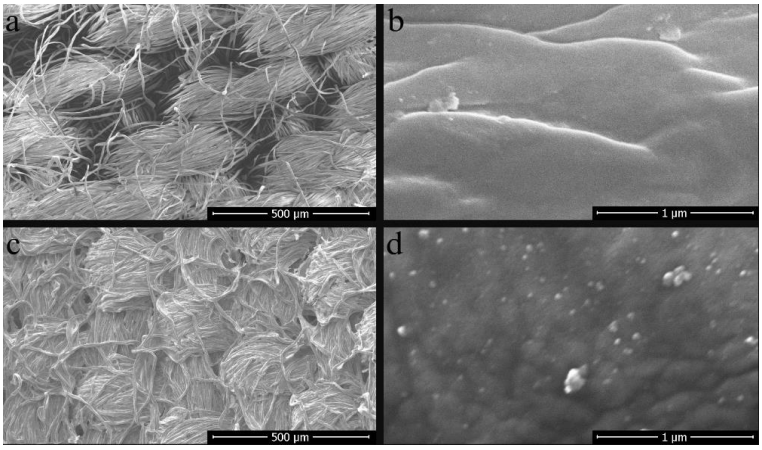

Fig. 36. SEM images showing surface topographies of untreated woven wool at magnification of a) 100, b) 50.000; Woven wool/PPy/Cl, control sample at magnification of c) 100, d) 50.000.

The morphology of the woven/PPy/dopant composite material is characterized using a scanning electron microscope (section *6.2.3.*). Specimens with dopant incorporations in an adhesive polymer matrix and aqueous Py monomer solution were examined and specific woven wool/PPy/dopant composites were chosen. From an array of samples, only the ones with the highest dopant concentrations for composite synthesis were analysed. Electron flux parameters for micrograph magnification for 3 kV, 0.8 nA were 100x, 250x, 1000x, 5000x, and 3 kV, 100 pA for 50.000x.

Wool/PPy/Dopant Composite SEM studies revealed that the surface of untreated woven wool has hollow cavities that are formed naturally during the weaving process (Fig. 36 a). The surface of the yarns itself is smooth and homogeneous (Fig. 36 b).

Meanwhile, by forming woven wool/PPy/Cl composite fabric, the adhesive PVA and $FeCl_3$ matrix fills the aforementioned cavities in the woven

wool and joins the yarns into a solid layer – composite. At higher magnifications (Fig. 36 d) wool/PPy/Cl composite surface micrograph indicates PPy globular agglomerates formed on the fabric and produces an inhomogeneous, wavy surface with some more unequally agglomerated areas.

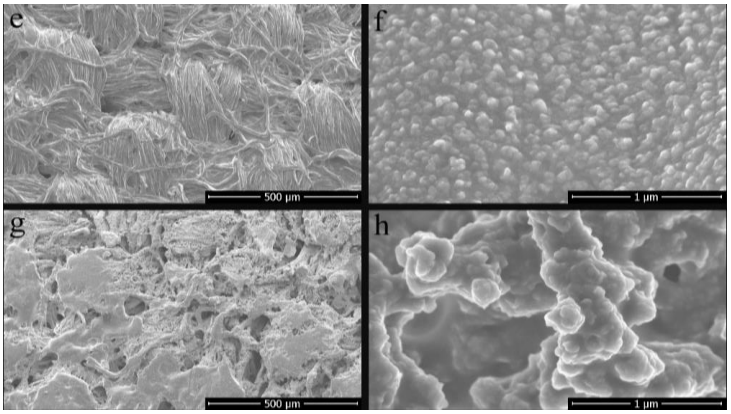

Fig. 37. Woven wool/PPy/dopant composite with 0.333 M DBS concentration: inside the matrix, at magnification of e) 100, f) 50.000, Py in monomeric solution, at magnification of g) 100, h) 50.000.

The woven wool/PPy/dopant composite, with 0.333 M DBS concentration inside an adhesive matrix, has a similar surface effect as in Fig. 37 e where PVA and $FeCl_3$ matrix fills up the voids in woven wool fabric and binds the yarns into a solid surface. Although at higher magnifications, one can indicate that the wool/PPy/DBS-M surface is homogeneously granulated.

Meanwhile, a composite of a woven wool/PPy/DBS composite fabric with a concentration of 0.333 M in the Py monomer solution surface reveals that by spray coating Py and dopant solution, PPy polymerization takes place on the fabric surface and penetrates deeper into woven wool PVA and $FeCl_3$ coated surface. Wool/PPy/DBS-P_y composite forms a highly agglomerated heterogeneous surface. At higher magnifications, wool/PPy/DBS-P_y composite surface exhibits a sponge-like morphology (Fig. 37 h).

The woven wool/PPy/dopant composite with 0.375 M DOSS concentration within the polymeric matrix and the composite with 0.188 M DOSS concentration in the Py monomer solution surfaces exhibit a web-like morphology at lower magnifications (Fig. 38 i, k). At higher magnifications, both wool/PPy/DOSS-M and wool/PPy/DOSS-Py composites surfaces show a homogeneous and agglomerated surface with PPy rough particle distribution

throughout the composite surface. Boukerma[229] and colleagues also reported that by comparing undoped PPy/Cl and DOSS doped PPy/Cl powder particles compared, the latter attributed a more compact globular morphology. Therefore, compared to woven wool/PPy/Cl composite, both DOSS dopant incorporated composites can offer high surface area properties.

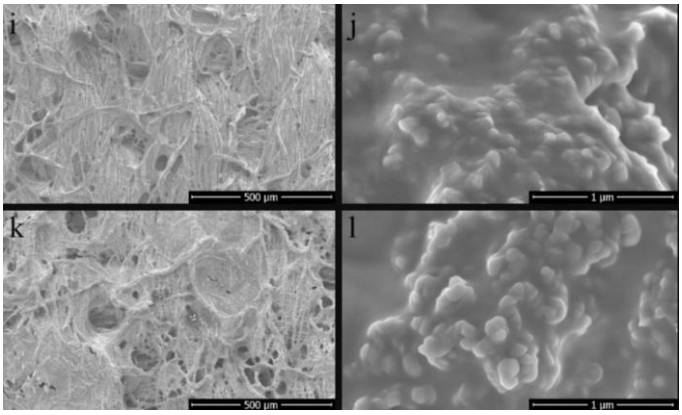

Fig. 38. Woven wool/PPy/dopant composite at 0.375 M DOSS concentration: inside the matrix, at magnification of i) 100, j) 50.000, 0.186 M Py in monomeric solution, at magnification of k) 100, l) 50.000.

Woven wool/PPy/dopant composite, when PSSA concentration inside an adhesive polymer matrix is 0.286 M, indicates a cracked surface with large voids on the textile composite surface (Fig. 39 m). Meanwhile, at higher magnifications (Fig. 39 n), wool/PPy/PSSA composite reveals a homogeneous surface comprised of highly compressed small granulated PPy particles produced during the Py monomer spray coating polymerization process. On the other hand, woven wool/PPy/dopant composite, with 0.286 M concentration PSSA dopant incorporated in Py monomer solution, forms a rough and wavy composite surface without any cracks on the fabric surface (Fig. 39 o). Meanwhile, at higher magnifications, wool/PPy/PPSA-P_y composite formed a heterogeneous and highly porous surface with large cavities (comprising sponge-like morphology) and much bigger agglomerated granules compared with Fig. 39 n during spray coating polymerization process.

The woven wool/PPy/dopant composite, with 0.336 M SDS concentration incorporated into a polymer matrix, the image shows a heterogeneous surface design with distinct bonding to the textile fabric yarns. Also, at lower magnifications, both wool/PPy/SDS composite surfaces (Fig. 40 q, s) obtained

a thin film with various different size voids comprising a web-like surface morphology where one can see woven wool weaving pattern. At higher magnifications, wool/PPy/SDS-M composite surface revealed a homogenous but highly agglomerated PPy particles (Fig. 40 r).

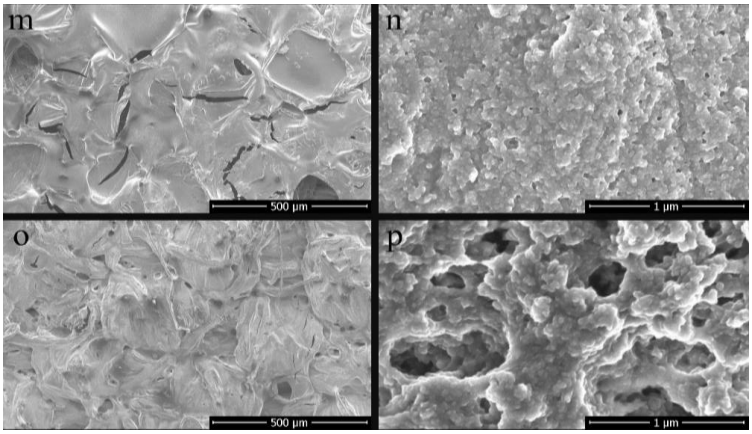

Fig. 39. Woven wool/PPy/dopant composite at 0.286 M PSSA concentration: inside the matrix, at magnification of m) 100, n) 50.000, Py in monomeric solution, at magnification of o) 100, p) 50.000.

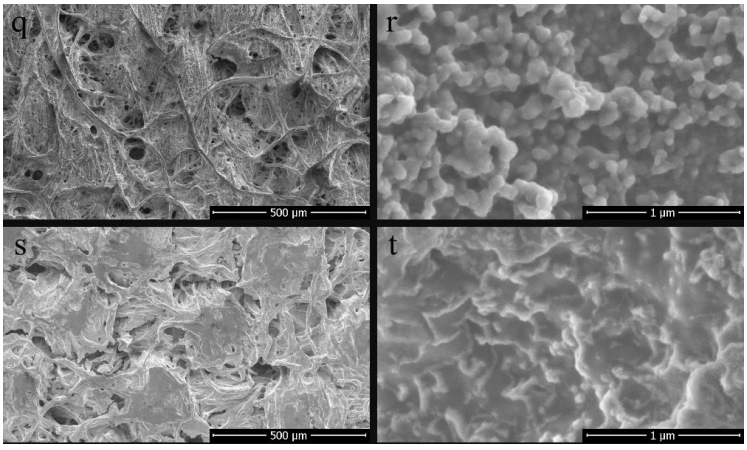

Fig. 40. Woven wool/PPy/dopant composite at 0.336 M SDS concentration: inside the matrix, at magnification of q) 100, r) 50.000, Py in monomeric solution, at magnification of s) 100, t) 50.000.

The woven wool/PPy/dopant composite, with 0.336 M SDS concentration in the Py monomer solution, exhibits a heterogeneous composite surface. At higher magnifications (Fig. 40 t) depicts that on the surface of PPy/SDS

composite obtained agglomerated particles (beads) are fused into one another and creates a highly rough and spiky active surface.

All in all, dopant incorporation into an adhesive polymeric matrix or into Py monomer aqueous solution has a great impact on obtained wool/PPy/dopant composite morphology.

11.3. Woven Wool/PPy/Dopant Composite Shielding Effectiveness Analysis

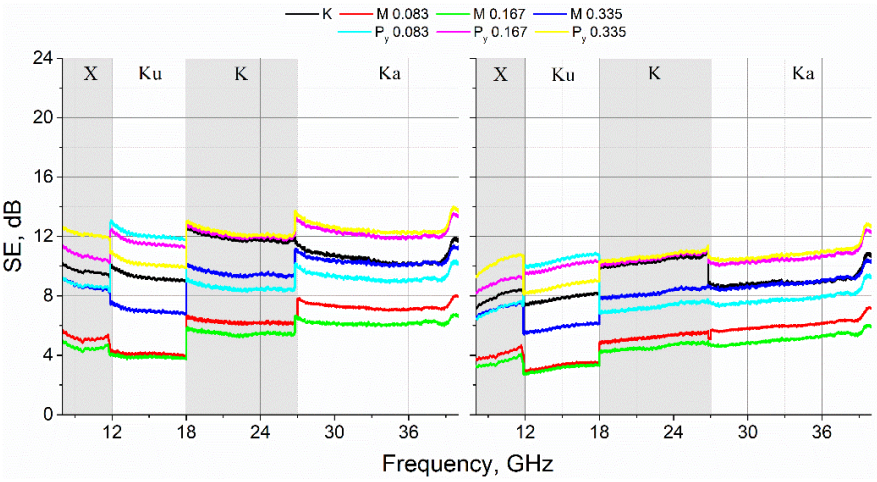

Fig. 41. SE of woven wool/PPy/DBS composite in rectangular waveguide (left) and free space (right) in the 8-38 GHz band. K-control sample; M – dopant is inside the matrix; Py – dopant is in a monomeric pyrrole solution.

A scalar waveguide circuit analyser investigates SE properties of a woven wool/PPy/dopant composite by electromagnetic radiation exposure and monitoring of the samples ability to reflect and transmit electromagnetic microwaves. In order to understand specimens SE capacity differences, an anionic dopant was incorporated in polymeric (PVA and $FeCl_3$) matrix and in Py monomer aqueous solution. Produced woven wool composite samples were then examined in rectangular waveguides.

For each dopant, an individually synthesized control sample was measured. Obtained results are recorded on an oscilloscope, PicoScope, pico Technology. The surface conductivity and shielding effectiveness are measured in a rectangular waveguide and then recalculated for free space

according to the analytical solution explained in (section *6.2.4.*) with the MatLab program.

SE improvement is evaluated by comparing prepared woven wool composites with an embedded dopant in polymeric matrix and aqueous Py monomer solution with the control sample (K – woven wool/Py polymerized with $FeCl_3$). An increase in shielding effectiveness of woven wool/PPy/DBS composite occurs when dopant DBS concentration in Py monomer solution is 0.167 M and 0.333 M. Compared to the control sample the evaluated difference is accordingly ~2 dB, and ~3 dB, while overall EMR shielding effectiveness corresponds to 11-13 dB and 8-10 dB in 8-38 GHz frequency range.

Meanwhile, when DBS is present in the polymeric matrix, shielding efficiency of the samples is weakened, especially when DBS concentrations are 0.083 M and 0.167 M. Shielding effectiveness results data in free space (Fig. 41) does not change the SE tendency, although all calculated data for free space indicates lower SE that measured in a rectangular waveguide.

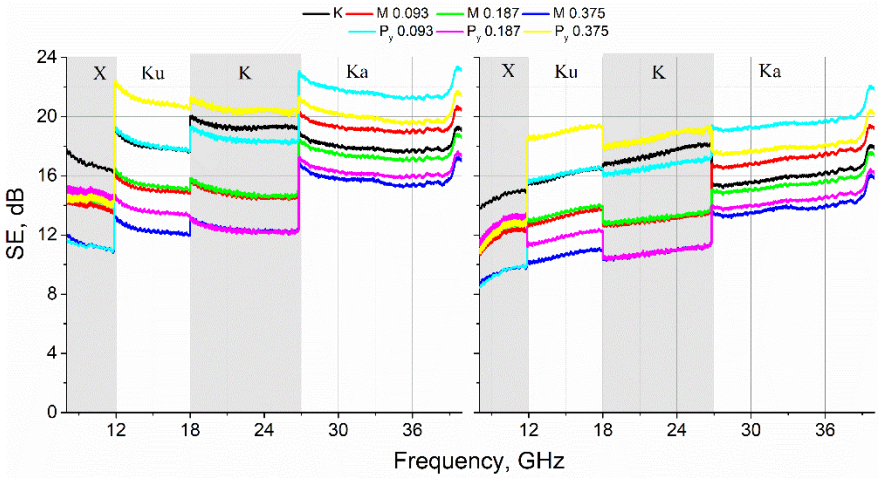

Fig. 42. SE of woven wool/PPy/DOSS composite in rectangular waveguide (left) and free space (right) in the 8-38 GHz band. K-control sample, M – dopant is inside the matrix, Py – dopant is in a monomeric pyrrole solution.

Woven wool/PPy/DOSS composite has uneven shielding effectiveness, which is depicted in Fig. 42 graphs. When dopant DOSS concentration in Py monomer solution is 0.375 M, then SE of woven wool/PPy/DOSS-P_y composite increases compared to the control sample in Ku, K, Ka frequency bands by approximately ~4 dB, whilst overall reaching around ~22 dB.

Meanwhile, all wool/PPy/DOSS-M composites, including wool/PPy/DOSS-P_y with dopant concentrations, demonstrate a decrease in composites SE properties, compared with the control sample. Calculated SE data in free space again does not change wool/PPy/DOSS composite SE tendencies, whilst indicating lower SE value than measured in a rectangular waveguide (Fig. 42 right).

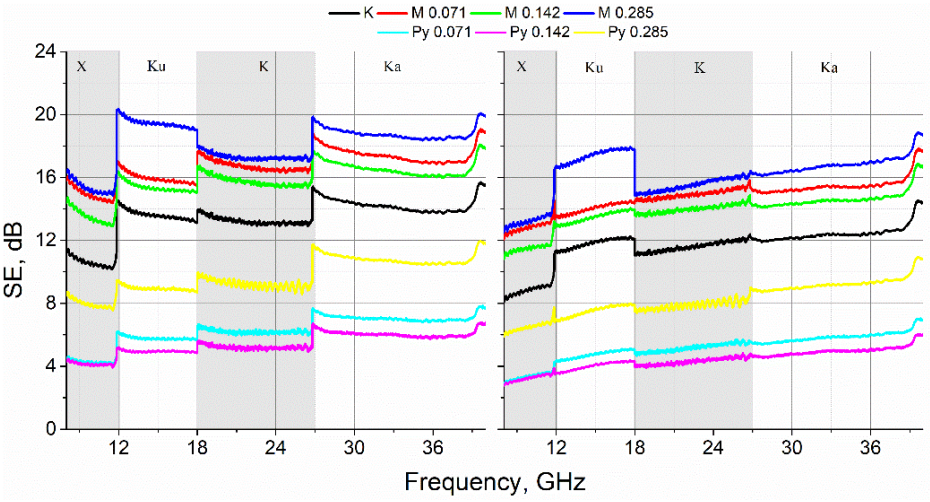

Fig. 43. SE of woven wool/PPy/PSSA composite in closed space (left) and open space (right) in the 8-38 GHz band. K-control sample, M – dopant is inside the matrix, Py – dopant is in a monomeric pyrrole solution.

Meanwhile, PSSA dopant incorporation into polymeric matrix proved to be a more efficient way to increase woven wool/PPy/PSSA composite shielding effectiveness compared with previous wool/PPy/DOSS composite SE investigations.

The composite with 0.285 M PSSA concentration in polymeric matrix, measured SE difference is ~5 dB and overall reaches 20 dB in Ku frequency range. However, when PSSA is incorporated into the Py monomeric solution, shielding efficiency decreases compared to the control sample. The weakest shielding efficiency is observed for composites with 0.142 M, 0.071 M and 0.285 M PSSA concentrations in Py monomer solution. The tendencies for recalculated SE data results from a rectangular waveguide to free space still remain lower than measured in a rectangular waveguide. However, the highest SE value demonstrated in the Ku frequency range reaches 17 dB.

Lastly, textile composite formation with an SDS dopant exhibits excellent SE values. All woven wool/PPy/SDS composites have improved shielding

effectiveness parameters compared to the control sample, except for the Ka band, where 0.083 M and 0.167 M SDS dopant concentrations in polymeric matrix result in SE decrease. Woven wool/PPy/SDS composite with 0.335 M SDS concentration in Py aqueous solution exhibited the highest SE difference comparing to the control sample and it reached ~9-12 dB. Accordingly, 0.083 M, SDS dopant concentration reached ~8-10 dB in 8-38 GHz frequency range. Moreover, highest overall SE value with SDS reaches 20 dB. Calculated SE data outcome in free space again does not change SE tendencies, while revealing lower SE values than measured in a rectangular waveguide.

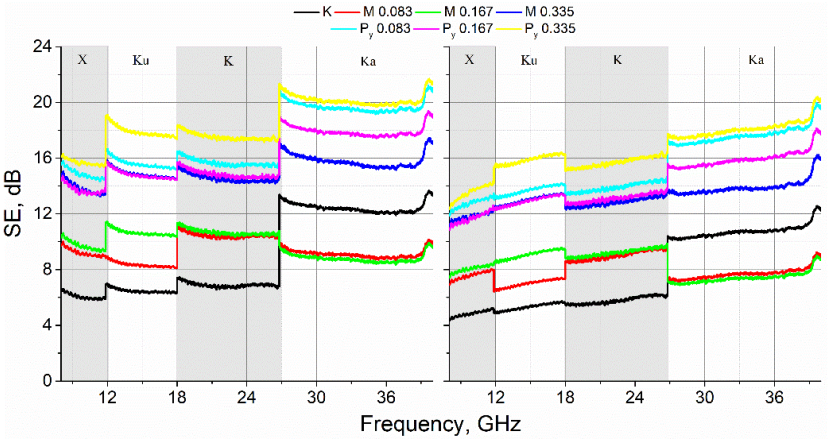

Fig. 44. SE of woven wool/PPy/SDS composite in rectangular waveguides (left) and free space (right) in the 8-38 GHz band. K-control sample, M – dopant is inside the matrix, Py – dopant is in a monomeric pyrrole solution.

Overall produced wool/PPy/dopant composites SE varied between 12-22 dB and in free when calculated to free space varied 10-19 dB. It is noteworthy to mention that all control samples also varied in EMI shielding efficiency levels, which leads to a conclusion that produced samples differed in homogeneity. Therefore, control samples should not be given much consideration in this study. In future there is a necessity to use a more efficient way of producing constant samples by using inject printer rather than screen printing technique.

11.4. Woven Wool/PPy/Dopant Composite 4-Point Probe Method, Resistance Analysis

The DC conductivity of the woven wool/PPy/dopant composites were measured with a 4-point probe method. The aforementioned method setup

consists of four equally spaced conducting tips mounted on a metallic support plate and placed on a tested sample. This test determines PPy/dopant material composites surface resistivity. DBS, DOSS, PSSA and SDS dopant composites with highest utilized dopant concentrations in Py monomer solution corresponding to 0.333 M, 0.375 M, 0.286 M and 0.336 M. Also, 0.286 M PSSA dopant composite in an adhesive polymer matrix was chosen for the 4-point probe resistivity measurements (Table 6). Only a few wool/PPy/dopant composites are primarily selected due to increased SE properties in the aforementioned studies (section *11.3*). Therefore, only those samples with the most efficient EMI shielding effectiveness were analysed.

Table. 6. Woven wool/PPy/dopant composite electrical resistance measurements.

Sample no.	Woven wool composite type	Average, R, kΩ
1	PPy/Cl, control	29.93
2	PPy/DBS, when dopant concentration 0.333 M in 1M Py monomer aqueous solution	55.13
3	PPy/DOSS, when dopant concentration 0.375 M in 1M Py monomer aqueous solution	0.90
4	PPy/PSSA, when dopant concentration 0.286 M in adhesive matrix solution	1.54
5	PPy/SDS, when dopant concentration 0.336 M in 1M Py monomer aqueous solution	39.50

According to the wool/PPy/dopant specimen results, the 4-point probe method test shows the lowest obtained composite electrical resistance is with specimen 3 when the concentration of DOSS in 1 M in Py monomer solution was 0.375 M, and the average surface resistance of the sample was 0.90 kΩ.

By comparing shielding effectiveness with surface resistance results, one must understand that the concept of conductivity in both cases. While 0.333 M wool/PPy/DBS-P_y and 0.336 M wool/PPy/SDS-P_y composite samples presented an increased SE compared to the control samples in Fig. 41, 44, thus determining higher electrical conductivity levels. However, composites electrical resistance results for specimens 2 and 5, demonstrated higher resistance than wool/PPy/DOSS-P_y sample, thus resulting in contrast to two methods. Contact resistance outcome is higher than we expected due to the

poor adhesion of the conductive silver paste with the surface of the PPy/dopant specimen, resulting in the need for further comparison of the composite resistance measurements with the results obtained by the electromagnetic wave absorption method or a better optimization of current 4-point probe method for accurate composite resistance measurements.

11.5. Woven Wool/PPy/Dopant Composite Thermal Imaging analysis

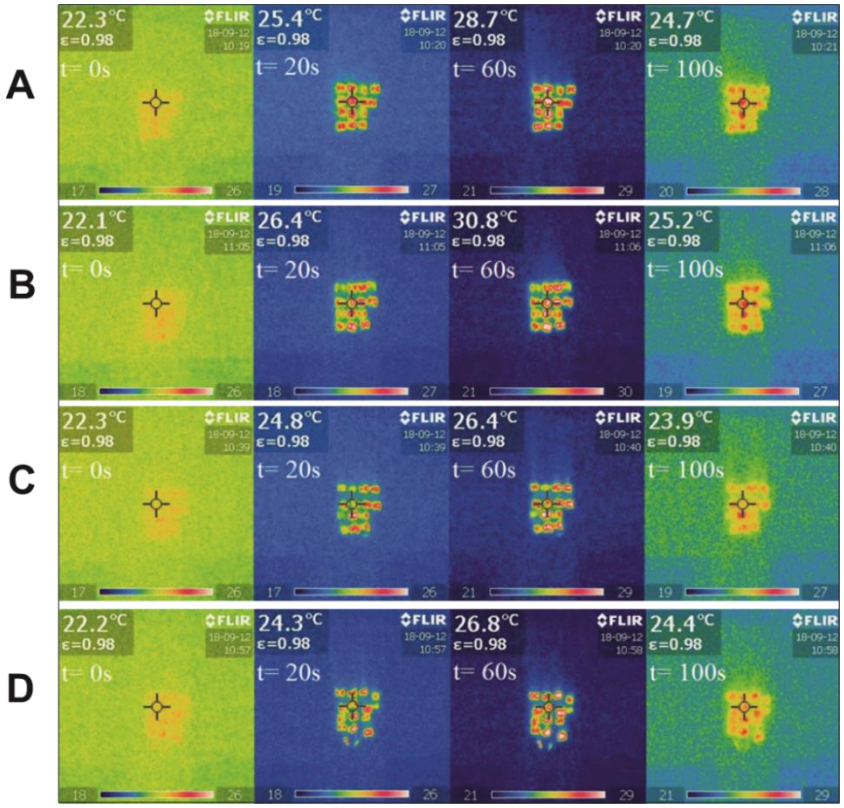

Fig. 45. Woven wool/PPy/dopant composites exposition to electromagnetic wave radiation during the thermoelectric properties study. Dopants: A – DBS, B – DOSS, C – PSSA, D – SDS.

All produced woven wool/PPy/dopant composite specimens were attached to a foam base and examined in an anechoic chamber using a FLIR camera (section *6.2.9.*). This study helped to determine the ability of produced woven wool/PPy/dopant composites to absorb electromagnetic waves and convert them into thermal energy expression.

Based on collected data, it can be stated that wool/PPy/DBS and wool/PPy/DOSS composites have shown the most promising thermoelectric properties, as their samples reach the highest temperature after 60 s of EM radiation. Meanwhile, wool/PPy/PSSA and wool/PPy/SDS composites demonstrate the weakest thermoelectric properties, as their temperature rises only a few degrees. Therefore, both wool/PPy/PSSA and wool/PPy/SDS composites will not be further discussed.

All woven wool/PPy/DBS composites when DBS dopant is incorporated into an adhesive polymeric matrix and in Py aqueous monomer solution with various dopant concentrations heats up till 28.7 °C which corresponds to 6.4 °C temperature difference. The highest temperature difference was obtained with wool/PPy/DBS-P_y composite with 0.333 M dopant concentration and the temperature difference between ambient room temperature and wool/PPy/DBS-P_y specimen was 8 °C Fig. 45 A. Although, 8 °C difference is considered high, it does not correlate with the results from EMI shielding when none of these mentioned specimens improve SE of woven wool/PPy/DBS composites compared to control sample Fig. 41.

Woven wool/PPy/DOSS composites, when dopant is incorporated into Py aqueous monomer solution at a concentration of 0.094 M reaches ~9 °C temperature difference compared to ambient room temperature, which correlates with SE of aforementioned composites in Fig. 42. An overall highest wool/PPy/dopant composite temperature was measured with 0.375 M DOSS composite when incorporated into adhesive polymeric matrix reaching 10 °C temperature difference. However, wool/PPy/DOSS composites do not improve the shielding efficiency compared to control sample, although FLIR analysis indicated temperatures even more raises the question whether all control samples should be considered, as wool/PPy/DOSS-P_y composites exhibits overall best SE of 22 dB (Fig. 42).

11.6. Discussion of the Main Results

The research has succeeded in synthesizing woven wool/PPy/dopant composites in both cases where the dopant is mixed in Py monomer aqueous solution and when the dopant is embedded in the adhesive matrix.

FT-IR spectroscopic analysis indicated and assigned O-H, aromatic C=C, C-C, C-N, C-H bonds, which confirmed the products obtained during composite formation corresponds to PPy, PVA. Meanwhile, S=O, C=O and C-O assigned bonds accordingly correspond to the anionic surfactants DBS, DOSS, PSSA, SDS presence in the produced composites.

SEM study was able to determine the morphological characteristics of woven wool/PPy/dopant composites. From the obtained results it can be stated that the incorporation of DOSS into the PVA adhesive matrix or 1 M concentration Py monomeric solution does not affect the morphological characteristics of the woven wool/PPy/dopant material, which is characterized by coarse agglomerated granules. Composites with DBS, PSSA or SDS anionic surfactant in the adhesive matrix have different sized, evenly distributed beaded (more agglomerated) surfaces. Composites when DBS and PSSA are present in a 1 M Py monomeric solution, acquires a porous surface.

In the study of EMI shielding effectiveness in a rectangular waveguide, was found that the best SE of all composites is woven/PPy/SDS composite, when the concentration of SDS in Py monomer solution is 0.336 M. The difference between SE of composite and control is equal to ~10 dB and overall SE reaches 20 dB. Although 0.375 M wool/PPy/DOSS composite SE compared with control is only 4 dB, yet overall composite demonstrates 22 dB shielding efficiency.

4-contact method layer resistance analysis showed that only two samples exhibited lower resistance than the control sample, respectively PPy/DOSS and PPy/PSSA layers. The PPy/DOSS layer at a DOSS concentration of 0.375 M in the 1 M Py monomer solution has the lowest resistance measured – 0.90 kΩ. Whilst, PPy/PSSA composite layer exhibited resistance of 1.54 kΩ, when dopant concentration in the adhesive polymer matrix was 0.286 M.

During the infrared thermographic analysis, all the composites of the woven wool/PPy/dopant material had demonstrated thermoelectric properties, when specimens temperature increased on average by ~7.0 °C. Most promising results were obtained with woven wool/PPy/DOSS composite, when the concentration of DOSS dopant in the adhesive polymeric matrix is 0.375 M. After 60 s exposure with 4.0 GHz EM radiation wool/PPy/DOSS-M composite revealed ~10.0 °C temperature difference.

In conclusion, dopant incorporation into Py aqueous monomer solution showed the most promising results with DOSS, PSSA and SDS dopants. These results give a bedrock for doped polymer composites use in the smart textile industry, which can be used to develop tunable electrical conductivity commercially available flexible smart electronics and thermoelectric devices.

CHAPTER 12. DOPANT INCORPORATION DIFFERENCES, WHEN DOPANT IS IN ADHESIVE MATRIX OR IN MONOMER MONOMER SOLUTION ON SYNTHETIC FABRIC

All specimens were formed with synthetic polyamide (PA) textile fabric. Nylon 6,6[230] is a high strength hydrophobic polyamide fabric and was chosen for its tremendous application possibilities in smart textiles (e.g., sportwear) and military purposes.

This study was carried out to understand the structural, thermal and shielding effectiveness differences between dopant incorporation stage. In continuation of previous work (section *6.1.7.*) with woven wool we optimised dopants SDS, PSSA, DBS, DOSS concentrations and added another dopant MWCNT. Also, PA/PPy/dopant composite sizes were substantially increased. The aforementioned five dopants were incorporated in to PA/PPy/dopant composite formation process by using two methods when:

M – dopant is in an adhesive polymer matrix;

P_y – dopant is in Py monomer solution.

12.1. PA/PPy/dopant Composite Thermal Imaging Analysis

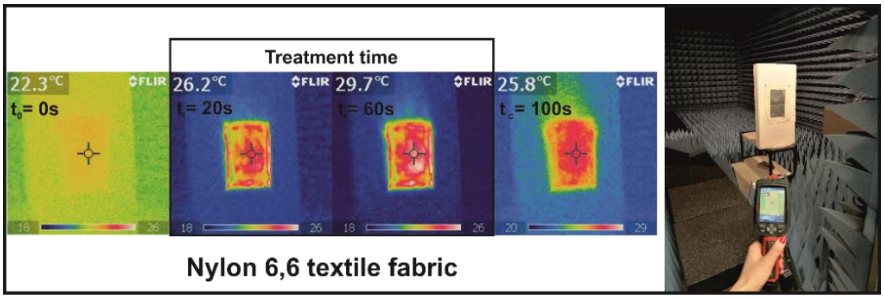

Fig. 46. Equipment set up for the measurement of thermoelectric properties (right). PA/PPy/Cl composite with PVA matrix exposition to electromagnetic wave radiation.

Nylon 6,6 fabric composites have been synthesised according to *6.1.7. Textile Composite Synthesis on Synthetic Fabric* methodology. The increase of composite temperature was analysed utilizing a thermal imaging camera. FLIR camera is able to detect temperature alterations on any given surface. During heating or cooling of the PA/PPy/Cl composite (section *6.2.9.*) thermal diffusivity was continuously recorded with an automated FLIR camera (Fig. 46). In this study, we reveal formed overall PPy distribution homogeneity and

the temperature difference is estimated. As one can see from Fig. 46 the temperature difference between PA/PPy/Cl composite sample in ambient state and in irradiated corresponds to 7.4 °C. The distribution on the textile fabric appears to be quite uniform throughout the produced composite.

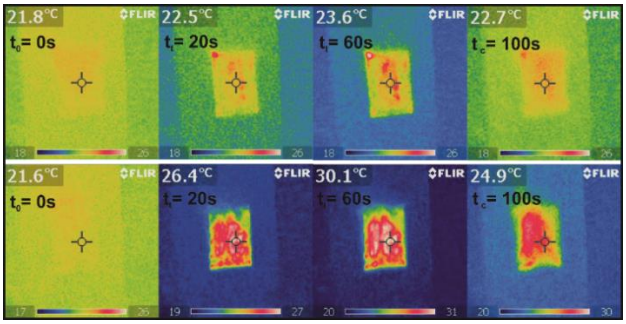

Fig. 47. PA/PPy/SDS composites exposition to electromagnetic wave radiation during the thermoelectric properties study. Top row images correspond to M; bottom row – P_y.

Based on PA/PPy/SDS composites images one can state that temperature difference between PA/PPy/SDS-M composite and PA/PPy/SDS-P_y is quite apparent. During heating (EM radiation) time composites thermal profile temperature changed compared to the ambient room temperature. PA/PPy/SDS-M composite temperature heated only up to 23.6 °C, whilst PA/PPy/SDS-P_y composite heat concentration reached 30.1 °C. Highest difference between the temperatures – 8.5 °C was achieved with P_y composite Fig. 47 bottom row.

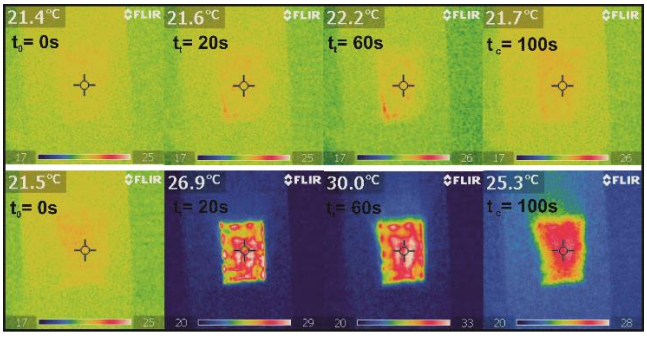

Fig. 48. PA/PPy/PSSA composites exposition to electromagnetic wave radiation during the thermoelectric properties study. Top row images correspond to M; bottom row – P_y.

Composites with PSSA dopant resulted in similar manner. PA/PPy/PSSA-M composite temperature barely reached 22.2 °C, but composite formed with spray coating with monomeric Py solution resulted in 30 °C which correspond to 8.5 °C temperature difference.

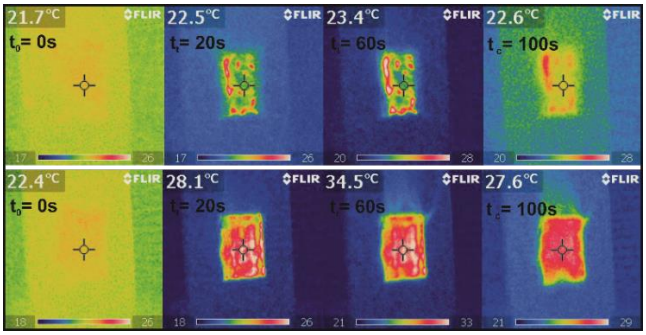

Fig. 49. PA/PPy/DBS composites exposition to electromagnetic wave radiation during the thermoelectric properties study. Top row images correspond to M; bottom row – P_y.

From detailed PA/PPy/DBS composites thermal imaging we can conclude that DBS mixed as a dopant offers higher thermal stability[231] of all considered PA textile specimens. PA/PPy/DBS-M composite thermal temperature reaches only 23.4 °C, whereas PA/PPy/DBS-P_y composites reaches 34.5 °C which corresponds to 12.1 °C temperature difference.

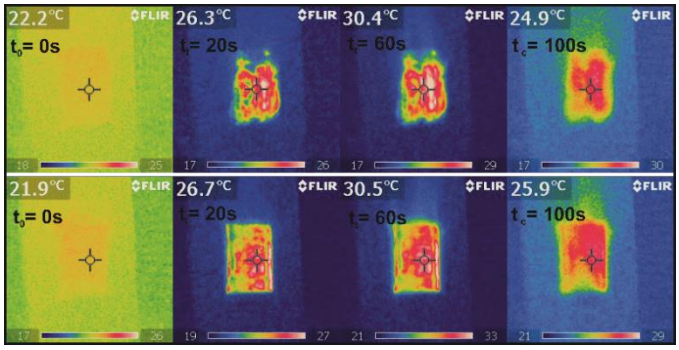

Fig. 50. PA/PPy/DOSS composites exposition to electromagnetic wave radiation during the thermoelectric properties study. Top row images correspond to M; bottom row – P_y.

On the other hand, PA/PPy/DOSS composites both thermal imaging series show promising thermal results. PA/PPy/DOSS-M composite displays a less

homogenic surface coverage, whereas measured temperature does not differ from the PA/PPy/DOSS-P_y composite, and results at around ~8.2 °C difference. PA/PPy/DOSS-P_y composites thermal profile reaches 30.5 °C, whist the composite when DOSS dopant is mixed into the polymeric matrix appears to be just 0.1 °C lower.

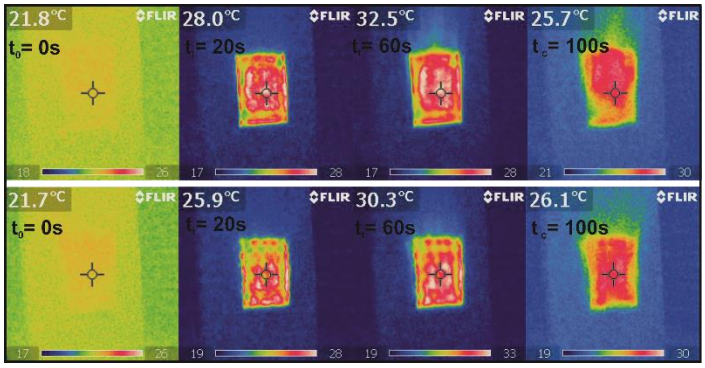

Fig. 51. PA/PPy/MWCNT composites exposition to electromagnetic wave radiation during the thermoelectric properties study. Top row images correspond to M; bottom row – P_y.

Meanwhile, PA/PPy/MWCNT composites thermal imaging exhibits elevated fabric temperatures. A more homogenic composite is formed when multiwalled carbon nanotubes are mixed in a polymeric PVA matrix before PPy polymerization process. Aforementioned composites temperature difference is 10.7 °C. PA/PPy/MWCNT-P_y composite reaches 30.3 °C, which corresponds to a lower 8.6 °C temperature difference.

12.2. PA/PPy/dopant Composite Contactless Microwave SE Method Analysis

This study was carried out to analyse and compare shielding effectiveness and electrical conductivity differences between dopant incorporation in adhesive polymeric matrix or in Py monomer solution. Contactless SE method generated results on nylon 6,6 fabric are shown in Fig. 52, indicating direct dependence of SE and electrical conductivity with different dopants.

One of the lowest SE properties were obtained with SDS dopant in either incorporation phases in a polymeric matrix or in monomer solution embedded SDS dopant composites shielding efficiency reaches only 0.4 and 4 dB respectively. Composites with PSSA dopant demonstrated similar

characteristics. When PA/PPy/PSSA composite is produced by embedding the dopant in matrix solution SE levels are at the lowest 2 dB, on the other hand PA/PPy/PSSA fabric composite when dopant is in Py monomer solution doubles shielding efficiency to 8 dB with electrical conductivity of 0.014 S. Nylon 6,6 composite with DOSS dopant exhibited polarizing results. While incorporated in adhesive polymeric matrix PA/PPy/DOSS-M composite shielding efficiency only reaches 0.1 dB, yet PA/PPy/DOSS-P_y composite exhibits SE at 11.1 dB with 0.0185 S electrical conductivity. Dopant dependence from incorporation variation is also observed with DBS dopant. SE for PA/PPy/DBS-M and PA/PPy/DBS-P_y composites is, 0.49 and 6.1 dB respectively, which correlates with section *12.1.* results, where PA/PPy/DBS-M composite was less absorbent of electromagnetic wave radiation and had little to none rise in composite temperature. Lastly, MWCNT doped composites offered promising results in SE improvement. Hence PA/PPy/MWCNT-M and PA/PPy/MWCNT-P_y composite electromagnetic wave radiation analysis resulted in shielding efficiency of 5 and 10.8 dB, respectively, with electrical conductivity of 0.0082 and 0.018 S.

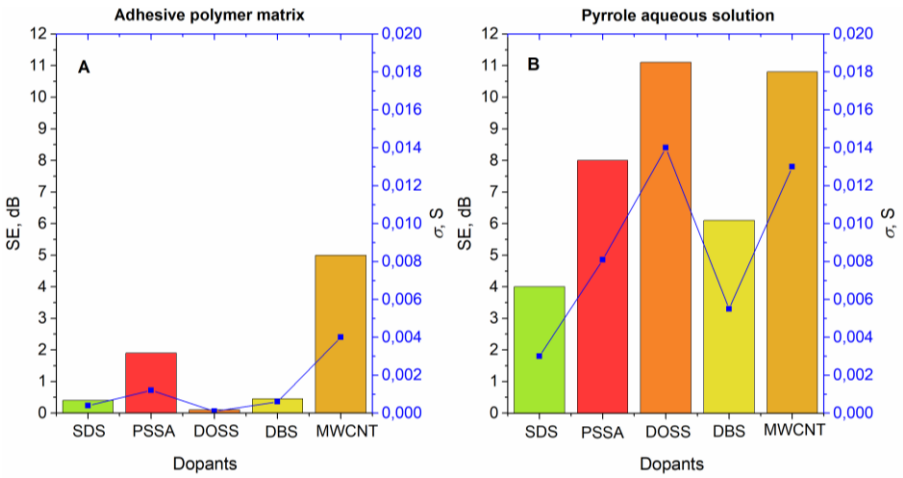

Fig. 52. Conductive PPy/dopant composites shielding effectiveness comparison on polyamide textile fabric substrate, when dopant is embedded in: A – adhesive polymer matrix solution, B – pyrrole monomer aqueous solution.

Overall, dopant incorporation into Py aqueous solution has a tendency to improve resulting textile composites electrical conductivity and SE possibilities.

12.3. PA/PPy/dopant Composite SEM Analysis

SEM study reveals PA/PPy/dopant textile composites diverse surface morphology. We try to compare morphological differences between PPy textile composites when a dopant is in aqueous pyrrole monomer solution versus PPy specimens when dopant is in adhesive polymer matrix. In the Fig. 53 we can indicate some differences between the surface areas of the specimens with PSSA and SDS dopants. When dopant is mixed in adhesive matrix both treated surfaces look smoother and homogenic (Fig. 53 left part) with otherwise PA/PPy specimens with dopants inside Py monomer solution. PA/PPy/PSSA-P_y surface is more agglomerated Fig. 53 top right. On the other hand, PA/PPy/SDS composite surface is cracked and uneven, although at higher magnification surface looks rough but homogenic.

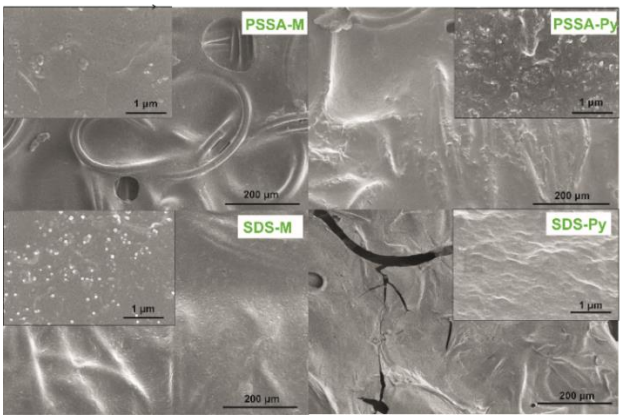

Fig. 53. SEM images comparing PA/PPy/PSSA and PA/PPy/SDS composites, when dopant is in adhesive polymer matrix M – left and in aqueous pyrrole solution P_y – right, at magnifications of 250 and 50.000 respectively.

However, PA/PPy composites with DBS and DOSS dopants exhibit significantly different surface characteristics. When comparing composites with DBS dopant one, can see that PA/PPy/DBS-M composite surface when dopant was incorporated in polymer matrix at lower magnifications appear to be smoother than PA/PPy/DBS-P_y composite. Although, at higher magnifications, PA/PPy/DBS-M (Fig. 54 left top) surface seems agglomerated with small granules located on top of each other. Also, PA/PPy/DBS-M composites surface wearing is visible, which is evidence of a thin layer formation on top of the fabric and efficient adhesive matrix

penetration into polyamide fabric. Meanwhile, PA/PPy/DBS-P_y composite surface at higher magnifications has a thicker layer (no visible textile weaving), which probably forms as a result of spray coating technique. PA/PPy/DBS-P_y composite surface at higher magnifications is much smoother without any noticeable agglomeration sites, exhibiting more of a wavy surface with steeper hills (Fig. 54 right top).

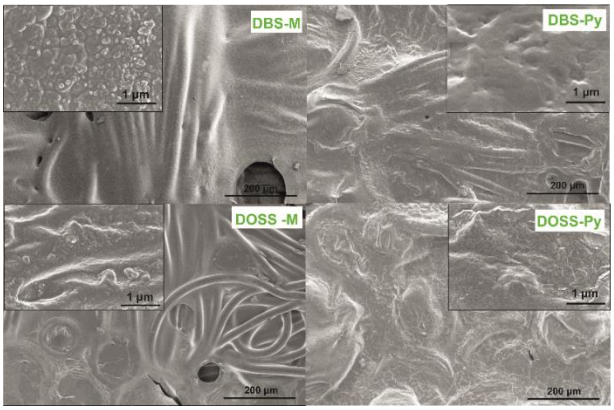

Fig. 54. SEM images comparing PA/PPy/DBS and PA/PPy/DOSS composites, when dopant is in adhesive polymer matrix M – left and aqueous in pyrrole solution P_y – right, at magnifications of 250 and 50.000 respectively.

On the other hand, both PA/PPy/DOSS composites images are more comparable and exhibit a wavy surface characteristic. The only difference is that PA/PPy/DOSS-M composite surface seems thinner and less evenly distributed throughout the composite surface, whereas PA/PPy/DOSS-P_y composite offers a homogeneously distributed thick, wavy and rough surface complexion where one cannot see the weaving of the fabric.

Between each other, PA/MWCNT composites differ the most compared to other anionic dopant composites (Fig. 56). At lower magnification textile surface weaving is visible, which reveals deep adhesive matrix penetration into textile fabric and ensures thin layer formation. However, at higher magnifications when textile composite is obtained by incorporating MWCNT in polymeric matrix it can result in largely agglomerated active surface. Although at MWCNT incorporation in polymer matrix, solution resulted in relatively high SE properties, PA/PPy/MWCNT-P_y composite at higher magnifications exhibited surface sponge-like morphology, which led to a more efficient SE parameters improvement (Fig. 52).

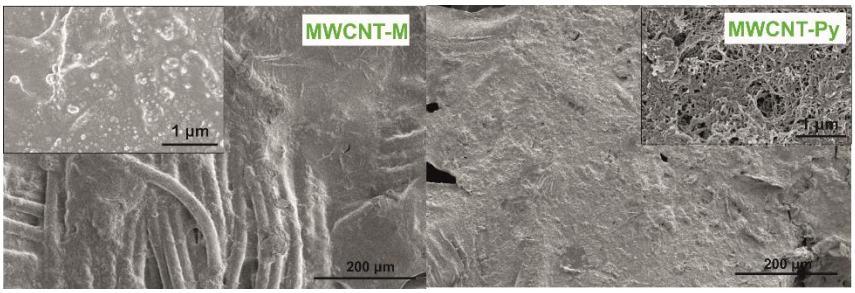

Fig. 56. SEM images comparing PA/PPy/MWCNT composite, when dopant is in adhesive polymer matrix M – left and in aqueous pyrrole solution P_y – right, at magnifications of 250 and 50.000 respectively.

Morphological analysis of PA/PPy/dopant fabric composites revealed that the presence of surfactant strongly influences the expected surface morphology which correlates with electrically conductive textile composites SE properties.

12.4. PA/PPy/dopant Composite XPS Analysis

Synthetic fabric composites with a dopant incorporated into polymerization matrix DOSS-M and MWCNT-M, as well as PPy composites formed with a dopant in aqueous monomer solution DOSS-P_y, MWCNT-P_y exhibited most promising SE properties (Fig. 67). Other PPy/dopant composites on nylon 6,6 weren't considered for XPS analysis, because of their lower electrical conductivity levels and SE characteristics.

The main PA/PPy/dopant composite core level peaks C 1s, N 1s, O 1s, S 2p3 and Cl 2p are centered at 285, 400, 532, 168 and 198 eV respectively. Furthermore, the binding energy of N 1s and Cl 2p may be assigned to pyrrole[30,232], thus confirming the presence of PPy in the prepared specimens. It is worth mentioning that, despite a thorough textile rinsing with deionised water DOSS and MWCNT containing composites still have localized iron (Fe2p at 741 eV) with a structure characteristic of Fe^{2+} is detected[233]. A considerable amount of Fe^{2+} was found in PA/PPy/DOSS-P_y composite, but in PA/PPy/DOSS-M and both PA/PPy/MWCNT composites were depicted to a much lesser extent.

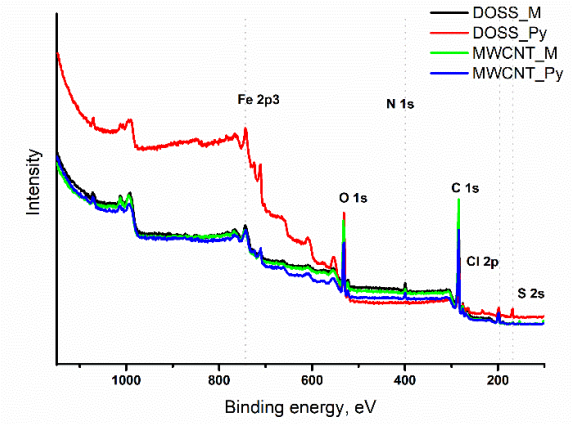

Fig. 57. XPS survey scans of PA/PPy composite with DOSS and MWCNT dopants embedded in M – adhesive polymer matrix and P_y – pyrrole aqueous solution.

Table 7. XPS composite surface composition atomic percentage analysis with anionic dopant DOSS and MWCNT aqueous solution.

Element	Atomic percentage of element on the surface, at. %			
	DOSS M	DOSS P_y	MWCNT M	MWCNT P_y
Fe2p3	1.54	4.08	0.93	1.69
Na1s	1.67	2.30	1.01	1.73
O1s	18.72	30.36	18.94	19.57
Cl2p	4.79	2.35	2.68	4.80
N1s	3.44	0.96	1.63	2.59
S2p	1.65	6.66	1.02	1.30
C1s	67.02	53.28	71.12	68.33

The apparent composite surface elemental compositions atomic percentage analysis with anionic dopant DOSS and MWCNT are reported in Table 7. The content of carbon changes slightly and decreases when the chosen dopant is incorporated in Py monomer solution versus incorporation in polymer matrix. The proportions of N and Cl in PA/PPy/DOSS composite decrease and the S and O contents increase upon comparing both DOSS composites[229]. It is evident that DOSS concentration in PA/PPy/DOSS-P_y composite is higher than in PA/PPy/DOSS-M, which ultimately exhibits higher conductivity levels (Fig. 52).

In addition to DOSS and MWCNT textile composite, further evaluation of their C1s peaks fittings were examined (Fig. 58). C1s fitted peaks spectra of PA/PPy/DOSS and PA/PPy/MWCNT composites were constructed with five

components and assigned by considering the chemical structure of DOSS[229] and MWCNT[234]. The aforementioned C1s fitted components are depicted in Fig. 58. The main peak at 284.7 eV is assigned to sp^2 C=C aromatic carbon for composites with MWCNT[235]. The peaks for all PA/PPy/dopant composites at 285.38–285.72 eV, which corresponds to sp^3 C–C bond or α-carbons[234],[202].

The position of the latter depends on the surrounding of this double bond whilst it is shifting slightly when hydrogen is incorporated. The peaks at 284.09-284.12 eV correspond to the β-carbons of Py ring. The peaks positioned at 286.01-288.87 eV represent $C–NH_x$ bonds, such as the peak at 286 eV is contributed by the polaron $=C–NH^+$ or C=N, and $C–SO^{3-}$ for DOSS dopant. Also, the peak at 287.06 eV for PA/PPy/DOSS-P_y composite is assigned to $–C=N^{+}$[202] and the shift can be attributed to the increase of sulphur 6.66% in the PA/PPy/DOSS-P_y composition. Moreover, 288 eV peaks represent (–COO).

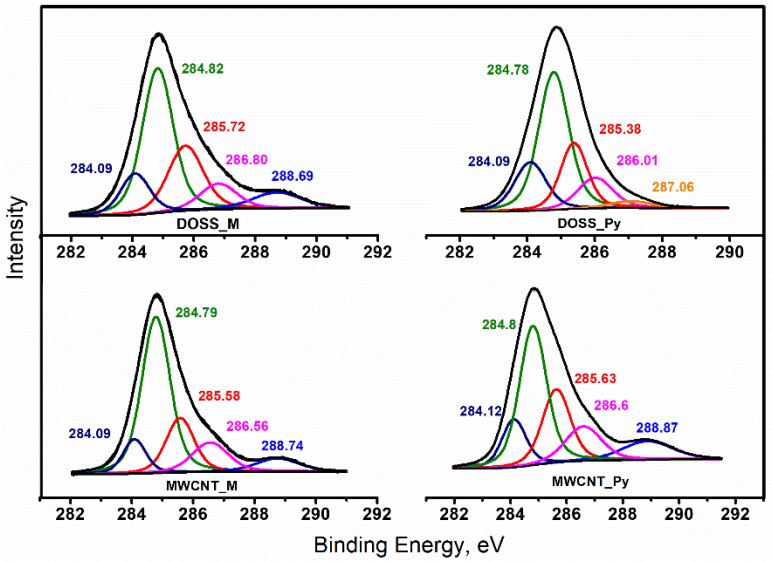

Fig. 58. PA/PPy/dopant composites XPS spectra analysis of high resolution C1s regions.

In general, it can be concluded that MWCNTs have close interaction with the *in situ* polymerized PPy moiety and can create very compact composite structures, as confirmed by SEM morphological analysis.

12.5. Review of the Main Results

Polyamide (nylon 6,6) textile composite studies incorporating anionic surfactants and MWCNT into polymeric matrix or in Py monomer aqueous solutions revealed that DOSS and MWCNT dopants offer the best electrical conductivity and thermal abilities.

DOSS shielding effectiveness almost reaches 12dB, when MWCNT shielding efficiency is at 11dB.

Experimental investigation of infrared thermography led to conclusions that conductive polymer distribution throughout all active composite surface was homogeneous.

FLIR analysis showed a tendency of temperature dependence from particular dopant with respect to dopant (DOSS, MWCNT) placement in the composite formation process. PA/PPy/DOSS-P_y and PA/PPy/MWCNT-P_y composites could later be used for development of novel thermoelectric materials.

From detailed XPS analysis one can conclude that higher levels of dopant incorporation into the textile composite is demonstrated with PA/PPy/DOSS and PA/PPy/MWCNT composites when dopant is embedded in the Py monomer solution.

Doped PPy textile composites using *in situ* polymerization process could be potentially used as a thermoelectric material for further TE device improvement. Doped polyamide textile composites with DOSS and MWCNT could be used as frame material for energy-storing textile fabrication.

CHAPTER 13. CONCLUTIONS

1. Bacteria *Streptomyces* spp. instigated biogenic polymerization process resulted in novel type of hollow BPPy microsphere formation varying at 20.3 μm and 24.5 μm sizes.

2. Sponge-like MPPy microspheres were fabricated by novel microemulsion polymerization in a microfluidic system varying between 30 and 40 μm in size.

3. A novel analytical model was adapted to measure SE and calculated electrical conductivity. The most suitable adhesive polymeric PVA matrix for PPy conductive composite formation was produced and demonstrated the best conductivity results from 13 to 18 S/cm in a 2-38 GHz frequency range.

4. Best textile for conductive composite formation was demonstrated with a wool substrate, which SE resulted in 14 dB in 2-20 GHz frequency range with possible applications in SRR production.

5. Most promising wool textile composite was obtained by spray coating technique when 0.375 M concentration anionic DOSS dopant was incorporated into Py aqueous monomer solution. Wool/PPy/DOSS composite exhibited SE of 22 dB in 8-38 GHz frequency range in a rectangular waveguide.

6. Highest measured SE in an anechoic chamber was demonstrated with electrically conductive PA/PPy/dopant textile composites at 12 and 11 dB in a 2-20 GHz frequency range where both DOSS and MWCNT dopants were embedded into Py aqueous monomer solution.

CHAPTER 14. LIST OF PUBLICATIONS AND CONFERENCE PARTICIPATION

14.1. Publications Included in Thesis

14.2. Articles in Journals

1. Stirke, R. M. Apetrei, **M. Kirsnyte**, L. Dedelaite, V. Bondarenka, V. Jasulaitiene, M. Pucetaite, A. Selskis, G. Carac, G. Bahrim, A. Ramanavicius, Synthesis of polypyrrole microspheres by *Streptomyces* spp., Polymer, Volume 84, 2016, 99-106.

   https://doi.org/10.1016/j.polymer.2015.12.029.

2. **M. Kirsnytė**, M. Jurkūnas, Ž. Kancleris, P. Ragulis, R. Simniškis, A. Vareikis, A. Abraitienė, K. Požėla, B. Whiteside, C.L. Tuinea-Bobe, A. Stirkė, Investigation of *in situ* formed conductive polymer composite in adhesive matrix, Synthetic Metals, Volume 258, 2019, 116181.

   https://doi.org/10.1016/j.synthmet.2019.116181

14.3. Published Patent

3. **M. Kirsnytė**, M. Jurkūnas, P. Ragulis, R. Simniškis, A. Stirkė, A method of fabricating polypyrrole in an adhesive polymeric matrix with embedded polymerization catalyst. Patent Nr. 6675, State Patent Bureau of the Republic of Lithuania 'Inventions' 2019 m. Nr. 21, 2019-11-11.

14.4. Attended Conferences

14.5. Oral Presentations

1. **M. Kirsnytė**, A. Stirkė, A. Janarauskas, Polipirolo sferų sintezė ir taikymas, FizTech 2015, Vilnius 2015 October 22-23d.
2. **M. Kirsnytė**, R. Simniškis, M. Jurkūnas, A.Stirkė, Polipirolo plonasluoksnių dangų laidumo ir paviršiaus ekranavimo efektyvumo tyrimas, FizTech 2016, Vilnius 2016 October 26-27d.
3. **M. Kirsnytė**, R Simniškis, Ž. Kancleris. Shielding effectiveness of screens from polypyrrole conducting layers, EUROEM 2016, London 2016 July 11-14d.
4. **M. Kirsnytė**, A. Sankauskaitė, P. Ragulis, A. Stirkė, Laidaus polimerinio sluoksnio tyrimas ir taikymas išmaniai tekstilei, FizTech 2017, Vilnius 2017 October 24-25d.

5. **M. Kirsnytė**, Ž. Kancleris, R. Simniškis, P. Ragulis, M. Jurkūnas, A. Šukys, A. Stirkė, Polypyrrole semiconductor films analysis and aplications for microvawe absorbers, 18th Lithuania-Belarus workshop, Vilnius 2017 December 8-9d.
6. **M. Kirsnytė**, P. Ragulis, A. Šukys, R. Simniškis, Ž. Kancleris, A. Stirkė, Conductive polypyrrole films analysis and application for microwave absorbers, FTMC, Vilnius 2018 February 21-22d.
7. **M. Kirsnytė**, A. Šukys, P. Ragulis, A. Stirkė, Legiruojančių medžiagų įtaka laidaus tekstilinio kompozito sintezėje, FizTech 2018, Vilnius 2018 October 17-18d.
8. **M. Kirsnytė**, A. Šukys, P. Ragulis, R. Simniškis, Ž. Kancleris, K. Požela, A. Stirkė, Doped polypyrrole textile composites thermoelectric analysis and characterization for energy storing materials, Open Readings 2019, Vilnius 2019 March 19-22d.

14.6. Poster Presentations

9. **M. Kirsnytė**, A. Stirkė, A. Janarauskas, R.M. Apetrei, Comparison of biogenic and by microemultion polymerized polypyrrole, Open Readings 2017, Vilnius 2017 March 14-17d.
10. **M. Kirsnytė**, A. Janarauskas, R. Celiešiūtė, A. Stirkė, L. Mažutis, Polypyrrole microsphere fabrication by biogenic and bioinspired polymerization processes, WCCE 10, Barcelona 2017 October 1-5d.
11. **M. Kirsnytė**, P. Ragulis, A. Šukys, R. Simniškis, Ž. Kancleris, A. Stirkė, Split-ring resonators formation on fabric using conductive polymer polypyrrole, Open Readings 2018, Vilnius 2018 March 20-23d.

REFERENCES

1. MacDiarmid, A. G., "Synthetic Metals": A Novel Role for Organic Polymers (Nobel Lecture). *Angewandte Chemie International Edition* **2001,** *40* (14), 2581-2590.
2. Umoren, S. A.; Solomon, M. M., Protective polymeric films for industrial substrates: A critical review on past and recent applications with conducting polymers and polymer composites/nanocomposites. *Progress in Materials Science* **2019,** *104*, 380-450.
3. Guimard, N. K.; Gomez, N.; Schmidt, C. E., Conducting polymers in biomedical engineering. *Progress in polymer science* **2007,** *32* (8-9), 876-921.
4. Liang, Y.; Yu, L., Development of semiconducting polymers for solar energy harvesting. *Polymer Reviews* **2010,** *50* (4), 454-473.
5. Cherenack, K.; van Pieterson, L., Smart textiles: Challenges and opportunities. *Journal of Applied Physics* **2012,** *112* (9), 091301.
6. Kwon, O. S.; Park, S. J.; Hong, J.-Y.; Han, A.-R.; Lee, J. S.; Lee, J. S.; Oh, J. H.; Jang, J., Flexible FET-type VEGF aptasensor based on nitrogen-doped graphene converted from conducting polymer. *Acs Nano* **2012,** *6* (2), 1486-1493.
7. Waltman, R.; Bargon, J., Electrically conducting polymers: a review of the electropolymerization reaction, of the effects of chemical structure on polymer film properties, and of applications towards technology. *Canadian Journal of Chemistry* **1986,** *64* (1), 76-95.
8. Pope, J.; Lekakou, C., Thermoelectric polymer composite yarns and an energy harvesting wearable textile. *Smart Materials and Structures* **2019,** *28* (9), 095006.
9. Chauhan, A.; Zubair, S.; Tufail, S.; Sherwani, A.; Sajid, M.; Raman, S. C.; Azam, A.; Owais, M., Fungus-mediated biological synthesis of gold nanoparticles: potential in detection of liver cancer. *International journal of nanomedicine* **2011,** *6*, 2305.
10. Sindhu, R.; Pandey, A.; Binod, P., Microbial diversity of nanoparticle biosynthesis. *Bio-Nanoparticles: Biosynthesis and Sustainable Biotechnological Implications* **2015**, 187-203.
11. Korbekandi, H.; Iravani, S.; Abbasi, S., Production of nanoparticles using organisms. *Critical reviews in biotechnology* **2009,** *29* (4), 279-306.
12. Mazutis, L.; Gilbert, J.; Ung, W. L.; Weitz, D. A.; Griffiths, A. D.; Heyman, J. A., Single-cell analysis and sorting using droplet-based microfluidics. *Nature protocols* **2013,** *8* (5), 870-891.
13. Skotheim, T. A.; Elsenbaumer, R. L.; Reynolds, J. R., *Handbook of conducting polymers*. 2nd ed.; M. Dekker: New York, 1998; p xiii, 1097 p.
14. Bolto, B. A.; McNeill, R.; Weiss, D., Electronic conduction in polymers. III. Electronic properties of polypyrrole. *Australian Journal of Chemistry* **1963,** *16* (6), 1090-1103.

15. Seliuta, D.; Šlekas, G.; Vaitkūnas, A.; Kancleris, Ž.; Valušis, G., Enhancement of higher-order plasmonic modes in a dense array of split-ring resonators. *Optics express* **2017,** *25* (21), 25113-25124.
16. Grancarić, A. M.; Jerković, I.; Koncar, V.; Cochrane, C.; Kelly, F. M.; Soulat, D.; Legrand, X., Conductive polymers for smart textile applications. *Journal of Industrial Textiles* **2018,** *48* (3), 612-642.
17. Eichelberger, L., Dr. Herbert Newby McCoy, Williams Gibbs Medalist. *Chem. Bull* **1937,** *24* (5), 171-174.
18. McCoy, H. N.; Moore, W. C., Organic amalgams: Substances with metallic properties composed in part of non-metallic elements. 2. *Journal of the American Chemical Society* **1911,** *33* (3), 273-292.
19. Garcia, E.; Cowley, A. H.; Bard, A. J., Quaternary ammonium amalgams as Zintl ion salts and their use in the synthesis of novel quaternary ammonium salts. *Journal of the American Chemical Society* **1986,** *108* (19), 6082-6083.
20. Tan, Y.; Ghandi, K., Kinetics and mechanism of pyrrole chemical polymerization. *Synthetic metals* **2013,** *175*, 183-191.
21. Skotheim, T. A., *Handbook of conducting polymers*. CRC press: 1997.
22. Polymers-Processing, C., Applications, ed. TA Skotheim and JR Reynolds. CRC Press, Boca Raton, FL: 2007.
23. Ateh, D.; Navsaria, H.; Vadgama, P., Polypyrrole-based conducting polymers and interactions with biological tissues. *Journal of the royal society interface* **2006,** *3* (11), 741-752.
24. Gardini, G., The oxidation of monocyclic pyrroles. In *Advances in Heterocyclic Chemistry*, Elsevier: 1973; Vol. 15, pp 67-98.
25. Das, T. K.; Prusty, S., Review on conducting polymers and their applications. *Polymer-plastics technology and engineering* **2012,** *51* (14), 1487-1500.
26. Bredas, J. L.; Street, G. B., Polarons, bipolarons, and solitons in conducting polymers. *Accounts of Chemical Research* **1985,** *18* (10), 309-315.
27. Stejskal, J.; Trchová, M.; Bober, P.; Morávková, Z.; Kopecký, D.; Vrňata, M.; Prokeš, J.; Varga, M.; Watzlová, E., Polypyrrole salts and bases: superior conductivity of nanotubes and their stability towards the loss of conductivity by deprotonation. *RSC advances* **2016,** *6* (91), 88382-88391.
28. Shirakawa, H., Nobel lecture: the discovery of polyacetylene film—the dawning of an era of conducting polymers. *Reviews of Modern Physics* **2001,** *73* (3), 713.
29. Kumar, D.; Sharma, R., Advances in conductive polymers. *European polymer journal* **1998,** *34* (8), 1053-1060.
30. Wang, J.; Zhang, C.; Du, Z.; Li, H.; Zou, W., Functionalization of MWCNTs with silver nanoparticles decorated polypyrrole and their application in antistatic and thermal conductive epoxy matrix nanocomposite. *RSC advances* **2016,** *6* (38), 31782-31789.
31. Chandrasekhar, P.; Zay, B.; McQueeney, T.; Birur, G.; Sitaram, V.; Menon, R.; Coviello, M.; Elsenbaumer, R., Physical, chemical, theoretical

aspects of conducting polymer electrochromics in the visible, IR and microwave regions. *Synthetic Metals* **2005,** *155* (3), 623-627.
32. Kanatzidis, M. G., Conductive polymers. *Chemical and Engineering News* **1990,** *68* (49).
33. Singh, M.; Kathuroju, P. K.; Jampana, N., Polypyrrole based amperometric glucose biosensors. *Sensors and Actuators B: Chemical* **2009,** *143* (1), 430-443.
34. Ates, M., A review study of (bio)sensor systems based on conducting polymers. *Materials Science and Engineering: C* **2013,** *33* (4), 1853-1859.
35. He, B.; Tang, Q.; Luo, J.; Li, Q.; Chen, X.; Cai, H., Rapid charge-transfer in polypyrrole–single wall carbon nanotube complex counter electrodes: Improved photovoltaic performances of dye-sensitized solar cells. *Journal of Power Sources* **2014,** *256*, 170-177.
36. Zou, Y.; Pisciotta, J.; Baskakov, I. V., Nanostructured polypyrrole-coated anode for sun-powered microbial fuel cells. *Bioelectrochemistry* **2010,** *79* (1), 50-56.
37. Madden, J. D.; Cush, R. A.; Kanigan, T. S.; Hunter, I. W., Fast contracting polypyrrole actuators. *Synthetic Metals* **2000,** *113* (1-2), 185-192.
38. Wan, Y.; Wu, H.; Wen, D., Porous-Conductive Chitosan Scaffolds for Tissue Engineering, 1. *Macromolecular bioscience* **2004,** *4* (9), 882-890.
39. Rasmussen, S. C., Early history of conductive organic polymers. *Conductive Polymers: Electrical Interactions in Cell Biology and Medicine; Zhang, Z., Rouabhia, M., Moulton, SE, Eds* **2018**, 1-21.
40. McNeill, R.; Siudak, R.; Wardlaw, J.; Weiss, D., Electronic conduction in polymers. I. The chemical structure of polypyrrole. *Australian Journal of Chemistry* **1963,** *16* (6), 1056-1075.
41. Bolto, B. A.; Weiss, D., Electronic conduction in polymers. II. The electrochemical reduction of polypyrrole at controlled potential. *Australian Journal of Chemistry* **1963,** *16* (6), 1076-1089.
42. Shirakawa, H.; Louis, E. J.; MacDiarmid, A. G.; Chiang, C. K.; Heeger, A. J., Synthesis of electrically conducting organic polymers: halogen derivatives of polyacetylene,(CH) x. *Journal of the Chemical Society, Chemical Communications* **1977,** (16), 578-580.
43. Zhou, D. D.; Cui, X. T.; Hines, A.; Greenberg, R. J., Conducting polymers in neural stimulation applications. In *Implantable Neural Prostheses 2*, Springer: 2009; pp 217-252.
44. Ghasemi-Mobarakeh, L.; Prabhakaran, M. P.; Morshed, M.; Nasr-Esfahani, M. H.; Baharvand, H.; Kiani, S.; Al-Deyab, S. S.; Ramakrishna, S., Application of conductive polymers, scaffolds and electrical stimulation for nerve tissue engineering. *Journal of tissue engineering and regenerative medicine* **2011,** *5* (4), e17-e35.
45. Meng, S.; Rouabhia, M.; Shi, G.; Zhang, Z., Heparin dopant increases the electrical stability, cell adhesion, and growth of conducting polypyrrole/poly (L, L-lactide) composites. *Journal of Biomedical Materials Research Part A:*

An Official Journal of The Society for Biomaterials, The Japanese Society for Biomaterials, and The Australian Society for Biomaterials and the Korean Society for Biomaterials **2008,** *87* (2), 332-344.
46. Lee, J.-W.; Serna, F.; Nickels, J.; Schmidt, C. E., Carboxylic acid-functionalized conductive polypyrrole as a bioactive platform for cell adhesion. *Biomacromolecules* **2006,** *7* (6), 1692-1695.
47. Kaur, G.; Adhikari, R.; Cass, P.; Bown, M.; Gunatillake, P., Electrically conductive polymers and composites for biomedical applications. *Rsc Advances* **2015,** *5* (47), 37553-37567.
48. Ghosh, S.; Maiyalagan, T.; Basu, R. N., Nanostructured conducting polymers for energy applications: towards a sustainable platform. *Nanoscale* **2016,** *8* (13), 6921-6947.
49. Bocchi, V.; Gardini, G.; Rapi, S., Highly electroconductive polypyrrole composites. *Journal of materials science letters* **1987,** *6* (11), 1283-1284.
50. Janata, J.; Josowicz, M., Conducting polymers in electronic chemical sensors. *Nature materials* **2003,** *2* (1), 19-24.
51. Sato, K.; Yamaura, M.; Hagiwara, T.; Murata, K.; Tokumoto, M., Study on the electrical conduction mechanism of polypyrrole films. *Synthetic metals* **1991,** *40* (1), 35-48.
52. Kang, E.; Tan, T.; Neoh, K.; Ong, Y., Halogen-induced charge transfer polymerization of pyrrole in aqueous media. *Polymer* **1986,** *27* (12), 1958-1962.
53. Sasso, C.; Beneventi, D.; Zeno, E.; Chaussy, D.; Petit-Conil, M.; Nortier, P.; Belgacem, N., Polypyrrole synthesis via carboxymethylcellulose-iron complexes. *BioResources* **2010,** *5* (4), 2348-2361.
54. Naarman, H., Electronic Properties of Conjugated Polymers, 76. Springer series in Solid State Science: 1987.
55. (a) Kulszewicz-Bajer, I.; Sobczak, J.; Hasik, M.; Pretula, J., Spectroscopic studies of polyaniline protonation with poly (alkylene phosphates). *Polymer* **1996,** *37* (1), 25-30; (b) Erdem, E.; Saçak, M.; Karakişla, M., Synthesis and properties of oxalic acid-doped polyaniline. *Polymer international* **1996,** *39* (2), 153-159.
56. Bakhshi, A., Electrically conducting polymers. *BULLETIN OF ELECTROCHEMISTRY* **1992,** *8*, 535-535.
57. Shalaby, S. W.; McCaig, M. S., Process for phosphonylating the surface of an organic polymeric preform. Google Patents: 1996.
58. Tessier, D.; Dao, L. H.; Zhang, Z.; King, M. W.; Guidoin, R., Polymerization and surface analysis of electrically-conductive polypyrrole on surface-activated polyester fabrics for biomedical applications. *Journal of Biomaterials Science, Polymer Edition* **2000,** *11* (1), 87-99.
59. Ohtani, A.; Shimidzu, T., Effective doping of polymer anion during chemical polymerization of pyrrole using Fe (OH) 3 oxidant. *Bulletin of the Chemical Society of Japan* **1989,** *62* (1), 234-238.

60. Gazotti Jr, W. A.; De Paoli, M.-A., High yield preparation of a soluble polyaniline derivative. *Synthetic Metals* **1996,** *80* (3), 263-269.
61. Martins, N.; e Silva, T. M.; Montemor, M.; Fernandes, J.; Ferreira, M., Electrodeposition and characterization of polypyrrole films on aluminium alloy 6061-T6. *Electrochimica Acta* **2008,** *53* (14), 4754-4763.
62. Herrasti, P.; Dıaz, L.; Ocón, P.; Ibáñez, A.; Fatas, E., Electrochemical and mechanical properties of polypyrrole coatings on steel. *Electrochimica acta* **2004,** *49* (22-23), 3693-3699.
63. Zhang, Z.; Roy, R.; Dugré, F. J.; Tessier, D.; Dao, L. H., In vitro biocompatibility study of electrically conductive polypyrrole-coated polyester fabrics. *Journal of Biomedical Materials Research: An Official Journal of The Society for Biomaterials, The Japanese Society for Biomaterials, and The Australian Society for Biomaterials and the Korean Society for Biomaterials* **2001,** *57* (1), 63-71.
64. Jiang, X.; Marois, Y.; Traoré, A.; Tessier, D.; Dao, L. H.; Guidoin, R.; Zhang, Z., Tissue reaction to polypyrrole-coated polyester fabrics: an in vivo study in rats. *Tissue engineering* **2002,** *8* (4), 635-647.
65. Leonavicius, K.; Ramanaviciene, A.; Ramanavicius, A., Polymerization model for hydrogen peroxide initiated synthesis of polypyrrole nanoparticles. *Langmuir* **2011,** *27* (17), 10970-10976.
66. Huczko, A., Template-based synthesis of nanomaterials. *Applied Physics A* **2000,** *70* (4), 365-376.
67. Shi, Y.; Peng, L.; Ding, Y.; Zhao, Y.; Yu, G., Nanostructured conductive polymers for advanced energy storage. *Chemical Society Reviews* **2015,** *44* (19), 6684-6696.
68. Gupta, S., Template-free synthesis of conducting-polymer polypyrrole micro/nanostructures using electrochemistry. *Applied physics letters* **2006,** *88* (6), 063108.
69. Reece, D. A.; Pringle, J. M.; Ralph, S. F.; Wallace, G. G., Autopolymerization of pyrrole in the presence of a host/guest calixarene. *Macromolecules* **2005,** *38* (5), 1616-1622.
70. Vaitkuviene, A.; Kaseta, V.; Voronovic, J.; Ramanauskaite, G.; Biziuleviciene, G.; Ramanaviciene, A.; Ramanavicius, A., Evaluation of cytotoxicity of polypyrrole nanoparticles synthesized by oxidative polymerization. *Journal of hazardous materials* **2013,** *250*, 167-174.
71. Kobayashi, S., Enzymatic polymerization. *Encyclopedia of polymer science and technology* **2002**.
72. Kobayashi, S., Enzymatic polymerization: a new method of polymer synthesis. *Journal of Polymer Science Part A: Polymer Chemistry* **1999,** *37* (16), 3041-3056.
73. Byrom, D., Polymer synthesis by microorganisms: technology and economics. *Trends in biotechnology* **1987,** *5* (9), 246-250.

74. Ramanavicius, A.; Kausaite, A.; Ramanaviciene, A., Self-encapsulation of oxidases as a basic approach to tune the upper detection limit of amperometric biosensors. *Analyst* **2008,** *133* (8), 1083-9.
75. Aizawa, M.; Wang, L.; Shinohara, H.; Ikariyama, Y., Enzymatic synthesis of polyaniline film using a copper-containing oxidoreductase: bilirubin oxidase. *Journal of biotechnology* **1990,** *14* (3-4), 301-309.
76. Samuelson, L. A.; Anagnostopoulos, A.; Alva, K. S.; Kumar, J.; Tripathy, S. K., Biologically derived conducting and water soluble polyaniline. *Macromolecules* **1998,** *31* (13), 4376-4378.
77. Bouldin, R.; Ravichandran, S.; Kokil, A.; Garhwal, R.; Nagarajan, S.; Kumar, J.; Bruno, F. F.; Samuelson, L. A.; Nagarajan, R., Synthesis of polypyrrole with fewer structural defects using enzyme catalysis. *Synthetic Metals* **2011,** *161* (15–16), 1611-1617.
78. Dias, H. R.; Fianchini, M.; Rajapakse, R. G., Greener method for high-quality polypyrrole. *Polymer* **2006,** *47* (21), 7349-7354.
79. Bruno, F. F.; Fossey, S. A.; Nagarajan, S.; Nagarajan, R.; Kumar, J.; Samuelson, L. A., Biomimetic synthesis of water-soluble conducting copolymers/homopolymers of pyrrole and 3, 4-ethylenedioxythiophene. *Biomacromolecules* **2006,** *7* (2), 586-589.
80. Tabačiarová, J.; Mičušík, M.; Fedorko, P.; Omastova, M., Study of polypyrrole aging by XPS, FTIR and conductivity measurements. *Polymer Degradation and Stability* **2015,** *120*, 392-401.
81. Nabid, M. R.; Entezami, A. A., A novel method for synthesis of water-soluble polypyrrole with horseradish peroxidase enzyme. *Journal of applied polymer science* **2004,** *94* (1), 254-258.
82. Chater, K. F.; Biró, S.; Lee, K. J.; Palmer, T.; Schrempf, H., The complex extracellular biology of Streptomyces. *FEMS Microbiology Reviews* **2010,** *34* (2), 171-198.
83. POPA, C.; FAVIER, L.; BAHRIM, G., TESTING OF THE NEW STREPTOMYCES STRAINS FOR PRODUCTION OF PHENOLOXIDASES. *Food Technology* **2013,** *37* (2), 35-46.
84. Wu, T.; Mei, Y.; Cabral, J. T.; Xu, C.; Beers, K. L., A new synthetic method for controlled polymerization using a microfluidic system. *Journal of the American Chemical Society* **2004,** *126* (32), 9880-9881.
85. Benhabib, M.; Chiesl, T. N.; Stockton, A. M.; Scherer, J. R.; Mathies, R. A., Multichannel capillary electrophoresis microdevice and instrumentation for in situ planetary analysis of organic molecules and biomarkers. *Analytical chemistry* **2010,** *82* (6), 2372-2379.
86. Bernard, A.; Michel, B.; Delamarche, E., Micromosaic immunoassays. *Analytical chemistry* **2001,** *73* (1), 8-12.
87. Burns, M. A.; Johnson, B. N.; Brahmasandra, S. N.; Handique, K.; Webster, J. R.; Krishnan, M.; Sammarco, T. S.; Man, P. M.; Jones, D.; Heldsinger, D., An integrated nanoliter DNA analysis device. *Science* **1998,** *282* (5388), 484-487.

88. Wu, M.-H.; Cai, H.; Xu, X.; Urban, J. P.; Cui, Z.-F.; Cui, Z., A SU-8/PDMS hybrid microfluidic device with integrated optical fibers for online monitoring of lactate. *Biomedical Microdevices* **2005,** *7* (4), 323-329.
89. Beebe, D. J.; Mensing, G. A.; Walker, G. M., Physics and applications of microfluidics in biology. *Annual review of biomedical engineering* **2002,** *4* (1), 261-286.
90. Whitesides, G. M., The origins and the future of microfluidics. *Nature* **2006,** *442* (7101), 368-373.
91. Fu, T.; Wu, Y.; Ma, Y.; Li, H. Z., Droplet formation and breakup dynamics in microfluidic flow-focusing devices: from dripping to jetting. *Chemical engineering science* **2012,** *84*, 207-217.
92. Tice, J. D.; Lyon, A. D.; Ismagilov, R. F., Effects of viscosity on droplet formation and mixing in microfluidic channels. *Analytica chimica acta* **2004,** *507* (1), 73-77.
93. Kaminski, T.; Garstecki, P., Controlled droplet microfluidic systems for multistep chemical and biological assays. *Chemical Society Reviews* **2017,** *46* (20), 6210-6226.
94. Vyawahare, S.; Griffiths, A. D.; Merten, C. A., Miniaturization and parallelization of biological and chemical assays in microfluidic devices. *Chemistry & biology* **2010,** *17* (10), 1052-1065.
95. Rogers, C. I.; Pagaduan, J. V.; Nordin, G. P.; Woolley, A. T., Single-monomer formulation of polymerized polyethylene glycol diacrylate as a nonadsorptive material for microfluidics. *Analytical chemistry* **2011,** *83* (16), 6418-6425.
96. Ng, J. M.; Gitlin, I.; Stroock, A. D.; Whitesides, G. M., Components for integrated poly (dimethylsiloxane) microfluidic systems. *Electrophoresis* **2002,** *23* (20), 3461-3473.
97. Yuan, C.; Li, P.; Shan, J.; Zhang, H., Influence of polymerization conditions on morphologies of polypyrrole. *Supramolecular Science* **1998,** *5* (5-6), 751-755.
98. Duchet, J.; Legras, R.; Demoustier-Champagne, S., Chemical synthesis of polypyrrole: structure–properties relationship. *Synthetic metals* **1998,** *98* (2), 113-122.
99. Zhang, X.; Zhang, J.; Song, W.; Liu, Z., Controllable synthesis of conducting polypyrrole nanostructures. *The Journal of Physical Chemistry B* **2006,** *110* (3), 1158-1165.
100. Li, W.; Pham, H. H.; Nie, Z.; MacDonald, B.; Güenther, A.; Kumacheva, E., Multi-step microfluidic polymerization reactions conducted in droplets: The internal trigger approach. *Journal of the American Chemical Society* **2008,** *130* (30), 9935-9941.
101. Qin, D.; Xia, Y.; Whitesides, G. M., Rapid prototyping of complex structures with feature sizes larger than 20 μm. *Advanced Materials* **1996,** *8* (11), 917-919.

102. McDonald, J. C.; Duffy, D. C.; Anderson, J. R.; Chiu, D. T.; Wu, H.; Schueller, O. J.; Whitesides, G. M., Fabrication of microfluidic systems in poly (dimethylsiloxane). *ELECTROPHORESIS: An International Journal* **2000,** *21* (1), 27-40.
103. McDonald, J. C.; Whitesides, G. M., Poly (dimethylsiloxane) as a material for fabricating microfluidic devices. *Accounts of chemical research* **2002,** *35* (7), 491-499.
104. Soper, S. A.; Ford, S. M.; Qi, S.; McCarley, R. L.; Kelly, K.; Murphy, M. C., Peer Reviewed: Polymeric Microelectromechanical Systems. ACS Publications: 2000.
105. Olanrewaju, A.; Beaugrand, M.; Yafia, M.; Juncker, D., Capillary microfluidics in microchannels: from microfluidic networks to capillaric circuits. *Lab on a Chip* **2018,** *18* (16), 2323-2347.
106. Abate, A. R.; Lee, D.; Do, T.; Holtze, C.; Weitz, D. A., Glass coating for PDMS microfluidic channels by sol–gel methods. *Lab on a Chip* **2008,** *8* (4), 516-518.
107. Abate, A. R.; Weitz, D. A., Syringe-vacuum microfluidics: A portable technique to create monodisperse emulsions. *Biomicrofluidics* **2011,** *5* (1), 014107.
108. Theberge, A. B.; Courtois, F.; Schaerli, Y.; Fischlechner, M.; Abell, C.; Hollfelder, F.; Huck, W. T., Microdroplets in microfluidics: an evolving platform for discoveries in chemistry and biology. *Angewandte Chemie International Edition* **2010,** *49* (34), 5846-5868.
109. Tewhey, R.; Warner, J. B.; Nakano, M.; Libby, B.; Medkova, M.; David, P. H.; Kotsopoulos, S. K.; Samuels, M. L.; Hutchison, J. B.; Larson, J. W., Microdroplet-based PCR enrichment for large-scale targeted sequencing. *Nature biotechnology* **2009,** *27* (11), 1025-1031.
110. Seemann, R.; Brinkmann, M.; Pfohl, T.; Herminghaus, S., Droplet based microfluidics. *Reports on progress in physics* **2011,** *75* (1), 016601.
111. Christopher, G. F.; Anna, S. L., Microfluidic methods for generating continuous droplet streams. *Journal of Physics D: Applied Physics* **2007,** *40* (19), R319.
112. Bibette, J.; Calderon, F. L.; Poulin, P., Emulsions: basic principles. *Reports on Progress in Physics* **1999,** *62* (6), 969.
113. Bibette, J.; Morse, D. C.; Witten, T.; Weitz, D., Stability criteria for emulsions. *Physical review letters* **1992,** *69* (16), 2439.
114. Baret, J.-C., Surfactants in droplet-based microfluidics. *Lab on a Chip* **2012,** *12* (3), 422-433.
115. Saini, D.; Basu, T., Synthesis and characterization of nanocomposites based on polyaniline-gold/graphene nanosheets. *Applied Nanoscience* **2012,** *2* (4), 467-479.
116. Percec, S.; Bolas, C.; Howe, L.; Brill, D. J.; Li, J., In situ polymerization and morphology of polypyrrole obtained in water-soluble polymer templates.

Journal of Polymer Science Part A: Polymer Chemistry **2012,** *50* (23), 4966-4976.
117. Porel, S.; Singh, S.; Harsha, S. S.; Rao, D. N.; Radhakrishnan, T., Nanoparticle-embedded polymer: in situ synthesis, free-standing films with highly monodisperse silver nanoparticles and optical limiting. *Chemistry of Materials* **2005,** *17* (1), 9-12.
118. Castano, H.; O'Rear, E. A.; McFetridge, P. S.; Sikavitsas, V. I., Polypyrrole thin films formed by admicellar polymerization support the osteogenic differentiation of mesenchymal stem cells. *Macromolecular bioscience* **2004,** *4* (8), 785-794.
119. Richardson-Burns, S. M.; Hendricks, J. L.; Martin, D. C., Electrochemical polymerization of conducting polymers in living neural tissue. *Journal of neural engineering* **2007,** *4* (2), L6.
120. Peramo, A.; Urbanchek, M. G.; Spanninga, S. A.; Povlich, L. K.; Cederna, P.; Martin, D. C., In situ polymerization of a conductive polymer in acellular muscle tissue constructs. *Tissue Engineering Part A* **2008,** *14* (3), 423-432.
121. Sun, X.; Sun, H.; Li, H.; Peng, H., Developing polymer composite materials: carbon nanotubes or graphene? *Advanced Materials* **2013,** *25* (37), 5153-5176.
122. Jayamurugan, P.; Ponnuswamy, V.; Subba Rao, Y. V.; Ashokan, S.; Meenakshisundar, S., Influence of spin coating rate on the thickness, surface modification and optical properties of water dispersed PPy composite thin films. *Materials Science in Semiconductor Processing* **2015,** *39*, 205-210.
123. Chatterjee, A.; Maity, S., A comparative study of reaction kinetics of in-situ chemical polymerization of polypyrrole onto various textile fibres. *Surface and Coatings Technology* **2017,** *324*, 569-576.
124. Lange, U.; Roznyatovskaya, N. V.; Mirsky, V. M., Conducting polymers in chemical sensors and arrays. *Analytica Chimica Acta* **2008,** *614* (1), 1-26.
125. Wang, Y.; Jiang, H.; Tao, Y.; Mei, T.; Liu, Q.; Liu, K.; Li, M.; Wang, W.; Wang, D., Polypyrrole/poly(vinyl alcohol-co-ethylene) nanofiber composites on polyethylene terephthalate substrate as flexible electric heating elements. *Composites Part A: Applied Science and Manufacturing* **2016,** *81*, 234-242.
126. Varshney, S.; Ohlan, A.; Jain, V.; Dutta, V.; Dhawan, S., Synthesis of ferrofluid based nanoarchitectured polypyrrole composites and its application for electromagnetic shielding. *Materials Chemistry and Physics* **2014,** *143* (2), 806-813.
127. Jiang, L.; Jun, H.-K.; Hoh, Y.-S.; Lim, J.-O.; Lee, D.-D.; Huh, J.-S., Sensing characteristics of polypyrrole–poly(vinyl alcohol) methanol sensors prepared by in situ vapor state polymerization. *Sensors and Actuators B: Chemical* **2005,** *105* (2), 132-137.

128. Chakraborty, M.; Mukherjee, D.; Mandal, B., Interpenetrating polymer network composites of polypyrrole and poly (vinyl acetate). *Synthetic metals* **1999,** *98* (3), 193-200.
129. Byko, M., From electric corsets to self-cleaning pants: the materials science and engineering of textiles. *Nanotechnology* **2004**.
130. Mattila, H., Yarn to Fabric: Intelligent Textiles. In *Textiles and Fashion*, Elsevier: 2015; pp 355-376.
131. Miravete, A., *3-D textile reinforcements in composite materials*. Woodhead Publishing: 1999.
132. Stoppa, M.; Chiolerio, A., Wearable electronics and smart textiles: a critical review. *sensors* **2014,** *14* (7), 11957-11992.
133. Van Langenhove, L.; Hertleer, C., Smart clothing: a new life. *International journal of clothing science and technology* **2004,** *16* (1-2), 63-72.
134. Ferrero, F.; Napoli, L.; Tonin, C.; Varesano, A., Pyrrole chemical polymerization on textiles: kinetics and operating conditions. *Journal of Applied Polymer Science* **2006,** *102* (5), 4121-4126.
135. Vatansever, D.; Siores, E.; Hadimani, R.; Shah, T., Smart woven fabrics in renewable energy generation. *Advances in modern woven fabrics technology* **2011**, 23-38.
136. Paul, G. M.; Cao, F.; Torah, R.; Yang, K.; Beeby, S.; Tudor, J., A smart textile based facial EMG and EOG computer interface. *IEEE sensors journal* **2013,** *14* (2), 393-400.
137. Cristian, I.; Nauman, S.; Cochrane, C.; Koncar, V., Electro-conductive sensors and heating elements based on conductive polymer composites in woven fabric structures. *Advances in Modern Woven Fabric Technology* **2011**, 1-22.
138. Gerard, M.; Chaubey, A.; Malhotra, B., Application of conducting polymers to biosensors. *Biosensors and bioelectronics* **2002,** *17* (5), 345-359.
139. Zhou, J.; Tzamalis, G.; Zaidi, N.; Comfort, N.; Monkman, A., Electrically conductive PANi multifilaments spun by a wet-spinning process. *Journal of materials science* **2001,** *36* (13), 3089-3095.
140. Jalili, R.; Razal, J. M.; Innis, P. C.; Wallace, G. G., One-step wet-spinning process of poly (3, 4-ethylenedioxythiophene): poly (styrenesulfonate) fibers and the origin of higher electrical conductivity. *Advanced Functional Materials* **2011,** *21* (17), 3363-3370.
141. Han, P.; Zhang, X.; Qiao, J., Intrinsically conductive polymer fibers from thermoplastic trans-1, 4-Polyisoprene. *Langmuir* **2016,** *32* (19), 4904-4908.
142. Wang, L., *Performance Testing of Textiles: Methods, Technology and Applications*. Woodhead Publishing: 2016.
143. Wildt, E., Embossing machine for textile materials. Google Patents: 1990.

144. Abbasi, A. M. R.; Militky, J., EMI shielding effectiveness of polypyrrole coated glass fabric. *Journal of Chemistry and Chemical Engineering* **2013,** *7* (3), 256.
145. Antunes, M.; Velasco, J. I., Multifunctional polymer foams with carbon nanoparticles. *Progress in Polymer Science* **2014,** *39* (3), 486-509.
146. Bharti, M.; Singh, A.; Samanta, S.; Aswal, D., Conductive polymers for thermoelectric power generation. *Progress in Materials Science* **2018,** *93*, 270-310.
147. Tritt, T. M.; Subramanian, M., Thermoelectric materials, phenomena, and applications: a bird's eye view. *MRS bulletin* **2006,** *31* (3), 188-198.
148. Snyder, G. J.; Toberer, E. S., Complex thermoelectric materials. In *Materials for sustainable energy: a collection of peer-reviewed research and review articles from Nature Publishing Group*, World Scientific: 2011; pp 101-110.
149. Hasan, M. N.; Wahid, H.; Nayan, N.; Mohamed Ali, M. S., Inorganic thermoelectric materials: A review. *International Journal of Energy Research* **2020**.
150. Khan, Z. U.; Edberg, J.; Hamedi, M. M.; Gabrielsson, R.; Granberg, H.; Wågberg, L.; Engquist, I.; Berggren, M.; Crispin, X., Thermoelectric polymers and their elastic aerogels. *Advanced Materials* **2016,** *28* (22), 4556-4562.
151. Chen, G.; Xu, W.; Zhu, D., Recent advances in organic polymer thermoelectric composites. *Journal of Materials Chemistry C* **2017,** *5* (18), 4350-4360.
152. Petsagkourakis, I.; Tybrandt, K.; Crispin, X.; Ohkubo, I.; Satoh, N.; Mori, T., Thermoelectric materials and applications for energy harvesting power generation. *Science and technology of advanced materials* **2018,** *19* (1), 836-862.
153. Zhang, Q.; Sun, Y.; Xu, W.; Zhu, D., Organic thermoelectric materials: emerging green energy materials converting heat to electricity directly and efficiently. *Advanced Materials* **2014,** *26* (40), 6829-6851.
154. Rowe, D. M., *Thermoelectrics handbook: macro to nano*. CRC press: 2018.
155. Li, C.; Jiang, F.; Liu, C.; Liu, P.; Xu, J., Present and future thermoelectric materials toward wearable energy harvesting. *Applied Materials Today* **2019,** *15*, 543-557.
156. Zuzok, R.; Kaiser, A.; Pukacki, W.; Roth, S., Thermoelectric power and conductivity of iodine-doped ‘‘new’’polyacetylene. *The Journal of chemical physics* **1991,** *95* (2), 1270-1275.
157. Yang, W.; Xu, H.; Li, Y.; Wang, W., Fabrications of Polyaniline Films by Pulse Electrodeposition in Acidic Solutions with Different Anions and Their Thermoelectric Performances. *Journal of Electronic Materials* **2017,** *46* (8), 4815-4824.

158. Li, J.; Du, Y.; Jia, R.; Xu, J.; Shen, S. Z., Flexible thermoelectric composite films of polypyrrole nanotubes coated paper. *Coatings* **2017,** *7* (12), 211.
159. Bender, K.; Gogu, E.; Hennig, I.; Schweitzer, D.; Müenstedt, H., Electric conductivity and thermoelectric power of various polypyrroles. *Synthetic Metals* **1987,** *18* (1-3), 85-88.
160. Jia, Y.; Shen, L.; Liu, J.; Zhou, W.; Du, Y.; Xu, J.; Liu, C.; Zhang, G.; Zhang, Z.; Jiang, F., An efficient PEDOT-coated textile for wearable thermoelectric generators and strain sensors. *Journal of Materials Chemistry C* **2019,** *7* (12), 3496-3502.
161. Jia, Y.; Li, X.; Jiang, F.; Li, C.; Wang, T.; Jiang, Q.; Hou, J.; Xu, J., Effects of additives and post-treatment on the thermoelectric performance of vapor-phase polymerized PEDOT films. *Journal of Polymer Science Part B: Polymer Physics* **2017,** *55* (23), 1738-1744.
162. Mordiguine, M., Interference Control in Computer and Microprocessors Based Equipments. *Don White Consultant Inc: Virginia* **1984**.
163. Mottahed, B. D.; Manoochehri, S., A review of research in materials, modeling and simulation, design factors, testing, and measurements related to electromagnetic interference shielding. *Polymer-Plastics Technology and Engineering* **1995,** *34* (2), 271-346.
164. Zamanian, A.; Hardiman, C., Electromagnetic radiation and human health: A review of sources and effects. *High Frequency Electronics* **2005,** *4* (3), 16-26.
165. Ebrahimi, I.; Gashti, M. P., Polypyrrole-MWCNT-Ag composites for electromagnetic shielding: Comparison between chemical deposition and UV-reduction approaches. *Journal of Physics and Chemistry of Solids* **2018,** *118*, 80-87.
166. Martin, P. M., *Handbook of deposition technologies for films and coatings: science, applications and technology*. William Andrew: 2009.
167. Huang, J. C., EMI shielding plastics: a review. *Advances in Polymer Technology: Journal of the Polymer Processing Institute* **1995,** *14* (2), 137-150.
168. Sparavigna, A. C., Applications of Polypyrrole/Polyester Textiles: A Review. *International Journal Of Sciences* **2017,** *6* (08), 98-107.
169. Ramasamy, S. In *A review of EMI shielding and suppression materials*, Proceedings of the International Conference on Electromagnetic Interference and Compatibility'99 (IEEE Cat. No. 99TH 8487), IEEE: 1997; pp 459-466.
170. White, D.; Mardiguian, M., Electromagnetic shielding. Interference Control Technologies. *Inc., Gainsville* **1988**.
171. Baker, Z.; Abdelazeez, M.; Zihlif, A., Measurements of the "Magnex DC" characteristics at microwave frequencies. *Journal of materials science* **1988,** *23* (8), 2995-3000.
172. Margolis, J., Conductive Polymers and Plastics (Chapman & Hall, New York, 1989).

173. Han, E. G.; Kim, E. A.; Oh, K. W., Electromagnetic interference shielding effectiveness of electroless Cu-plated PET fabrics. *Synthetic Metals* **2001,** *123* (3), 469-476.
174. Ortlek, H. G.; Saracoglu, O. G.; Saritas, O.; Bilgin, S., Electromagnetic shielding characteristics of woven fabrics made of hybrid yarns containing metal wire. *Fibers and polymers* **2012,** *13* (1), 63-67.
175. Niranjanappa, A.; Biliya, R.; Trivedi, D., Seminar on State of the Art in EMI—EMC and Future Trends. India: 1996.
176. Stafström, S.; Bredas, J.; Epstein, A.; Woo, H.; Tanner, D.; Huang, W.; MacDiarmid, A., Polaron lattice in highly conducting polyaniline: theoretical and optical studies. *Physical Review Letters* **1987,** *59* (13), 1464.
177. Liu, C.; Li, F.; Ma, L. P.; Cheng, H. M., Advanced materials for energy storage. *Advanced materials* **2010,** *22* (8), E28-E62.
178. Gaponik, N. P.; Talapin, D. V.; Rogach, A. L.; Eychmüller, A., Electrochemical synthesis of CdTe nanocrystal/polypyrrole composites for optoelectronic applications. *Journal of Materials Chemistry* **2000,** *10* (9), 2163-2166.
179. MacDiarmid, A. G., Polyaniline and polypyrrole: where are we headed? *Synthetic Metals* **1997,** *84* (1-3), 27-34.
180. Geetha, S.; Satheesh Kumar, K.; Rao, C. R.; Vijayan, M.; Trivedi, D., EMI shielding: Methods and materials—A review. *Journal of applied polymer science* **2009,** *112* (4), 2073-2086.
181. Kim, B. R.; Lee, H.-K.; Park, S.; Kim, H.-K., Electromagnetic interference shielding characteristics and shielding effectiveness of polyaniline-coated films. *Thin Solid Films* **2011,** *519* (11), 3492-3496.
182. Kathirgamanathan, P., Unusual electromagnetic shielding characteristics of inherently conducting polymer-coated metal powder/polymer composites. *Journal of Materials Chemistry* **1993,** *3* (3), 259-262.
183. Lakshmi, K.; John, H.; Mathew, K.; Joseph, R.; George, K., Microwave absorption, reflection and EMI shielding of PU–PANI composite. *Acta Materialia* **2009,** *57* (2), 371-375.
184. Rubežienė, V.; Abraitienė, A.; Baltušnikaitė-Guzaitienė, J.; Varnaitė-Žuravliova, S.; Sankauskaitė, A.; Kancleris, Ž.; Ragulis, P.; Šlekas, G., The influence of distribution and deposit of conductive coating on shielding effectiveness of textiles. *The Journal of The Textile Institute* **2018,** *109* (3), 358-367.
185. Giddens, H.; Paul, D.; Hilton, G.; McGeehan, J. In *Influence of body proximity on the efficiency of a wearable textile patch antenna*, 2012 6th European Conference on Antennas and Propagation (EUCAP), IEEE: 2012; pp 1353-1357.
186. Wang, Z.; Zhang, L.; Psychoudakis, D.; Volakis, J. L. In *Flexible textile antennas for body-worn communication*, 2012 IEEE International Workshop on Antenna Technology (iWAT), IEEE: 2012; pp 205-208.

187. Gupta, B.; Sankaralingam, S.; Dhar, S. In *Development of wearable and implantable antennas in the last decade: A review*, 2010 10th Mediterranean Microwave Symposium, IEEE: 2010; pp 251-267.
188. Cotarlet, M.; Bahrim, G.; Negoita, T.; Stougaard, P., Screening of polar streptomycetes able to produce cold-active hydrolytic enzymes using common and chromogenic substrates. *Rom Biotechnol Lett* **2008,** *13*, 69-80.
189. Arribas, C.; Rueda, D., Preparation of conductive polypyrrole-polystyrene sulfonate by chemical polymerization. *Synthetic metals* **1996,** *79* (1), 23-26.
190. Hoshina, Y.; Zaragoza-Contreras, E. A.; Farnood, R.; Kobayashi, T., Nanosized polypyrrole affected by surfactant agitation for emulsion polymerization. *Polymer bulletin* **2012,** *68* (6), 1689-1705.
191. Joo, J.; Lee, J.; Baeck, J.; Kim, K.; Oh, E.; Epstein, J., Electrical, magnetic, and structural properties of chemically and electrochemically synthesized polypyrroles. *Synthetic metals* **2001,** *117* (1-3), 45-51.
192. Jang, K. S.; Moon, B.; Oh, E. J.; Lee, H., Characteristics of tantalum electrolytic capacitors using soluble polypyrrole electrolyte. *Journal of power sources* **2003,** *124* (1), 338-342.
193. Kancleris, Z.; Slekas, G.; Matulis, A., Modeling of two-dimensional electron gas sheet in FDTD method. *IEEE Transactions on Antennas and Propagation* **2013,** *61* (2), 994-996.
194. Rybicki, T.; Stempień, Z.; Rybicki, E.; Szugajew, L., EMI Shielding Effectiveness of Polyacrylonitrile Fabric With Polyaniline Deposition by Reactive Ink-Jet Printing and Model Approach. *IEEE Transactions on Electromagnetic Compatibility* **2016,** *58* (4), 1025-1032.
195. Orfanidis, S., Electromagnetic waves and antennas (pp. 227–250). *New Brunswick, NJ: Rutgers University* **2002**.
196. Ragulis, P.; Simniškis, R.; Kancleris, Ž., Shift and elimination of microwave Fabry-Perot resonances in a dielectric covered with a thin metal layer. *Journal of Applied Physics* **2015,** *117* (16), 165302.
197. EN, S., 1149-3: 2004. *Protective clothing—Electrostatic properties—Part 3*.
198. Yang, Y.; Chu, Y.; Yang, F.; Zhang, Y., Uniform hollow conductive polymer microspheres synthesized with the sulfonated polystyrene template. *Materials Chemistry and Physics* **2005,** *92* (1), 164-171.
199. Novák, P.; Rasch, B.; Vielstich, W., Overoxidation of polypyrrole in propylene carbonate: An in situ FTIR study. *Journal of the Electrochemical Society* **1991,** *138* (11), 3300.
200. Lu, X.; Chao, D.; Chen, J.; Zhang, W.; Wei, Y., Preparation and characterization of inorganic/organic hybrid nanocomposites based on Au nanoparticles and polypyrrole. *Materials letters* **2006,** *60* (23), 2851-2854.
201. P. Louette, F. B., J.-J.Pireaux, Poly(pyrrole) (PPY) XPS reference core level and energy losss spectra. *Surface Science Spectra* **2005,** *Vol. 12*, 84-89.

202. Sabbatini, L.; Malitesta, C.; De Giglio, E.; Losito, I.; Torsi, L.; Zambonin, P., Electrosynthesised thin polymer films: the role of XPS in the design of application oriented innovative materials. *Journal of Electron Spectroscopy and Related Phenomena* **1999,** *100* (1-3), 35-53.
203. A.L.Harreus, *Pyrrole*. 2007.
204. Gardner, S. D.; Singamsetty, C. S. K.; Booth, G. L.; He, G.-R.; Pittman Jr, C. U., Surface characterization of carbon fibers using angle-resolved XPS and ISS. *Carbon* **1995,** *33* (5), 587-595.
205. Delpeux, S.; Beguin, F.; Benoit, R.; Erre, R.; Manolova, N.; Rashkov, I., Fullerene core star-like polymers—1. Preparation from fullerenes and monoazidopolyethers. *European Polymer Journal* **1998,** *34* (7), 905-915.
206. Bùi, L. N.; Thompson, M.; McKeown, N. B.; Romaschin, A. D.; Kalman, P. G., Surface modification of the biomedical polymer poly (ethylene terephthalate). *Analyst* **1993,** *118* (5), 463-474.
207. Yamamoto, S.; Bluhm, H.; Andersson, K.; Ketteler, G.; Ogasawara, H.; Salmeron, M.; Nilsson, A., In situ x-ray photoelectron spectroscopy studies of water on metals and oxides at ambient conditions. *Journal of Physics: Condensed Matter* **2008,** *20* (18), 184025.
208. Frateur, I.; Lecoeur, J.; Zanna, S.; Olsson, C. O. A.; Landolt, D.; Marcus, P., Adsorption of BSA on passivated chromium studied by a flow-cell EQCM and XPS. *Electrochimica Acta* **2007,** *52* (27), 7660-7669.
209. Kang, E. T.; Neoh, K. G.; Ong, Y. K.; Tan, K. L.; Tan, B. T. G., X-ray photoelectron spectroscopy studies of deprotonated polypyrrole and its complexes. *Polymer* **1991,** *32* (8), 1354-1360.
210. Tan, K. L.; Tan, B. T. G.; Kang, E. T.; Neoh, K. G., The chemical nature of the nitrogens in polypyrrole and polyaniline: A comparative study by x-ray photoelectron spectroscopy. *The Journal of Chemical Physics* **1991**.
211. Liu, J.; He, Z.; Xue, J.; Tan, T. T. Y., A metal-catalyst free, flexible and free-standing chitosan/vacuum-stripped graphene/polypyrrole three dimensional electrode interface for high performance dopamine sensing. *Journal of Materials Chemistry B* **2014,** *2* (17), 2478-2482.
212. Guo, H.; Zhu, H.; Lin, H.; Zhang, J., Polypyrrole–multi-walled carbon nanotube nanocomposites synthesized in oil–water microemulsion. *Colloid and Polymer Science* **2008,** *286* (5), 587-591.
213. Kostić, R.; Raković, D.; Stepanyan, S.; Davidova, I.; Gribov, L., Vibrational spectroscopy of polypyrrole, theoretical study. *The Journal of chemical physics* **1995,** *102* (8), 3104-3109.
214. Xu, L.; Li, X.; Zhai, M.; Huang, L.; Peng, J.; Li, J.; Wei, G., Ion-Specific Swelling of Poly(styrene sulfonic acid) Hydrogel. *The Journal of Physical Chemistry B* **2007,** *111* (13), 3391-3397.
215. Omastová, M.; Boukerma, K.; Chehimi, M. M.; Trchová, M., Novel silicon carbide/polypyrrole composites; preparation and physicochemical properties. *Materials Research Bulletin* **2005,** *40* (5), 749-765.

216. Cho, M. S.; Park, S. Y.; Hwang, J. Y.; Choi, H. J., Synthesis and electrical properties of polymer composites with polyaniline nanoparticles. *Materials Science and Engineering: C* **2004,** *24* (1), 15-18.
217. Omastová, M.; Trchová, M.; Kovářová, J.; Stejskal, J., Synthesis and structural study of polypyrroles prepared in the presence of surfactants. *Synthetic Metals* **2003,** *138* (3), 447-455.
218. Bose, S.; Kuila, T.; Uddin, M. E.; Kim, N. H.; Lau, A. K. T.; Lee, J. H., In-situ synthesis and characterization of electrically conductive polypyrrole/graphene nanocomposites. *Polymer* **2010,** *51* (25), 5921-5928.
219. Tabačiarová, J.; Mičušík, M.; Fedorko, P.; Omastová, M., Study of polypyrrole aging by XPS, FTIR and conductivity measurements. *Polymer Degradation and Stability* **2015,** *120*, 392-401.
220. Chebil, S.; Monod, M.; Fisicaro, P., Direct electrochemical synthesis and characterization of polypyrrole nano-and micro-snails. *Electrochimica Acta* **2014,** *123*, 527-534.
221. Yang, H.; Dai, J.; Liu, X.; Lin, Y.; Wang, F.; Liu, P., Synthesis and enhanced microwave absorption properties of PVB/Co2Z/RGO layered composite. *Journal of Alloys and Compounds*.
222. Sudhamani, S.; Prasad, M.; Sankar, K. U., DSC and FTIR studies on gellan and polyvinyl alcohol (PVA) blend films. *Food Hydrocolloids* **2003,** *17* (3), 245-250.
223. Arora, K.; Chaubey, A.; Singhal, R.; Singh, R. P.; Pandey, M.; Samanta, S.; Malhotra, B.; Chand, S., Application of electrochemically prepared polypyrrole–polyvinyl sulphonate films to DNA biosensor. *Biosensors and Bioelectronics* **2006,** *21* (9), 1777-1783.
224. Tian, B.; Zerbi, G., Lattice dynamics and vibrational spectra of polypyrrole. *The Journal of chemical physics* **1990,** *92* (6), 3886-3891.
225. Jayamurgan, P.; Ponnuswamy, V.; Ashokan, S.; Mahalingam, T., The effect of dopant on structural, thermal and morphological properties of DBSA-doped polypyrrole. *Iranian Polymer Journal* **2013,** *22* (3), 219-225.
226. Omastová, M.; Trchová, M.; Pionteck, J.; Prokeš, J.; Stejskal, J., Effect of polymerization conditions on the properties of polypyrrole prepared in the presence of sodium bis (2-ethylhexyl) sulfosuccinate. *Synthetic Metals* **2004,** *143* (2), 153-161.
227. Jang, K. S.; Lee, H.; Moon, B., Synthesis and characterization of water soluble polypyrrole doped with functional dopants. *Synthetic metals* **2004,** *143* (3), 289-294.
228. Yue, B.; Wang, C.; Ding, X.; Wallace, G. G., Polypyrrole coated nylon lycra fabric as stretchable electrode for supercapacitor applications. *Electrochimica Acta* **2012,** *68*, 18-24.
229. Boukerma, K.; Omastová, M.; Fedorko, P.; Chehimi, M. M., Surface properties and conductivity of bis (2-ethylhexyl) sulfosuccinate-containing polypyrrole. *Applied surface science* **2005,** *249* (1-4), 303-314.

230. Vagholkar, P., Nylon (Chemistry, Properties and Uses). *Chemistry* **2016,** *5* (9).
231. Oh, E. J.; Jang, K. S.; Park, S. Y.; Han, S. S.; Suh, J. S., Electrochemical synthesis and characterization of strechable polypyrrole films. *Molecular Crystals and Liquid Crystals Science and Technology. Section A. Molecular Crystals and Liquid Crystals* **2001,** *371* (1), 243-246.
232. Gemeiner, P.; Kuliček, J.; Mikula, M.; Hatala, M.; Švorc, Ľ.; Hlavatá, L.; Mičušík, M.; Omastová, M., Polypyrrole-coated multi-walled carbon nanotubes for the simple preparation of counter electrodes in dye-sensitized solar cells. *Synthetic Metals* **2015,** *210*, 323-331.
233. Moulder, J. F.; Chastain, J., *Handbook of X-ray Photoelectron Spectroscopy: A Reference Book of Standard Spectra for Identification and Interpretation of XPS Data*. Physical Electronics Division, Perkin-Elmer Corporation: 1992.
234. Okpalugo, T.; Papakonstantinou, P.; Murphy, H.; McLaughlin, J.; Brown, N., High resolution XPS characterization of chemical functionalised MWCNTs and SWCNTs. *Carbon* **2005,** *43* (1), 153-161.
235. Bouchet-Fabre, B.; Zellama, K.; Godet, C.; Ballutaud, D.; Minéa, T., Comparative study of the structure of a-CNx and a-CNx: H films using NEXAFS, XPS and FT-IR analysis. *Thin Solid Films* **2005,** *482* (1-2), 156-166.

ACKNOWLEDGEMENTS

First of all, I would like to thank my alma mater Vilnius University and Center for Physical Science and Technology for the opportunity to not only start my PhD studies but also helping me to grow as a member of a broad scientific community. Over all my PhD years, there were many professors, supervisors, lab co-workers, family and friends that helped me in various circumstances on this ongoing road for improvement. So naturally, I would like to express my deepest gratitude for all of them.

Therefore firstly, I would like to thank my supervisor Dr. Arūnas Stirkė for believing in me and ultimately suggesting this PhD position. I am thankful for your guidance, support, strong leadership and comforting words, which throughout the years kept me moving forward and growing not only as a scientist but also as an individual human being. Thanks for the times when I needed a push and for the times when I needed a friend.

Moreover, I would like to express my gratitude to the whole Functional Materials and Electronics department. I would especially like to thank Prof. Habil. Dr. S. Balevičius and Prof. Dr. N. Žurauskienė for sharing their scientific knowledge and their rewarding discussions with a cup of coffee. All my Bioelectrics lab colleagues throughout the years. Furthermore, I must thank Dr. R. Celiešiūtė-Germanienė for her sincere support and motivation.

Also, I wish to extend my gratitude to our various collaborators. Dr. R. M. Apetrei for her microbiological knowledge and on collaboration when preparing my first manuscript. Microwave laboratory Prof. Habil. Dr. Ž. Kancleris, Dr. P. Ragulis and Dr. R. Simniškis for their patience, help with data interpretations and overall physics knowledge. Also, I want to acknowledge Prof. Dr. A. Selskis and Dr. V. Jasulaitienė for their assistance with SEM and XPS measurements. Also, Dr. A. Abraitienė and all the colleagues from the Textile Institute for their conductive textile measurements as well as fruitful discussions and advice. L. Mažutis for the opportunity to conduct research in the Microfluidics laboratory. Prof. Dr. E. G. Bogdanienė from VAA for her artistic ideas. Likewise, to my dear students, a sincere thank you to M. Jurkūnas, A. Šukys, A. Janarauskas and others. Also, I would like to thank my friend, fellow PhD, and now Dr. M. Mackoit-Sinkevičienė, for her inspiring spirit and example in science.

Finally, I wish to express my deepest gratitude to my amazing, beloved family: grandfather, father and especially my mum, who always made her priority to help me even when I was frustrated and down. And of course, my extended family thank you for your infinite encouragement and support.

NOTES

Vilniaus universiteto leidykla
Saulėtekio al. 3, LT-10222 Vilnius
El. p. info@leidykla.vu.lt,
www.leidykla.vu.lt
Tiražas 20 egz.
139